VILNIUS UNIVERSITY

Milda
ZILNYTĖ

Characterization of Pore-forming Toxin Vaginolysin from *Gardnerella vaginalis*

DOCTORAL DISSERTATION

Natural Sciences,
Biochemistry N 004

VILNIUS 2019

This doctoral thesis work was performed from 01/10/2014 to 30/09/2018 at Vilnius University, Life Sciences Center, Institute of Biotechnology. The research was supported by the Research Council of Lithuania (promotional scholarships), Vilnius University (Erasmus+ funding for the internship).

ACKNOWLEDGEMENTS

3

CONTENTS

ABBREVIATIONS

18:1 DGS-NTA(Ni) – 1,2-dioleoyl-sn-glycero-3-[(N-(5-amino-1-carboxypentyl)iminodiacetic acid)succinyl] (nickel salt)

Ab – antibody; Abs – antibodies

AUC – analytical ultracentrifugation

BV – bacterial vaginosis

CDC – cholesterol-dependent cytolysin; CDCs – cholesterol-dependent cytolysins

CDRs – complementarity-determining regions

CHO – Chinese hamster ovary cells

ClyA – cytolysin A secreted by *Escherichia coli, Salmonella enterica, Shigella flexneri*

cryo-EM – cryo-electron microscopy

cryo-ET – cryo-electron tomography

DMEM - Dulbecco's Modified Eagle Media

ELISA – enzyme-linked immunosorbent assay

FBS – fetal bovine serum

FITC – fluorescein isothiocyanate

HB1, 2 – helical bundle 1, 2

HD50 – CDC concentration inducing half-maximal erythrocyte lysis

HEK293 – human embryonic kidney 293 cells

Hla – α-haemolysin

Hlg – γ-haemolysin

HP 1,2 – β-hairpin 1, 2

HRP – horseradish peroxidase

ILY – intermedilysin from *Streptococcus intermedius*

INY – inerolysin from *Lactobacillus iners*

LLO – listeriolysin from *Listeria monocytogenes*

LLY – lectinolysin from *Streptococcus mitis*

MAb – monoclonal antibody; MAbs – monoclonal antibodies

MAC – membrane attack complex

MACPF – membrane attack complex-perforin

MACPF/CDC – membrane attack complex-perforin/cholesterol-dependent cytolysin

MFI – a median of fluorescence intensity

NET – neutrophil extracellular trap; NETs – neutrophil extracellular traps

nMFI – a normalised median of fluorescence intensity

PBS – phosphate-buffered saline

PE - phycoerythrin

PFO – perfringolysin from *Clostridium perfringens*
PFP – pore-forming protein; PFPs – pore-forming proteins
PFT – pore-forming toxin; PFTs – pore-forming toxins
PLY – pneumolysin from *Streptococcus pneumoniae*
PVDF – polyvinylidene fluoride
RBCs – red blood cells
RCF – relative centrifugal force
RPM – revolutions per minute
RT – room temperature
SLO – streptolysin O from *Streptococcus pyogenes*
SRB – sulforhodamine B
TMH1, 2 – transmembrane helix 1, 2
UDP – undecapeptide
VLY – vaginolysin from *Gardnerella vaginalis*
α-PFT – α-pore-forming toxin; α-PFTs – α-pore-forming toxins
β-PFT – β-pore-forming toxin; β-PFTs – β-pore-forming toxins

INTRODUCTION

Pore formation is widely used by different living organisms to target the membranes in the cells starting from the plasma membrane and extending to the membranes inside the cell. Similarly to the human immune system, which uses proteins capable of oligomerising and punching the holes in transformed or virus-infected cells, pathogens use similar mechanisms to target and compromise host cells. The puncture of the membranes can serve various purposes, such as disrupting the homeostasis across the membrane, delivering toxic material or opening up a tunnel for the pathogen itself to travel to the other side of the membrane, for example, to escape out of the specific organelles or cells.

Many pathogenic bacteria secrete soluble proteins, pore-forming toxins (PFTs), that bind to host cells with high affinity and assemble into a ring- or arc-shaped structures puncturing the membrane. The class of bacterial PFTs, which is widely distributed among human bacterial pathogens, is cholesterol-dependent cytolysins (CDCs). Interestingly, CDCs are a part of the same protein superfamily as membrane-attack complex/perforin (MACPF) proteins that play a vital role in the immune system.

Many recent studies suggest that bacteria use CDCs as the main asset during their pathogenesis (Los et al., 2013). For example, pneumolysin from *Streptococcus pneumoniae* was shown to play a role in the clearance of *S. pneumoniae* from the upper respiratory tract followed by promoting successful transmission of the bacterium (Zafar et al., 2017). Moreover, perfringolysin secreted by *Clostridium perfringens* helps the bacterium to evade the immune response by escaping from the macrophages (O'Brien and Melville, 2004). In the case of facultative intracellular *Listeria monocytogenes*, its CDC, listeriolysin, serves as a tool for the bacteria to get out from the phagosome and multiply in the cytosol of the host cell or allows it to replicate in vacuole of macrophages (Birmingham et al., 2008; Ruan et al., 2016).

The sole requirement for cholesterol in the membrane that CDCs target highlights their tropism for eukaryotic cells. Even though cholesterol is necessary and sufficient for most of the CDCs to form membrane pores, some CDCs use cellular receptors, such as specific glycans or membrane proteins, to facilitate their pore-forming activity (Farrand et al., 2008; Shewell et al., 2014; Soltani et al., 2007). One of such CDCs is the object of this study – vaginolysin (VLY) secreted by bacterium *Gardnerella vaginalis* (Gelber et al., 2008). This bacterium is believed to be a leading or initiating cause of the vaginal microflora imbalance known as bacterial vaginosis (BV) (Catlin,

1992; Schellenberg et al., 2017). The mechanism of BV is not well understood, but it is based on the dominance of anaerobic bacterial species over usually abundant *Lactobacillus* spp. Moreover, the presence of *G. vaginalis* is not necessarily related to BV as it can be found in a normal vaginal state as well (Ma et al., 2012; Schellenberg et al., 2017). Specific subspecies of *G. vaginalis* alone or in accord with other anaerobic bacteria are believed to lead to features that cause the imbalance of normal vaginal microflora. However, for now, the definitive features that could switch *G. vaginalis* phenotype from the one that is unrelated to microflora changes to the pathogenic one have not been found. According to the virulence potential of other CDCs, VLY is proposed to be one of the most likely players in the virulence of *G. vaginalis* (Los et al., 2013).

In this study, firstly, we focused on VLY and CD59 interaction and its role in VLY tropism for human cells. Secondly, we attempted to disentangle the roles of cholesterol and CD59 in VLY pore formation. Lastly, we sought to describe how VLY monomers interact with each other to form a pore.

The goal of the study

To investigate and characterise the features of *Gardnerella vaginalis* toxin vaginolysin and its pore-forming mechanism using *in vitro* systems.

Objectives

- To compare vaginolysin (VLY) and other cholesterol-dependent cytolysins in their cytolytic activity and tropism towards human cells.
- To design and optimise artificial membranes for the monitoring of VLY pore formation dynamics.
- To investigate the role of human protein CD59 in VLY pore formation.
- To investigate the role of membrane-embedded cholesterol in VLY pore formation.
- To define the interface between VLY and CD59 and identify the key amino acids that constitute the interface.
- To investigate the nature of the VLY monomer-monomer interface.

Scientific novelty

In this study, we advanced the experimental frontier to reveal that CD59 pre-concentrates VLY to enable efficient pore formation in cholesterol-containing membranes. We developed an experimental system to measure the kinetics of pore formation on artificial membrane models of liposomes containing cholesterol and CD59. Furthermore, we showed that unlike another cholesterol-dependent cytolysin (CDC), intermedilysin, which is unable to form pores without interacting with CD59, VLY successfully perforates membranes lacking CD59 but with much lower efficiency. Moreover, we lay the groundwork for the understanding of the interaction between VLY and its receptor CD59 as well as between adjacent VLY molecules in a growing chain of an oligomer that is to become a pore. Both of these processes are based on β-sheet extension either between VLY and CD59 or between two adjacent VLY molecules in a growing oligomer.

During this study, the crystal structure of vaginolysin in the complex with its receptor CD59 was solved by another group working in parallel (Lawrence

et al., 2016). However, the structure was not validated by mutagenesis until our study. The results of mutagenesis confirmed the interface of VLY-CD59 complex resolved from the crystal structure. Furthermore, our work elucidates the nature of VLY's tropism for human cells. We demonstrated for the first time the role of membrane protein CD59 in the dynamics of CDC pore formation. Our study makes a significant contribution to the understanding of CDCs' pore-forming mechanism.

Our study also provided a clinical case demonstrating the pathogenic potential of VLY. We identified, to date, the only patient, who developed *G. vaginalis*-related encephalopathy and provided indirect evidence, that the level of secreted VLY may correlate with the virulence of *G. vaginalis*, thus indicating the long-proposed importance of VLY in the pathogenesis of *G. vaginalis* infection.

Defended statements

- Vaginolysin (VLY) displays tropism towards human cells and forms pores more efficiently in the cells expressing human protein CD59.
- Membrane-bound CD59 triggers VLY oligomerisation and expedites the rate of VLY pore formation.
- Membrane-embedded cholesterol is necessary and sufficient for VLY pore formation.
- The interface of VLY-CD59 complex is based on the β-sheet extension between VLY D4 domain and CD59.
- VLY monomer-monomer interface is based on the β-sheet extension via the D3 domains of the neighbouring VLY molecules.

LITERATURE OVERVIEW

1   Cellular membrane remodelling

Membrane bilayer works as a barrier shielding the content of the cell from the exterior. This division has, likely, allowed life as we know it to emerge. During evolution, membranes became much more versatile and sophisticated. Various components were later added to the membrane to permit sensing of the surroundings of the cell, communication with the other cells or even enabled their movement (Bayraktar et al., 2017; Perez-Pascual et al., 2016; Zhang and Yang, 2017).

While these later evolutionary additions made membranes much more than just barriers, membranes are primarily barriers still. Efficient inter- and intracellular communication by transducing signals or transporting cargo depends on many processes. Most, if not all of these processes, rely on some degree of membrane remodelling that includes but is not limited to the following four processes.

1. Changing the membrane's physical properties, such as stiffness or softness, thickness, curvature. Local changes of membrane lipid composition or expression of various membrane interacting proteins, such as BAR proteins, can change overall physical characteristics of the membrane (Mim and Unger, 2012).

2. Microdomain formation that relies on the dynamic nature of the lipids and other components in the membrane. A good example is cholesterol and sphingolipids segmenting into transient microdomains called lipid rafts, whose composition allows them to serve as signal transduction islands (Simons and Toomre, 2000).

3. Membrane fusion and fission, such as is found during fission and fusion of mitochondria, cell division or gamete fusion (Pernas and Scorrano, 2015). Furthermore, a lot of intracellular communication is carried out by extracellular vesicles that carry cargo between cells and either bud from the eminent cell or fuse with the receiving cells (Balaj et al., 2011; Bayraktar et al., 2017; Zhang and Yang, 2017).

4. Changing membrane permeability that is enacted mostly through channel or transporter proteins to produce semi-permeable nature of the membrane (Borgnia et al., 1999; Huang and Czech, 2007; Jørgensen and Andersen, 1988; Mueckler et al., 1985), however, extreme changes in membrane permeability are achieved via pore-forming proteins that are the topic of the next chapter.

Lastly, it is important to note that all of these processes are used by cells to maintain homeostasis under various conditions, but are also, not surprisingly, used by the pathogens for their own needs.

2 Pore-forming proteins in membrane remodelling

Pore formation is a sophisticated adaptation to interrupt membrane integrity. All kingdoms of life have developed ways to execute pore formation either for defence or attack. Thus, the functions of pore-forming proteins (PFPs) are diverse (Dal Peraro and Van der Goot, 2016). The most widely spread and well studied PFPs are related to pathogen-host interaction. Pathogen aims to compromise host cell homeostasis or even kill it, whereas host cells retaliate against the pathogen and aim to kill it directly or to get rid of its infected cells. The actual function of the pore, however, may be to induce ion imbalance across the membrane, to help to transport toxic molecules into the target cell or even to serve as a tunnel for bacteria's safe escape out of endosomes. The large disparity in the diameter of different pores is characteristic to the family of a particular PFPs and is closely related to its function.
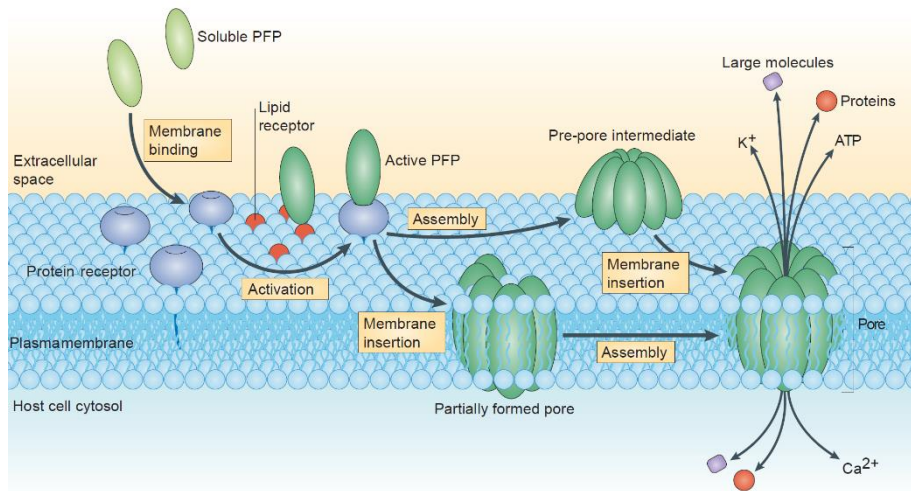
Figure 1. Schematic representation of pore formation by a major class of pore-forming proteins. The monomers of PFPs bind to the membrane through their lipid, glycan or protein receptors and subsequently oligomerise into a complete or partial ring-shaped structures that can punch a hole in the membrane. Opened membrane pores change membrane permeability and depending on the size and stability of the pores can lead to various outcomes, e.g. leaking of ions, signalling molecules or even proteins. Figure adapted from Dal Peraro and Van der Goot, 2016.

Generally, PFPs form pores in a three-step process. Firstly, monomeric PFPs bind to the membrane of a cell they target. Secondly, monomers oligomerise into a circular prepore that, finally, becomes a functional pore and punches a hole in the membrane (Figure 1) (Dal Peraro and Van der Goot, 2016). The first step is usually based on high protein-membrane affinity, and the membrane works as a platform for individual proteins to concentrate on, while the oligomerisation of individual membrane-bound proteins into a prepore is the rate-limiting step (Hotze et al., 2002; Thompson et al., 2011). The dynamics of prepore formation become quite distinct when considering pores of different diameters. It is generally supposed that the pores of a smaller size (that are composed of a small number of monomers) insert into the membrane more quickly and thus the number of prepores is kept low (Lee et al., 2016).

In contrast, PFPs that form large pores (of >20 monomers) take much longer to assemble fully (Lee et al., 2016). Therefore, maintaining a high number of growing oligomers ensures more insertions into the membrane. Aside from this, large enough oligomers can perforate the membrane without necessarily being completed. Thus, larger pores are more heterogeneous in size (Lee et al., 2016). In addition to the intrinsic PFPs' characteristics, the final step of the pore formation, the conversion from a prepore to a pore, is dependent on membrane characteristics. Less ordered membranes permit pores to be inserted more efficiently and, as such, facilitate the insertion of incomplete oligomers (Rojko and Anderluh, 2015).

In the chapters ahead, main PFP protein families are reviewed and discussed, with the emphasis on pore-forming toxins.

2.1 MACPF/CDC superfamily

Membrane attack complex-perforin/cholesterol-dependent cytolysin (MACPF/CDC) protein superfamily is one of the largest classes of PFPs, and its members are found among bacteria, fungi, animals, plants and a group of parasitic protozoa called apicomplexans. MACPF/CDC superfamily links a great diversity of PFPs playing a vital role in innate and adaptive immunity, animal venoms, bacterial virulence (Rosado et al., 2008). The diversity of these proteins has been reviewed many times (Anderluh and Gilbert, 2014; Lukoyanova et al., 2016; Ni and Gilbert, 2017; Reboul et al., 2016; Tweten et al., 2015). For example, mammalian perforins and complement proteins C6-C9 constitute an essential defence arm against pathogens and transformed (virus-infected) cells. Meanwhile, bacterial pathogens secrete CDCs that can lyse host cells or compromise them in other ways. Moreover, apicomplexan

parasites (*Toxoplasma* spp., *Plasmodium* spp.) secrete perforin-like proteins that are essential for maintaining the life cycle of these parasites (Amino et al., 2008; Kafsack et al., 2009; Wirth et al., 2014). Apart from that, the diversity of MACPF/CDC superfamily does not end here. A group of development-related proteins contain membrane attack complex/perforin (MACPF) domain, but they are not known to form pores (Ni and Gilbert, 2017). Astrotactins are one of the examples – they are known to play an essential role in the development of vertebrate central nervous system mediating neuronal-glial interactions and neural migration (Chang, 2017). Another example is *Drosophila* Torso-like proteins that are related to the development in invertebrates – termination of embryonic patterning, growth control, initiation of metamorphosis, development of immune cells (Johnson et al., 2017b).

Previously, it was thought that MACPF and CDC families are separate as their constituent members do not share any detectable sequence similarity. A breakthrough was achieved when the crystal structures of Plu-MACPF from bacterium *Photorhabdus luminescens*, human complement protein C8α alone and in the complex with C8γ were solved (Hadders et al., 2012; Rosado et al., 2007; Slade et al., 2008). By comparing it to the existing structures of bacterial CDCs, perfringolysin (PFO) and intermedilysin (ILY) (Polekhina et al., 2005; Rossjohn et al., 1997), a common fold between MACPF domain and N-terminal part of CDCs was found. MACPF and CDC families were joined into a superfamily and named MACPF/CDC. The structural conservation implies that MACPF and CDC share a common ancestor and that the mechanism of pore formation through this common pathway is well adapted for the roles it plays (Rosado et al., 2008).

2.2 Pore-forming toxins

A group of PFPs secreted by pathogens and playing an important role in their virulence are classified as pore-forming toxins (PFTs). PFTs comprise one of the largest known group of natural toxins (Anderluh and Lakey, 2008). Pathogens evolved to target essential membrane components of the host cell membrane and direct the toxic action towards required cell types or even particular cellular compartments (Los et al., 2013). Conversely, the membrane composition is versatile and can undergo reorganisation and reparation to resist damage (Cooper and McNeil, 2015). Thus, altogether opens more opportunities for the arms race between a pathogen and its host.

PFTs can be broadly classified into two groups based on the secondary structures that perforate the membrane, namely α-pore-forming toxins

(α-PFTs) and β-pore-forming toxins (β-PFTs). α-PFTs perforate the membrane by a set of α-helices, while β-PFTs form a transmembrane β-barrel, which can be a complete ring or an arc-shaped structure (Dal Peraro and Van der Goot, 2016; Gilbert et al., 2014; Gonzalez et al., 2008).

2.2.1 α-pore-forming toxins

The class of α-PFTs is very diverse in their origins and structures. A prototypical family of this class is the colicin family. What is interesting about colicins is that under stress conditions, *E. coli* secretes these toxins that are directed towards neighbouring *E. coli* or other closely related bacterial strains. The mechanism of action was thoroughly reviewed a long time ago by Lakey et al. (Lakey et al., 1994) describing the differences among different colicins. The typical function of all colicins is to cross the outer and inner membrane and translocate into the cytoplasm of the targeted bacterial cell. Once they are translocated, they reveal one of the three toxic activities – pore formation, degradation of nucleic acids or interruption of peptidoglycan synthesis. Colicins are encoded by a plasmid together with a protein ensuring immunity against that colicin. In this way, colicin plasmid containing *E. coli* cell is not compromised by the toxin it secretes, even though it has all the required receptors for the protein to be translocated. Colicins share a common fold composed of hydrophobic helical hairpin sheltered within a bundle of amphipathic α-helices (Figure 2, A) (Dal Peraro and Van der Goot, 2016; Parker et al., 1989). After required conformational changes, hydrophobic helical hairpin inserts into the membrane and forms a nonspecific voltage-gated channel (Lakey et al., 1991).

Another highly diverse family is cytolysin A (ClyA) family. ClyA family proteins target eukaryotic membranes. Even though proteins of ClyA family share a common fold of five bundled α-helices, the overall structure is highly versatile (Figure 2, B). The resulting pore can be assembled from one, two or even three different proteins (Bräuning and Groll, 2018). The prototype of this family is ClyA secreted by pathogenic strains of *E. coli*, *Salmonella enterica*, *Shigella flexneri*. Monomeric ClyA, in addition to a bundle of five α-helices, has a β-hairpin flanked by short α-helices. β-hairpin dips into the membrane and refolds into an α-helical motif, which, together with N-terminal α-helix, inserts into the membrane (Mueller et al., 2009). ClyA spans the eukaryotic membranes by homododecameric pores. Cholesterol was shown to be an essential component of the membrane for ClyA to form pores efficiently. However, in contrast to cholesterol-dependent cytolysins (described below), interaction with cholesterol does not affect the binding but stabilises

intermediary oligomers and boosts pore formation (Sathyanarayana et al., 2018).
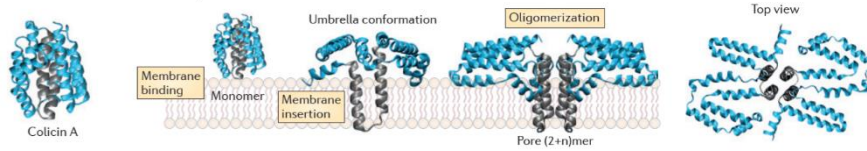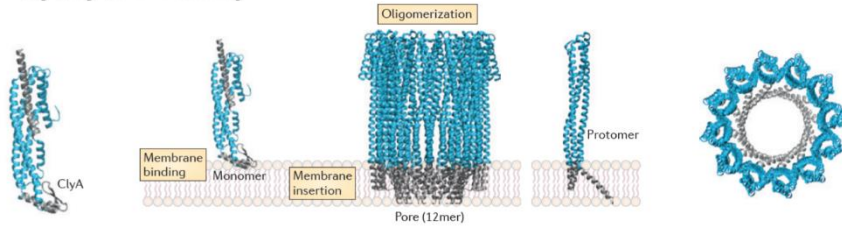
Figure 2. Structural architectures of monomers and oligomers among different families of α-pore-forming toxins (α-PFTs). Transmembrane α-helices in monomeric and oligomeric states are coloured in grey. A – the prototypical member of the colicin family, colicin A; the structure of the monomer was solved (PDB ID: 1COL), oligomeric structure provided is hypothetical; B – the prototypical member of the ClyA family, cytolysin A (ClyA); the monomer structure of ClyA (PDB ID: 1QOY) and the structure of dodecameric oligomer (PDB ID:2WCD) was solved; C – the prototypical member of the actinoporin family, fragaceatoxin C (FraC); FraC structures were solved for lipid-bound monomer form (PDB ID: 4TSL), dimeric intermediate (PDB ID: 4TSN) and octameric pore intercalated with sphingomyelin moieties (PDB ID: 4TSY). Figure adapted from Dal Peraro and Van der Goot, 2016.

In contrast to previously described α-PFTs families, actinoporins are eukaryotic toxins secreted by sea anemones (reviewed in Črnigoj Kristan et al., 2009; Peraro and Goot, 2016; Rojko et al., 2016). Actinoporins are one of the constituents of the venom that sea anemones use to attack their prey or defend themselves from predators. Actinoporins are small single-domain proteins sharing a common fold of β-sandwich flanked by two α-helices (Figure 2, C). N-terminal amphipathic α-helix disengages from the core and spans the membrane. The presence of sphingomyelin and the membrane phase boundaries between ordered and disordered domains were shown to promote binding of actinoporins to the membrane and enhance membrane

permeabilisation (Bakrač et al., 2008; Schön et al., 2008). Interestingly, apart from lipids, at least some actinoporins can bind glycans to enhance their haemolytic activity (Tanaka et al., 2017).

2.2.2 β-pore-forming toxins

β-pore-forming toxins (β-PFTs) received a tremendous amount of attention after the virulence factors of opportunistic human pathogen *Staphylococcus aureus* were identified and characterised (Bhakdi and Tranum-Jensen, 1991; Burnet, 1929). *S. aureus* produces a list of toxins, which constitute the whole class of β-PFTs called haemolysins (Dal Peraro and Van der Goot, 2016), which contribute to *S. aureus* pathogenesis by either the disruption or evasion of the immune system or by breaking epithelial barriers, thus facilitating tissue invasion. *S. aureus* haemolysins are single domain compact proteins rich in β-strands that contribute three-stranded β-sheets to form transmembrane β-hairpins (Figure 3, A). The archetype of this family is α-haemolysin (Hla) that assembles into a heptameric pore spanning the membrane by the fourteen-stranded β-barrel. Aside from Hla, *S. aureus* secretes a set of other β-PFTs of a similar fold, but the pores they form are composed of two components and form sixteen-stranded β-barrels. These two-component toxins are γ-haemolysin AB, HlgCB, leukocidin ED, Panton-Valentine leukocidin and leukocidin AB. They have evolved to target different cell types through the binding to specific cell surface proteins (Alonzo and Torres, 2014; Dumont and Torres, 2014).

The widest-spread family of β-PFTs is aerolysin family. These proteins are found among all kingdoms of life, including vertebrates (Szczesny et al., 2011). The prototypical member of this family is aerolysin from human pathogen bacterium *Aeromonas hydrophila*. Aerolysin is a four-domain protein that targets eukaryotic cells by binding to glycans on GPI-anchored proteins (Diep et al., 2002) (Figure 3, B). Interestingly, the monomers of aerolysin are secreted as an inactive proaerolysins. Proteolytic cleavage is required to remove C-terminal propeptide to proceed in forming a prepore (Iacovache et al., 2011). High-resolution complete pore structures of aerolysin and another aerolysin-like protein lysenin from the earthworm strikingly revealed a novel fold of two concentric β-barrels, both, in prepores and pores (Bokori-Brown et al., 2016; Cirauqui et al., 2017; Iacovache et al., 2016). The double β-barrel was credited with the extreme stability of aerolysin oligomers (Iacovache et al., 2016; Lesieur et al., 1999). The double β-barrel region is highly conserved among the other aerolysin-like proteins. Thus, it is hypothesised that the mechanism of pore formation might be similar, whereas

membrane-binding domains are highly versatile, suggesting diversity in the cells they target (Cirauqui et al., 2017).
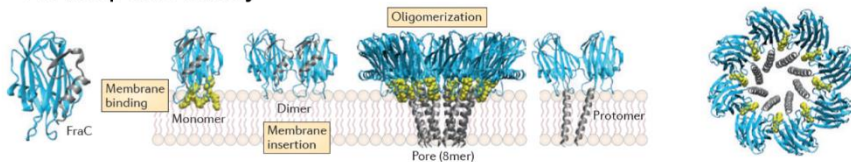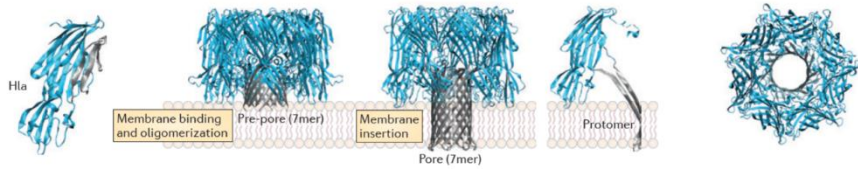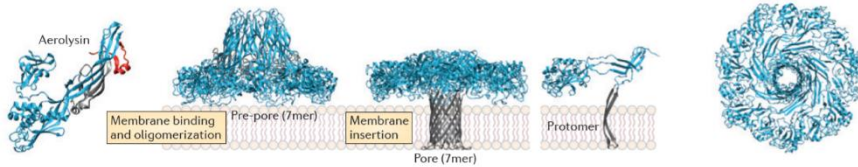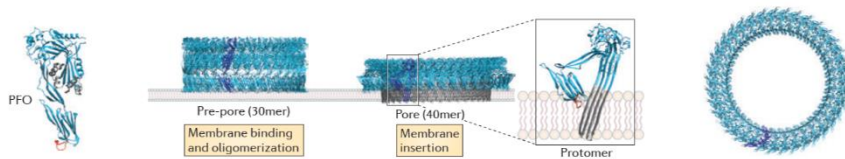

Figure 3. Structural architectures of monomers and oligomers among different families of β-pore-forming toxins (β-PFTs). Transmembrane α-helices in monomeric and oligomeric states are coloured in grey. A – the prototypical member of haemolysin family, α-haemolysin (Hla); the structures of Hla are solved in monomeric form (PDB ID: 4IDJ), single-component heptameric oligomer (PDB ID: 7AHL); heptameric prepore was modelled on the experimentally solved structure of γ-haemolysin (PDB ID: 4P1Y); haemolysin family also contains bi-component leukocidins, which form octameric pores of similar architecture; B – the prototypical member of aerolysin family, aerolysin; the structure of aerolysin was solved in monomeric form (PDB ID: 1PRE); aerolysin first assembles into a prepore, which eventually converts into a heptameric form, as shown by integrative modelling; C – the prototypical member of cholesterol-dependent cytolysin family, perfringolysin (PFO); the structure of PFO is solved in monomeric form (PDB ID: 1PFO); CDCs oligomerise into large prepore, which converts into membrane-inserted pores; prepore and pore structures were solved for pneumolysin (PDB ID: 2BK1, 2BK2, 5LY6). Figure adapted from Dal Peraro and Van der Goot, 2016.

Another large family of β-PFTs secreted by many human pathogens, called cholesterol-dependent cytolysins (Figure 3, C), is described in the next chapter.

3 Cholesterol-dependent cytolysins

3.1 Diversity and physiological role of CDCs

Cholesterol-dependent cytolysins (CDCs) are a family of β-PFTs. CDCs are predominantly found in Gram-positive bacteria, usually, pathogenic to animals (Christie et al., 2018). CDCs were also found in many human pathogens, including *Clostridium*, *Streptococcus*, *Listeria* (Los et al., 2013). CDCs target eukaryotic cells and share the ability to form pores in the membrane. The characteristic feature of CDCs is their interaction with the membrane-embedded cholesterol via direct binding. Amino acid sequences of CDCs are highly conserved (~40% identity among all family members), especially in motifs that are required for pore formation. The most variable regions are responsible for binding to membrane components other than cholesterol, thus enabling CDCs to display tropism for various cells. Nevertheless, the structures and the core mechanism of the pore formation are believed to be similar among different CDCs.

One of the most studied CDC with regards to its functional properties is pneumolysin (PLY). PLY is secreted by the bacterium *Streptococcus pneumoniae*, one of the leading agents behind human respiratory diseases (Hirst et al., 2004). Moreover, PLY was demonstrated to play a role in the transmission of *S. pneumoniae* (Lipsitch and Moxon, 1997; Matthias et al., 2014; Zafar et al., 2017). Due to its strong pro-inflammatory features in the mucosa, PLY speeds up the clearance of *S. pneumoniae* from the upper respiratory tract. The role of PLY in the transmission of *S. pneumoniae* is related to its pore-forming activity as a mutant with impaired pore-forming activity show reduced transmission of the pathogen (Zafar et al., 2017). PLY helps to enhance the survival of bacteria *ex vivo* after the escape from the host. It ensures that a sufficient amount of nutrients are released into the nasal secretions under inflammation (Zafar et al., 2017). Moreover, PLY was demonstrated to promote neutrophil extracellular trap (NET) formation. Although the formation of NETs is a way of defence against bacteria; high levels of NETs lead to an undesirable inflammation (Nel et al., 2016).

Lastly, it is interesting to note that the gene encoding PLY lacks a secretion signal peptide, which is responsible for the secretion of all other identified CDCs. It is suggested that PLY's release occurs in phagolysosomes in phagocytes when they lyse *S. pneumoniae*. Upon PLY pore formation, bacterial proteins flood into the cytosol where they activate inflammasome followed by a pro-inflammatory phagocyte death (Davis et al., 2011; Lemon and Weiser, 2015; Zafar et al., 2017). Moreover, Shak et al. visualised

biofilms of *S. pneumoniae* using confocal microscopy and immunogold-based electron microscopy and observed that at least some PLY is located on the surface of *S. pneumonia* (Shak et al., 2013). The specific PLY localisation hints its role as a matrix protein.

Group A *Streptococcus* bacteria were shown to use their CDC, streptolysin O (SLO) to promote immune evasion and affect host epithelial cells. Upon phagocytosis, bacteria secrete SLO, which can trigger macrophage apoptosis (Timmer et al., 2009). Furthermore, extracellular Group A *Streptococci* were shown to use SLO to elevate intracellular Ca^{2+} ion concentration in host epithelial cells and thus induce their apoptosis (Cywes-Bentley et al., 2005).

Another human pathogen *Clostridium perfringens,* the causal agent of gas gangrene, was shown to use its secreted CDC, perfringolysin O (PFO), in the course of gas gangrene pathogenesis. PFO was shown to promote bacteria's escape out of macrophages and thus, evasion of immune-induced elimination (O'Brien and Melville, 2004). Furthermore, the synergistic effect of PFO and another *C. perfringens* virulence factor α-toxin was observed, with α-toxin mostly damaging muscle tissue and PFO impairing vital leukocyte infiltration into the damaged sites (Awad et al., 2001).

The human pathogen, *Listeria monocytogenes*, is a facultative intracellular parasite, which causes foodborne diseases. *L. monocytogenes* exhibits a cell-to-cell spread life cycle. Upon entry into the host cell, the bacterium becomes encapsulated into a phagosome. It then uses CDC listeriolysin (LLO) to damage the membrane of phagosome interfering the phagosome-lysosome fusion, promoting escape from the phagosome and proceeds to multiply in the cytosol. LLO differs from other CDCs as its pore formation was shown to be regulated by the acidity of its environment. Even though it can form pores in both, acidic and neutral pH, the membrane pore conductances differ suggesting disparate the ways they affect membranes in particular environments (Bavdek et al., 2012; Podobnik et al., 2015; Ruan et al., 2016; Shaughnessy et al., 2006). Aside from this, the role of LLO was extended studying the virulence factor for persistent *L. monocytogenes* infection as LLO enables *L. monocytogenes* replication within macrophage vacuoles (Birmingham et al., 2008).

Pore-forming activity is not the only possible pathogenic outcome induced by CDCs. Sublytic concentrations of CDCs were shown to induce a variety of outcomes. For example, PLY triggers *S. pneumoniae* internalisation into macrophages by direct protein-protein interaction between PLY and mannose receptor C type 1 (Subramanian et al., 2018). Aside from this, SLO and PFO were shown to help the pathogen to evade immunity by triggering membrane shedding as a part of membrane repair. As SLO and PFO bind to

cholesterol-rich microdomains, shedding of these membrane regions resulted in a loss of immune signalling proteins, such as toll-like receptor 4 and type I interferon-γ receptor (Bhattacharjee and Keyel, 2018). Membrane binding without pore formation of LLO, PLY, and PFO was related to an epigenetic histone modification resulting in lower transcription of certain host genes including key immune components (Hamon et al., 2007).

Interestingly, few CDCs were identified in Gram-negative bacteria that are supposed to be non-pathogenic at least in animals (Hotze et al., 2013). Novel CDCs, namely enterolysin, desulfolysin, are produced by anaerobic soil-resident bacteria, *Enterobacter lignolyticus*, *Desulfobulbus propionicus*, respectively. These cytolysins maintain the pore-forming ability and the characteristic cholesterol-rich membrane binding. However, they lack secretion signal peptide that is typical for all CDCs except PLY discussed above. It is hypothesised that *E. lignolyticus* and *D. propionicus* might target their protozoan predators in a fight for resources in soil and aquatic environments.

3.2   CDC targets in the membrane

Membrane binding is the initial and crucial step for all cholesterol-dependent cytolysins (CDCs) no matter whether their function is to form a pore or to induce some other signal. CDCs possess a membrane-binding domain at the C-terminus – the tip of the protein (designated as domain 4, D4) (Figure 4). The namesake membrane target for CDCs is cholesterol embedded in the eukaryotic membranes.
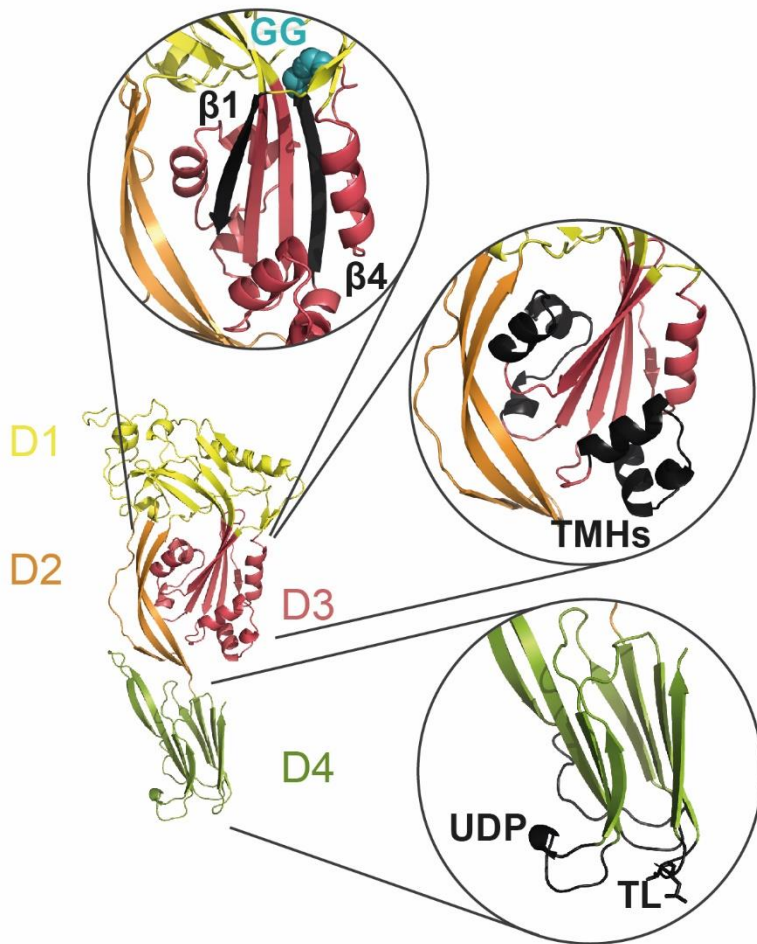
Figure 4. Structure of prototypical cholesterol-dependent cytolysin (CDC) perfringolysin (PFO) (PDB ID: 1PFO). Domains are designated as D1 (yellow), D2 (orange), D3 (red), D4 (green). Highlighted in black are β1- and β4-strands and a highly conserved Gly-Gly motif in D1, transmembrane helical (TMHs) motifs (black) in D3 domain and characteristic loops in D4 – undecapeptide (UDP) (black) and L1 loop bearing Thr-Leu (TL) amino acid pair (visualised as a stick model).

Additionally, many CDCs were shown to bind to glycans (Shewell et al., 2014). However, only one known CDC, lectinolysin (LLY) contains a *bona fide* lectin domain responsible for glycan-binding at its N-terminus (Farrand et al., 2008). Lastly, a small class of CDCs share tropism towards human cells. In addition to cholesterol and/or glycans, they engage human cluster of differentiation protein CD59.

3.2.1 Cholesterol is a lipid receptor for CDCs

Cholesterol is vital for a variety of cellular processes carried out in eukaryotes maintaining membrane permeability and fluidity (Pollard et al., 2017). The amount of cholesterol is tightly regulated to fulfil the functional requirements of different membranes across the cell (Brown and Goldstein, 1997; Gill et al., 2008; Jeon and Osborne, 2012).
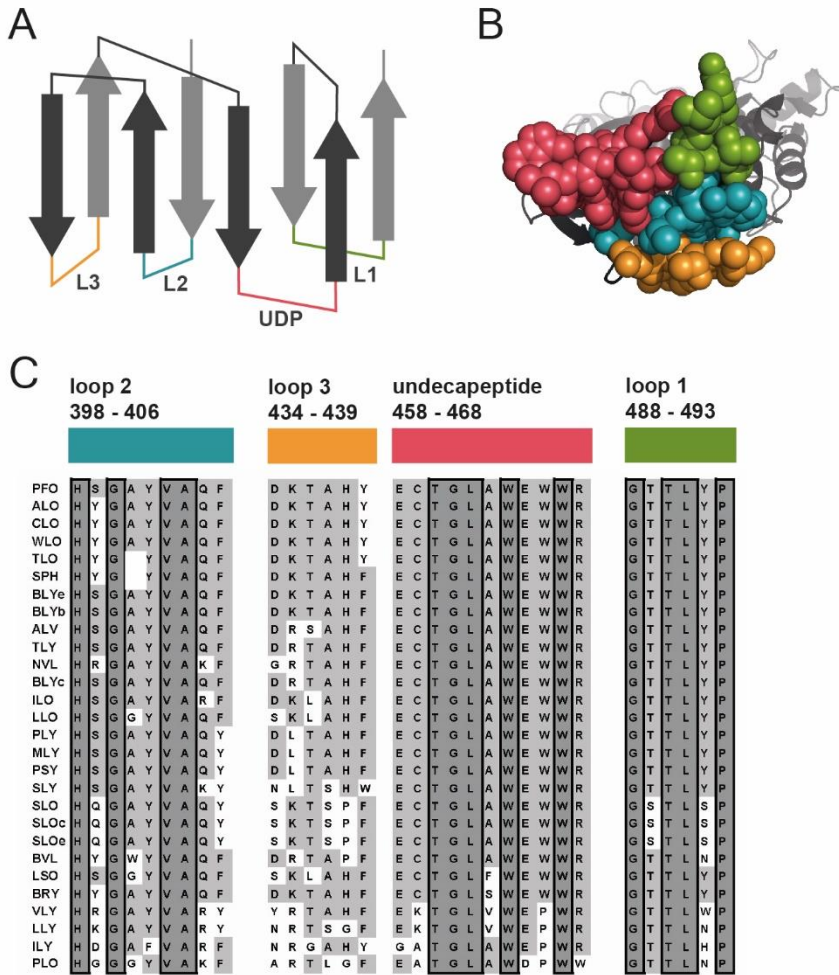
Figure 5. Membrane binding loops in the D4 domain of cholesterol-dependent cytolysins (CDCs). A – schematic representation of membrane-binding D4 domain of CDCs highlighting four loops, L1 (green), L2 (blue), L3 (orange), undecapeptide (UDP) (red); B – four loops in D4 domain are exposed on the tip of CDC monomer visualised in space-fill model of perfringolysin (PDB ID: 1PFO); C – multiple sequence alignment of the loops in D4 domains of different CDC family members highlighting highly conserved motifs in L1, L2 and UDP. Figure adapted from Savinov and Heuck, 2017.

The threshold of cholesterol concentration *in vitro* required for CDC activity is around 30-40 molar per cent of total membrane lipids (Christie et al., 2018). However, the amount of surface-exposed (accessible from solution) cholesterol *in vivo* differs and not necessarily relates to the total amount of cholesterol in the membrane. Phospholipid composition in the membrane was shown to play a significant role in sequestering cholesterol across the membrane (Chakrabarti et al., 2017).

CDCs exploit this necessary component of the membrane by using cholesterol as a receptor. CDCs have an 11-residue cholesterol sensing loop in their D4 domain historically called undecapeptide (UDP). Through UDP and a two-residue Thr-Leu motif located on one of the loops, L1, of the D4 domain, CDCs establish direct contacts with the cholesterol-rich membrane (Farrand et al., 2010) (Figure 5).

To confound matters further, aside from being an integral part of the eukaryotic membrane, cholesterol is a hallmark of lipid rafts, which are transient assemblies of lipids of different physical characteristics (such as sphingomyelins or gangliosides). Cholesterol, with its lipid raft partners, is known to be a major player defining membrane fluidity and bilayer thickness (Schroeder et al., 2010). Therefore, it may be the case that CDCs not only target cholesterol as a cellular receptor but also as a signpost that attracts them to the parts of the membrane they were tailored, by evolution, to insert into.

3.2.2 CD59 is a protein receptor for some CDCs

The only known protein receptor for CDCs so far is human protein CD59, which is a GPI-anchored protein expressed on the majority of the human cell types. Three CDCs, namely intermedilysin (ILY), vaginolysin (VLY) and lectinolysin (LLY) are known to engage human CD59 during pore formation (Giddings et al., 2003; Tabata et al., 2014). Furthermore, several hypothetical CD59-dependent CDCs are predicted to be produced by *Streptococcus tigurinus* and *Streptococcus pseudopneumoniae* (Wade et al., 2015). Ironically, in human cells, CD59 blocks pore-forming action of complement C8, C9 proteins interrupting the formation of membrane attack complex (MAC) and, therefore, inhibiting complement-mediated cell lysis. Thus, CD59 allows the complement to differentiate between self- and non-self cells, but on the other hand, it assists these particular CDCs to find their targets (Davies and Lachmann, 1993; Davies et al., 1989).

The early study of ILY interaction with CD59 showed that ILY binds to the species-specific region of CD59 (Giddings et al., 2004; LaChapelle et al., 2009). For instance, rabbit erythrocytes do not permit ILY pore formation

while the ones from non-human primates do, however, to a 100-fold lesser extent (Nagamune et al., 1996). Moreover, replacement of human-specific region of CD59 with rabbit-specific region resulted in a complete abrogation of ILY pore formation and conferred resistance to rabbit complement-mediated lysis (Giddings et al., 2004; Zhao et al., 1998).

Boyd et al. suggested transitory roles for CD59 and cholesterol during ILY pore formation (Figure 6) (Boyd et al., 2016). Primary ILY interaction with the membrane is thought to be maintained through membrane-attached CD59 proceeding to oligomerisation and early prepore formation. The transition from an early prepore to a late prepore requires the vertical collapse of the prepore structure during which CD59 is released. Hence, cholesterol mediates the transition from a late prepore to a pore. The requirement for ILY to disengage from CD59 was highlighted even earlier by showing that ILY or CD59 mutants that strengthen their interaction resulted in lower ILY cytolytic activity (Wickham et al., 2011).
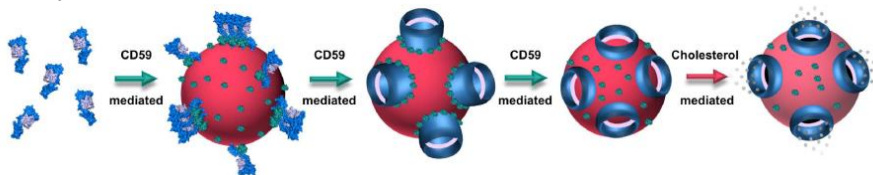
Figure 6. The model for the temporal role of CD59 receptor in the intermedilysin (ILY) pore formation. ILY is coloured in blue and grey; CD59 is coloured in green. The model suggests that CD59 mediates ILY binding to the membrane, sets specific geometry of ILY pore structure and triggers the vertical collapse of the prepore structure but is released in the final step of pore formation which is mediated by membrane-embedded cholesterol. Modified from Boyd et al., 2016.

Crystal structures of monomer-locked ILY and VLY (ILY[ML] and VLY[ML]) in the complex with human CD59 envisioned the interface that is based on the β-sheet extension between D4 domain of a CDC and CD59 (Feil et al., 2012; Johnson et al., 2013; Lawrence et al., 2016). Although it was expected that the mechanism of pore formation would be similar, the interfaces of ILY[ML]-CD59 and VLY[ML]-CD59 complexes were shown to overlap only partly (Lawrence et al., 2016). Moreover, as CD59 is necessary for ILY but conditional for VLY, this highlights the possibility that CD59 plays a different role during the action of these toxins.

3.2.3 Glycan receptors for CDCs

Novel insights in CDC-membrane interfaces were brought into light when CDCs were observed to bind to glycans with high affinity (Shewell et al.,

2014). Screening PLY and SLO using glycan arrays revealed a list of potential glycan receptors. Moreover, their ability to inhibit CDC haemolytic action was demonstrated. The haemolytic activity of PLY on human red blood cells was shown to be dependent on Lewis histo-blood group sialyl LewisX (sLeX) glycolipids. Preincubating PLY with sLeX significantly reduced the haemolytic activity of PLY by binding to the D4 domain and competing with the sLeXs on the surface of RBCs. Similarly, SLO was shown to bind to a list of glycans bearing terminal galactosyl, N-acetylglucosaminyl, N-acetylgalactosaminyl, glucosyl, fucosyl, sialyl structures. Preincubation with lacto-N-neotetraose had the most robust reduction in SLO binding to RBCs and interference with haemolysis.

A single known CDC, lectinolysin produced by *Streptococcus mitis*, contains an additional lectin binding domain at its N-terminal end (Farrand et al., 2008; Feil et al., 2012). The lectin domain of LLY is composed of F-type lectin fold of two β-sheets interconnected by five hypervariable loops (CDRs, complementarity-determining regions) forming so-called jellyroll fold on one end of this domain. F-type lectins are known to bind fucosylated structures; therefore, as predicted, the potential of LLY to bind difucosylated Lewis y and b antigens was shown (Feil et al., 2012). F-type lectins were thoroughly reviewed by Vasta et al. that are widely distributed from viruses to vertebrates (Vasta et al., 2017). F-type lectins play a crucial role in innate immunity (in both vertebrates and invertebrates) where they recognise surface-exposed glycans of microbial pathogens. Thus, the self-/nonself-recognition is thought to be a characteristic of this type of lectins.

3.3   The structure of CDCs

3.3.1 Monomer structure of CDCs

A list of monomeric CDC structures has been solved to date (Figure 7, A). A general structure of a CDC can be divided into two parts, MACPF domain and Ig-like domain (Figure 7, B). Aside from this, a single CDC, lectinolysin (LLY) from *Streptococcus mitis* is known to contain an additional lectin domain at the N-terminal end (called D0) (Farrand et al., 2008). The core of a CDC is the MACPF domain, which is directly responsible for the pore formation. Historically, the MACPF domain in CDCs was segmented into three domains, creatively named domain 1 (D1), domain 2 (D2) and domain 3 (D3) (Figure 4). D3 domain maintains the monomer-monomer interface and provides α-helices (TMHs, transmembrane helices) to form transmembrane β-hairpins (Figure 4).

A – a list of solved monomeric CDC structures.

	PDB ID	Resolution (Å)	Reference
Perfringolysin O (PFO)	1PFO	2.2	Rossjohn et al., 1997
	1M3J	3.0	Rossjohn et al., 2007
	1IMEI	2.9	Rossjohn et al., 2007
Intermedilysin (ILY)	1S3R	2.6	Polekhina et al., 2005
	4BIK	3.5	Johnson et al., 2013
	5IMW	2.89	Lawrence et al., 2016
	5IMT	2.7	Lawrence et al., 2016
Anthrolysin (ALO)	3CQF	3.1	Bourdeau et al., 2009
Suilysin (SLY)	3HVN	2.85	Xu et al., 2010
Streptolysin O (SLO)	4HSC	2.1	Feil et al., 2014
Listeriolysin O (LLO)	4CDB	2.15	Koster et al., 2014
Pneumolysin (PLY)	4QQA	2.8	Park et al., 2016
	4ZGH	2.9	Lawrence et al., 2015
	5CR6	1.98	Marshall et al., 2015
	5AOD	2.4	van Pee et al., 2016
Vaginolysin (VLY)	5IMY	2.4	Lawrence et al., 2016

Figure 7. Monomeric crystal structures of cholesterol-dependent cytolysins (CDCs). A – a list of solved monomeric CDC structures. B – the structure of perfringolysin (PDB ID: 1PFO). Membrane-attack complex/perforin (MACPF) fold comprising D1, D2 and D3 domains are highlighted in black, and immunoglobulin-like (Ig-like) fold comprises D4 domain, depicted in green.

In addition to highly interconnected MACPF domain, a discrete Ig-like domain, named domain 4 (D4), is located at the C-terminal end of the protein. D4 is responsible for membrane recognition and binding (Figure 7, B).

Structurally, proteins in the CDC family are highly conserved that is reflected in the above-mentioned sequence identity of around 40 % across the whole family. The architecture of all of the solved CDC structures are as follows: D1 contains a seven-stranded β-sheet surrounded by α-helices. D2 harbours long β-strands that link D1 and D3 with D4 (Figure 4).

D3 is a central domain composed of a twisted β-sheet surrounded by α-helices. The twisted five-stranded β-sheet works for a β-sheet extension during monomer-monomer interactions where β4-strand from one monomer interacts with a β1-strand from the neighbouring monomer (Figure 4) (Dowd and Tweten, 2012; Ramachandran et al., 2004). Moreover, a motif of two glycines is highly conserved throughout the whole MACPF/CDC superfamily and is thought to act as a hinge around which the rotation occurs during oligomerisation (Figure 4) (Ramachandran et al., 2004). As a donor for

transmembrane insertion, D3 contains two bundles of short α-helices (TMH1 and TMH2), which refold into β-hairpins and upon pore formation span the membrane (Shatursky et al., 1999; Shepard et al., 1998).

D4 and D0 domains share a structure of β-sandwich (layered β-sheets) with the functionally important loops interconnecting β-strands at the tip of the domains that, respectively, are responsible for cholesterol-rich membrane recognition or binding to glycans. D4 contains four loops, namely loop 1 (L1), loop 2 (L2), loop 3 (L3) and UDP.

3.3.2 Prepore and pore structures of CDCs

An intermediate oligomer during CDC pore formation is called a prepore. A prepore is an oligomer, which has not perforated the membrane yet. Interestingly, as opposed to α-PFTs, CDCs are thought to maintain a high number of prepores. This is likely because CDC prepores and pores contain 20-60 monomers, whereas α-PFTs rarely contain more than 10. Therefore it takes much longer for the complete individual pore of CDCs to be formed. However, CDCs do not necessarily need to form a full-ring structure to perforate the membrane. So-called arc structures are thought to be appropriate to perforate the membrane more times with less amount of toxin (Figure 8) (Gilbert and Sonnen, 2016; Gilbert et al., 2014; Leung et al., 2014; Ruan et al., 2016; Sonnen et al., 2014). Interestingly, the ability to insert into the membrane as an arc strictly depends on the membrane characteristics, e.g. fluidity, as the more fluid membrane can accommodate arc-shaped pores more easily (Rojko and Anderluh, 2015).

Therefore, CDC pores do not share well-defined structures as the oligomers are heterogeneous in size (Shepard et al., 1998; Shatursky et al., 1999). The heterogeneity may not be physiologically relevant. However, it determines their structure challenging.
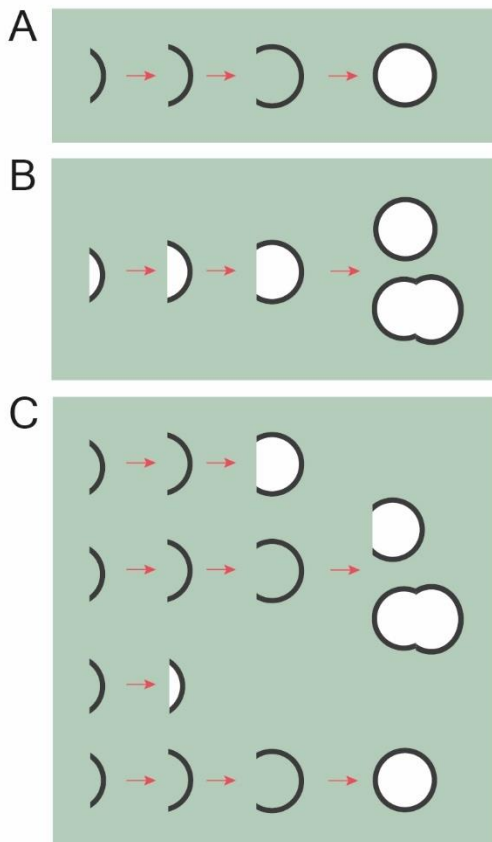
Figure 8. Schematic representation of three different proposed models for pore formation by CDCs. A – a model suggesting that only complete ring-shaped oligomers can insert into the membrane and perforate it and all incomplete ring-shaped oligomers are prepores (Heuck et al., 2003); B – a model proposing that the nascent CDC oligomer is membrane-inserted and is able to grow and fuse with other oligomers. This model neglects the existence of prepore structures, however (Palmer et al., 1998). C – a hybrid model suggesting that either a complete or incomplete ring-shaped oligomer can exist in prepore or membrane-inserted pore structures and incomplete membrane-inserted oligomers can fuse enlarging the pore size. Based on Gilbert, 2005.

Advances in cryo-electron microscopy allowed a high-resolution visualisation of the prepore and pore structures. In 2017 Pee et al. solved a 4.5 Å cryoEM structure of the ~2.2 MDa pore complex of PLY (van Pee et al., 2017). The giant pore structure contained 168-stranded β-barrel that adopted two β-hairpins from every monomer, 42 monomers in total. Moreover, the β-barrel was stabilised by electrostatic interactions between the β-barrel and the internal α-barrel. Using cryo-electron tomography (cryo-ET), the structure of a prepore was determined. It helped to get the finer glimpse into the mechanism of membrane perforation (van Pee et al., 2017).
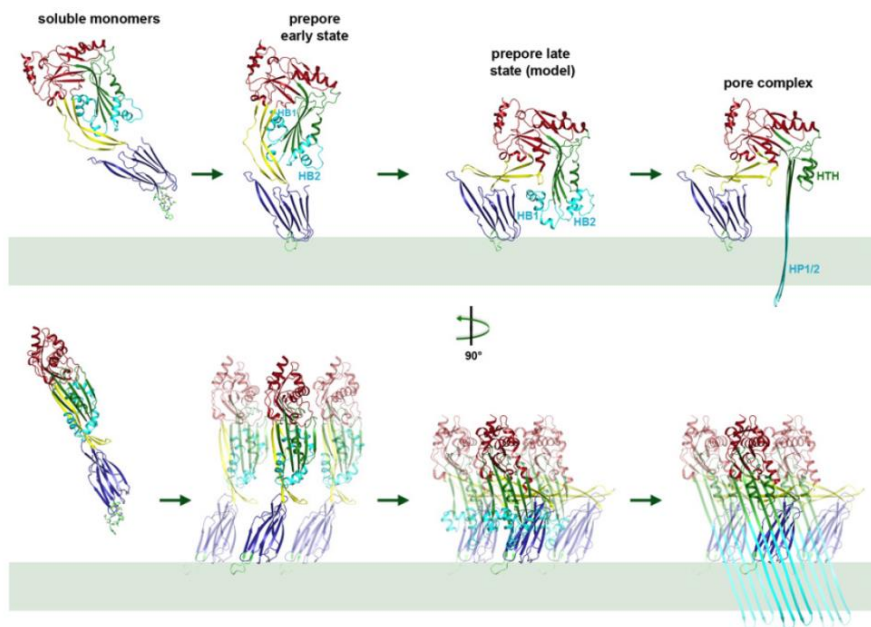
Figure 9. The model for pneumolysin (PLY) pore formation. Conformational changes taking place in the PLY molecule during the pore formation are visualised in the above panel from the side view of the individual monomer and in the bottom panel from the pore-centred view. A 90° rotation of D2 domain moves D1 and D3 domains (comprising transmembrane helices, alternatively named as helical bundles, HB1/2) towards the membrane in the late prepore. Final membrane-inserted pore structure comprises 168-strands, 260 Å β-barrel (van Pee et al., 2017).

The prepore stage can be subdivided into early prepore and late prepore stages. Although at both stages, prepores do not span the membrane, the overall structure of the oligomers differs greatly (van Pee et al., 2017). The early prepore consists of assembled monomers in a similar conformation as monomers in the crystal structures, sitting side by side on the plane of the membrane. This became apparent both from the crystal structures of soluble monomers as well as linear assemblies of monomers in the crystals (Lawrence et al., 2015; Marshall et al., 2015; Pee et al., 2016; van Pee et al., 2017). Subsequent conformational movement serves to bring transmembrane domain (D3), which are farther away, into the proximity of the membrane. Late prepore is an oligomer, which has already vertically collapsed (Figure 9), as it is characterised by the reduction of the oligomer height (Czajkowsky et al., 2004; van Pee et al., 2017; Ramachandran et al., 2005; Tilley and Orlova, 2005). Cryo-ET data provided evidence of a D2 rigid body rotation from its vertical position by 90° to an orientation parallel to the membrane plane (van

Pee et al., 2017). Nonetheless, at the point of late prepore, the membrane is still intact. Late prepore to pore transition requires the unfurling of α-helices (TMH1 and TMH2 or, alternatively, HB1 and HB2) and refolding into β-hairpins that can span the membrane as a β-barrel.

4 *Gardnerella vaginalis* and its role in the pathogenesis of bacterial vaginosis

The bacterium that was to be *Gardnerella vaginalis* was first identified by Leopold in 1953 (Leopold, 1953). Later on, in 1955, it was named as *Haemophilus vaginalis* by Gardner and Dukes, and it was finally identified as the causal agent of the until then nonspecified aetiology of vaginitis (vaginal infection/inflammation) (Gardner and Dukes, 1955). Vaginal squamous epithelial cells that were densely covered with *H. vaginalis*, because of their unique appearance, were called clue cells. These clue cells gave (and still gives) the clue of the presence of vaginal infection.

Later on, in 1980, due to the lack of similarity to any described genus, Greenwood and Picket assigned *H. vaginalis* to a new genus, *Gardnerella*, and renamed the bacterium to *Gardnerella vaginalis* in the honour of Gardner, who was one of the first people to realise its importance (Greenwood and Pickett, 1980).

G. vaginalis has an unusual cell wall with a thin peptidoglycan layer. Thus by current definitions should be Gram-positive, but upon Gram staining, it can appear Gram-negative and is therefore described as Gram-variable (Verstraelen et al., 2010). *G. vaginalis* is rod-shaped bacterium of 0.5 µm by 1.0 to 1.5 µm, non-encapsulated, nonmotile, and not observed to form filaments.

Characteristics and clinical considerations of *G. vaginalis* were thoroughly reviewed long ago by Catlin et al. (Catlin, 1992). *G. vaginalis* is classified as β-haemolytic that means that when grown on blood agar, it completely lyses surrounding red blood cells. It is worth to note that haemolysis was observed on human, horse or rabbit but not sheep erythrocytes. *G. vaginalis* is a facultative anaerobe, and its growth and induced haemolysis are promoted under anaerobic conditions. *G. vaginalis* is closely related to, or even causative agent, of vaginal microflora imbalance, called bacterial vaginosis (BV).

The most widely spread and still used criteria to diagnose BV is Amsel criteria of vaginal discharge (Amsel et al., 1983) and Nugent score of vaginal swabs (Nugent et al., 1991). For Amsel criteria, the presence of at least three characteristics out of the following four confirms the state of BV: non-viscous

consistency, elevated pH, fishy trimethylamine odour after treatment with potassium hydroxide, the presence of clue cells, reduced levels of *Lactobacillus* species and increased levels of *G. vaginalis* or other anaerobe species. For Nugent score, Gram staining-based evaluation of present bacterial species is evaluated.

What constitutes a healthy or imbalanced vaginal microbiota, in general, is still unclear as the composition of the urogenital microbiota and, most importantly, its dynamics over time is not well understood (Onderdonk et al., 2016; Schellenberg et al., 2017). Dynamic microbiota of the urogenital tract can be classified as *Lactobacillus* dominant (normal/healthy), *G. vaginalis* dominant or *G. vaginalis* codominant with other anaerobic bacteria (prone to BV). The main hint of BV seems to be the disappearance of *Lactobacillus* (*L. crispatus*, *L. jensenii*) and the ability of commonly subdominant anaerobic species to form biofilms. However, the interrelationship of microbiota and the driving forces that allow anaerobic species to attain their dominance remain under discussion. One point of view suggests that *Lactobacillus* and *G. vaginalis* are engaged in a constant struggle for their dominance in vaginal microbiota. As *Lactobacillus* produces hydrogen peroxide, lactic acid and other bacteriocins, *G. vaginalis* with the help of other anaerobic bacterial species fight to access the mucosal surface and establish biofilm phenotype. *G. vaginalis* may be the leading cause in changing the conditions required for the successful growth of anaerobic species such as *Atopobium*, *Prevotella* and others (Schellenberg et al., 2017). Moreover, the synergy between *G. vaginalis* and *Prevotella* was observed on a nutritional basis (ammonia production by *Prevotella bivia* and consumption of it by *G. vaginalis*) as well as the promotion of biofilm formation (Machado and Cerca, 2015; Pybus and Onderdonk, 1997). Biofilm formation is suggested to be a successful strategy to overcome natural defences from the opposing microbiota species and the antibiotic treatment (Hardy et al., 2017).

Aside from this, BV is not necessarily related to pathogenic outcome and can easily be unrecognised as it may not induce any apparent symptoms. The switch into the recognisable state has not been defined yet (Ma et al., 2012). It may not only be restricted to the general composition of vaginal microflora but rely on particular subspecies that are featured by specific levels of virulence factors (Janulaitiene et al., 2017, 2018; Schellenberg et al., 2016).

One of the challenges that need to be overcome in the study of urogenital tract microbiota is the establishment of appropriate and representative *in vitro* and *in vivo* models to study dynamic interactions between different species (Ma et al., 2012; Onderdonk et al., 2016; Schellenberg et al., 2017). As it

stands, the most direct ways to modulate the desired processes remain inaccessible.

Nevertheless, *G. vaginalis* can be considered a hallmark of BV state as it is found in all patients experiencing BV (Schellenberg et al., 2017). The phenotypic properties of *G. vaginalis* are extraordinarily variable, and extensive attempts are being made to divide the bacterium into subtypes, which might help to explain its role in health or disease. Vaginal microbiota was shown to contain a mixed community of *G. vaginalis* strains that vary in their phenotypes and virulence potential (Albert et al., 2015; Balashov et al., 2014; Janulaitiene et al., 2018; Schellenberg et al., 2017). Four groups of *G. vaginalis* subtypes were identified by different criteria, including variability of *cpn60* gene for chaperonin (Hill et al., 2005; Jayaprakash et al., 2012) and a whole genome-based typing (Ahmed et al., 2012; Schellenberg et al., 2016). However, the phenotypic properties of *G. vaginalis* subtypes cannot be inferred from genotyping alone. So far it has been observed that all members of group B (clade 2) and some of group C (clade 1) share sialidase activity (Lewis et al., 2013; Schellenberg et al., 2016), whereas the members of group A (clade 4) are unified by lipase activity (Jayaprakash et al., 2012). Moreover, group A (clade 4) was found the most homogeneous compared with group C (clade 1) and group B (clade 2) featured by low secretion of sialidase and VLY (Janulaitiene et al., 2018). However, more investigation is needed here to prove this relationship and identify the other possible markers of subspecies.

The most discussed and studied virulence factors of *G. vaginalis* are vaginolysin and sialidase, which are suggested to play a role in biofilm formation, mucosal access and immune modulation (Schellenberg et al., 2017). Sialidase is produced in high amounts by various BV-associated bacteria and, as expected, is not observed in high amounts in the non-BV state (Briselden et al., 1992). Moreover, sialidase is linked to the pathogenicity by the degradation of mucosal sialoglycans and complex N-glycans of secretory IgA (Lewis et al., 2012). Women's reproductive tract is known to be rich in sialoglycoproteins that shield the epithelial cells and restricts the direct access to them. Aside from the benefit that the pathogen might gain by approaching the epithelial cells, sialidase was shown to promote bacterial growth and biofilm formation (Lewis and Lewis, 2012).

4.1   Vaginolysin from *Gardnerella vaginalis*

Vaginolysin (VLY), the object of this thesis, is a member of MACPF/CDC protein superfamily produced by the bacterium *Gardnerella vaginalis*. VLY

is one of the most probable virulence factors of *G. vaginalis*, as discussed above. VLY contains a signal peptide at its N-terminus, which is responsible for the secretion of the cytolysin out of the bacterium.

Even though it was not demonstrated *in vivo*, the link between vaginolysin and BV state is believed to be plausible by analogy with other CDCs playing a critical role in the pathogenesis of microorganisms that produce them (e.g. PLY from *Streptococcus pneumoniae*) as described above. VLY concentration was shown to be higher in women whose vaginal microbiota lacks dominant *Lactobacillus* species (Nowak et al., 2018). Moreover, an increase in anti-VLY IgA response was observed in BV state together with higher levels of interleukin-1β, thus, highlighting the mucosal immune response to the presence of VLY (Cauci et al., 1996, 2002). However, despite extensive attempts to study mucosal immune responses, a consensus has not been reached, partly due to the lack of animal models (Mitchel and Marrazzo, 2014).

Early studies on VLY and its haemolytic activity demonstrated the tropism of VLY activity towards human erythrocytes. However, VLY was shown to display haemolytic, albeit decreased, activity on erythrocytes of other species as well (Cauci et al., 1993). When tested on erythrocytes from different species, concentration of VLY needed to lyse 50 % of the cells was increased in the following proportions when compared to human erythrocytes: cat (11-fold), pig (31-fold), cow (67-fold), dog (71-fold), rabbit (143-fold), horse (167-fold), sheep (>1000-fold). A possible way to explain these differences was suggested to rely on the affinity of VLY to certain cell membrane components be it lipids, glycans or proteins. Hence, the discovery of its human protein receptor CD59 helped to explain the tropism towards human cells (Gelber et al., 2008).

The role of VLY in the course of *G. vaginalis* infection is not clearly understood, and one of the limitations for understanding is the lack of abilities to modify the genome of *G. vaginalis* together with above-mentioned animal models for studying the vaginal state of BV.

5   The importance of pore-forming toxins

As antibiotic resistance becomes more widespread, alternative options for treatment or disease prevention are becoming more desirable. Because pore-forming toxins constitute an essential part in the pathogenesis of many bacterial diseases, they are an important object to be studied. For example, PLY is the primary driver behind tissue invasion and colonisation (Zafar et al., 2017). Thus, by understanding mechanisms of pore formation and the role

of toxins in pathogenesis or life cycles of microorganisms, we stand to benefit our medical options. This is especially true for bacterial diseases, which do not pose a deadly risk. Furthermore, secreted toxins can be used as biomarkers to diagnose certain bacterial infections.

Secondly, pore-forming proteins have valuable traits that can be exploited as tools. As they target specific membrane components to initiate pore formation, we can exploit monomer-locked versions of toxins to label various non-protein components of the membrane. A prime example of this is perfringolysin O (PFO), which, like all CDCs, binds to membrane cholesterol (Johnson et al., 2017a).

Another application is to use toxins as delivery agents for various compounds. For example, many of the biologicals, including siRNAs, DNA or proteins are uptaken by cells via endocytosis pathway. To release them from endosomes, the cell can use membrane pores (Varkouhi et al., 2011).

Another interesting and unusual application was reported for ILY, which is a CDC strictly dependent on human protein CD59. Using genetic engineering, several groups have made mice expressing human protein CD59 under tissue-specific promoters. Upon administration of intravenous ILY, the ablation of specific cell populations expressing CD59 is induced. This was shown as a hugely powerful tool to study neuronal populations and other populations of cells by removing some of them (Feng et al., 2016; Hu et al., 2007).

Lastly, pore-forming toxins and pores they form are used in the third generation sequencing approach called nanopore sequencing, where DNA sequences are electrophoretically passed through the pores of, e.g. α-hemolysin or *Mycobacterium smegmatis* porin A (Derrington et al., 2010). Reading out changes in conductivity as different nucleotides of the DNA sequence passes through the pore allows for sequencing. Such approaches are very appealing due to avoiding amplification of DNA before sequencing. Furthermore, it is foreseen that nanopores could also be used for protein sequencing if proper ways to unfold them were developed (Nivala et al., 2013).

Aside from easily listable benefits we derive from studying pore-forming toxins, it is important to add that like with all fundamental research, it is impossible to foretell whence the next advance will come from and where the characterisation of the next pore-forming toxin may lead us.

METHODS

1   Generation and purification of recombinant proteins

1.1   VLY and VLY mutants

Recombinant N-terminally-6xHis-tagged VLY lacking the putative signal sequence (1-31 aa) was cloned into pUC57(+) (Thermo Fisher Scientific) and pET28a(+) (Novagen Merck Millipore) plasmid vectors previously in our laboratory (Zvirbliene et al., 2010).

VLY was mutagenised using a site-directed mutagenesis. The mutations were introduced by PCR amplification of pUC57-VLY plasmid using primers with BpiI restriction endonuclease sites, one of which had a mismatched codon for the amino acid substitution. PCR products were digested with BpiI restriction endonuclease, and the DNA fragment was ligated using T7 DNA ligase. *E.coli* DH10B strain was transformed with recircularised plasmids encoding mutant VLY proteins, and the correct gene sequences were confirmed by DNA sequencing. The genes were transferred to pET28a(+) vector via NdeI and BamHI restriction endonuclease sites followed by the transformation of *E. coli* strains that were used for the expression of VLY variants.

VLY and all the VLY mutants were expressed in *E. coli* Tuner (DE3) or BL21 (DE3) strain. The overnight culture was diluted 30 times into fresh LB media and incubated at 37 °C with shaking at 220 rpm until OD_{600nm} reached 0.6-0.8. Induction was carried out by adding 0.1 mM (for *E. coli* Tuner (DE3)) or 1 mM (for *E. coli* BL21 (DE3)) isopropyl β-D-1-thiogalactopyranoside and incubating cells at 26 °C with shaking at 220 rpm for 4.5 hours. Harvested biomass was resuspended in lysis buffer (50 mM Tris-HCl (pH 7.5 at 4 °C), 500 mM, NaCl, 50 mM imidazole) into which PMSF protease inhibitor (1 mM final concentration) was added, and the sample was sonicated. The cleared lysate was purified using HisTrap FF and HisTrap SP columns (GE Healthcare) followed by the size-exclusion chromatography using Superdex 75 16/60 column in 20 mM sodium acetate (pH 5.5 at 25 °C) (or 20 mM MES (pH 5.5 at 25 °C)) 100 mM ammonium sulphate buffer. VLY and its mutants were stored in 20 mM sodium acetate (pH 5.5 at 25 °C) (or 20 mM MES (pH 5.5 at 25 °C)), 100 mM ammonium sulphate buffer supplemented with 0.01 % Tween-80.

For the experiments with the liposomes containing 18:1 DGS-NTA(Ni) (1,2-dioleoyl-sn-glycero-3-[(N-(5-amino-1-carboxypentyl)iminodiacetic acid)succinyl] (nickel salt)) lipids, His-tag was removed from the purified

VLY proteins to avoid undesired VLY binding to the liposomes via the 6xHis-tag. The 6xHis-tag was cleaved by adding thrombin protease and incubating overnight at 4 °C while dialysing against 20 mM Tris-HCl (pH 8.4 at 4 °C), 150 mM NaCl, 2.5 mM CaCl$_2$ buffer. After 6xHis-tag cleavage, the protein was loaded on HisTrap HP column. The column was washed with 25mM Tris-HCl (pH 7.5 at 4 °C), 200mM NaCl buffer. Cleaved VLY was eluted using imidazole gradient (50 mM Tris-HCl (pH 7.5 at 4 °C), 500 mM NaCl, 0-100 mM imidazole). Cleaved VLY eluted at a significantly lower concentration of imidazole than the construct bearing 6xHis-tag. 6xHis-tag cleavage was confirmed using Western blot by the analysis of the samples before and after cleavage probed with primary mouse anti-6xHis (HIS.H8 clone, Cat. No. MA121315, Thermo Fisher Scientific) antibodies and secondary goat anti-mouse IgG HRP-labelled antibodies (Bio-Rad).

1.2 ILY

The gene for ILY was amplified from *Streptococcus intermedius* isolate 14654 (a kind gift from Lithuanian National Public Health Surveillance Laboratory, Vilnius, Lithuania) and sequenced previously in our laboratory. The gene encoding ILY lacking the putative signal sequence (1-33 amino acids) was cloned into pET28(+) vector (Novagen Merck Millipore) fusing the gene with N-terminal 6xHis-tag. The generated plasmid was subsequently used for *E. coli* BL21(DE3) transformation. His-tagged ILY was expressed and purified as described for VLY in *Methods* 1.1 section. Purified protein was stored in 20 mM sodium acetate (pH 5.5 25 °C), 100 mM ammonium sulphate supplemented with 0.01 % Tween-80.

1.3 PLY

The gene for PLY was amplified from *Streptococcus pneumoniae* isolate 7170 (a kind gift from Lithuanian National Public Health Surveillance Laboratory, Vilnius, Lithuania) and sequenced previously in our laboratory. The gene encoding PLY was cloned into pET28(+) vector (Novagen Merck Millipore) fusing the gene with N-terminal 6xHis-tag. The generated plasmid was subsequently used for *E. coli* BL21(DE3) transformation. 6xHis-tagged PLY was expressed and purified as described for VLY in *Methods* 1.1 section. Purified protein was stored in 20 mM HEPES (pH 7.5 at 25 °C), 200 mM NaCl, 0.01 Tween-80 buffer.

1.4   CD59 and its variants

Human protein CD59 was expressed in mammalian HEK293T cells (ATCC Cat. No. CRL-321) as a soluble protein secreted into the media as it lacked the sequence coding for the GPI-anchor attachment. In order to purify the protein, its gene was fused with a 6xHis-tag at C-terminal end. C-terminal 6xHis-tag was used to attach the protein to the surface of DGS-NTA(Ni) lipids-containing liposomes.

The coding sequence for human protein CD59 was amplified from the pFUSE-CD59 construct (described in *Methods* 2 section) and cloned into a mammalian cell expression vector pHLsec (Aricescu et al., 2006) via AgeI and KpnI restriction endonuclease sites fusing the gene with secretion signal sequence at the N-terminal end and 6xHis-tag at the C-terminal end. The internal N-linked glycosylation site was disrupted by Asn-16 substitution to Gln. HEK293T cells were transiently transfected with pHLsec-CD59 plasmid. An artificial N-linked glycosylation site was introduced downstream of the *CD59* gene at the junction with KpnI restriction endonuclease site as it improved the amount of media-secreted CD59. N-linked glycosylation was subsequently removed during the protein purification. Protein expression was carried out in 12 roller bottles (2125 cm^2 growth area) by transfecting the cells with 0.5 mg of plasmid and 1 mg of polyethylenimine per roller bottle followed by the incubation at 37 °C for five days. After the media was collected, it was cleared by centrifugation at 5000 g for 20 min, filtered through 0.22 µm filter membrane and buffer-exchanged into 20 mM HEPES (pH 7.5 at 25 °C), 300 mM NaCl 5 mM imidazole buffer using QuixStand system. All purification steps were carried out at RT. The media was loaded onto HisTrap HP column (GE Healthcare), which was subsequently washed with 20 mM HEPES (pH 7.5 at 25 °C), 300 mM NaCl, 5 mM imidazole. The protein was eluted by imidazole gradient (20 mM HEPES (pH 7.5 at 25 °C), 300 mM NaCl 5-500 mM imidazole). Eluted protein was treated with PNGase F (Cat. No. P0704S, New England BioLabs) at 37 °C for 72 h to remove artificially introduced N-linked glycan. The removal of glycans was proved by SDS-PAGE. After PNGase F treatment, the protein was further fractionated using size-exclusion chromatography Superdex S75 16/60 column (GE Healthcare) in 20 mM HEPES (pH 7.5 at 25 °C), 150 mM NaCl buffer.

Table 1. Overlapping oligonucleotides for linker insertion at the N-terminal end of the CD59-encoding gene.

	Forward oligonucleotide	Reverse oligonucleotide
2n linker	5'-CATGGCCGAAGCT GCAGCCAAAGAGGCC GCTGCAAAGGCT-3'	5'-CGGCTTCGACGTCG GTTTCTCCGGCGACGT TTCCGACATGGTAC-3'
4n linker	5'-CATGGCCGAAGCT GCAGCCAAAGAGGCC GCAGCTAAGGAGGCC GCTGCAAAGGCT-3'	5'-CGGCTTCGACGTCG GTTTCTCCGGCGTCGA TTCCTCCGGCGACGTT TCCGAGTAC-3'

For CD59 constructs bearing linkers the rigid helical linkers of A(EAAAK)$_2$A (CD59-2n construct) or A(EAAAK)$_4$ALEA(EAAAK)$_4$A (CD59-4n construct) at the C-terminus between the gene for CD59 and 6xHis-tag were introduced. The linkers were introduced by a pair of oligonucleotides, which were annealed, extended and cloned into the plasmid through KpnI restriction endonuclease cutting site (Table 1). Expression and purification protocol applied for these CD59 variants was the same as described above for CD59.

2 Generation of CHO cell line expressing human CD59

To characterise VLY tropism to human CD59-bearing cells, we generated a set of stable cell lines by transfecting non-human origin CHO cells with a plasmid encoding GPI-anchored human CD59. As the protocol was based on random integration into the genome, different clones expressed different levels of surface-exposed CD59.

The plasmid encoding GPI-anchored human CD59 was constructed in our laboratory previously by Dr Milda Plečkaitytė. pFUSE (InvivoGen) vector bearing zeocin-resistance gene was used into which a synthetic gene for human CD59 (GenScript) comprising 1-76 amino acids of CD59 together with GPI-anchoring encoding sequence at the C-terminal end was inserted. The N-linked glycosylation site was disrupted by the single amino acid substitution of Asn-18 into Gln. This mutation was previously shown not to affect the activity of CD59 (Yu et al., 1997). During this work, CHO cells were transfected, and surface-exposed CD59 expression was assessed by labelling it with FITC conjugated anti-CD59 antibodies (Cat. No. 555763, BD Pharmingen) followed by the flow-cytometric analysis.

CHO cells (ECACC Cat. No. 8505030) were cultivated in DMEM:Ham's F-12 (1:1) media supplemented with 10 % heat-inactivated fetal bovine serum (FBS). The transfection was carried out using TurboFect reagent (Thermo

Fisher Scientific). For the transfected cell selection, the cell growth media was supplemented with 250 µg/ml zeocin (InvivoGen). After selection, the cells were cloned, and the clones were screened by labelling intact cells with FITC-conjugated anti- CD59 antibodies and analysing using flow cytometry. The level of surface-exposed CD59 was evaluated by a normalised median of fluorescence intensity (nMFI) in the FITC channel. MFI was normalised by dividing the MFI value of the anti-CD59 antibody-labelled cells by the averaged MFI value of the isotype control (Cat. No. 555573, BD Pharmingen). Each experiment was repeated three times. The value of nMFI, together with standard deviation, was calculated for each clone. Four clones (CHO-CD59[4A9], CHO-CD59[4A11], CHO-CD59[3E9], CHO-CD59[4F1]) characteristic of an increasing level of CD59 expression were selected for further experiments (*Methods* 4, 6 sections).

3 Haemolytic assay

The haemolytic assay was used as one of the approaches for evaluating the cytolytic activity of CDCs (Cauci et al., 1993). It is based on the ability of CDCs to lyse human erythrocytes and release haemoglobin, which can be measured spectrophotometrically.

Five ml of blood from a volunteer was collected, and the erythrocytes were washed to remove the blood plasma using sterile PBS by centrifugation at 200 RCF at RT. Erythrocytes were suspended in 950 µl PBS for each reaction, which was carried out in 1.5 ml microtubes. The dilution of erythrocyte suspension was chosen to get an absorbtion at 415 nm (A_{415nm}) equal to 2.5-2.7 when lysed by deionised H_2O representing maximal lysis of erythrocytes. CDCs were serially diluted in PBS, 50 µl of diluted CDCs were used for an individual reaction. Upon erythrocyte treatment with CDCs, the tubes were incubated for 15 min at RT, followed by centrifugation for 5 min at 200 RCF at RT. One-hundred µl of the supernatant of each data point was transferred to a 96-well plate, and A_{415nm} was measured. PBS without CDCs was used as a negative lysis control; the A_{415nm} value of it was subtracted from each data point as a background. The percentage of maximal lysis (positive control acquired with deionised H_2O) was evaluated for each data point. Erythrocyte lysis versus CDC concentration was fitted with a four-parameter dose-response curve using GraphPad Prism. Each experiment was repeated three times. HD50 value that represented the CDC concentration inducing half-maximal erythrocyte lysis, for each data set was calculated together with standard deviation.

4   Cell proliferation MTS assay

MTS assay was used to measure the effect of CDCs on cell proliferation as opposed to their cytolytic activity. The assay was based on MTS (3-(4,5-dimethylthiazol-2-yl)-5-(3-carboxymethoxyphenyl)-2-(4-sulfophenyl)-2H-tetrazolium) compound that is reduced by NAD(P)H-dependent dehydrogenases in metabolically active cells generating the soluble coloured formazan product.

Adherent HEK293 (human embryonic kidney) (ATCC Cat. No. CCL-2), CHO (Chinese hamster ovary) (ECACC Cat. No. 8505030) and CHO-CD59 (*Methods* 2 section) cell lines were used in the MTS assay. HEK293 cells were cultivated in DMEM media supplemented with 10 % heat-inactivated FBS. CHO cells were cultivated in DMEM:Ham's F12 media (1:1) supplemented with 10 % heat-inactivated FBS. CHO-CD59 cells were cultivated in DMEM:Ham's F12 media (1:1) supplemented with 10 % heat-inactivated FBS and 250 μg/ml zeocin. The cells were cultivated in 96-well plates at 37 °C 5 % CO_2 to the confluence of approximately 70 %. The cell monolayer was washed twice with serum-free DMEM. Recombinant CDCs (VLY, PLY, ILY) were serially diluted in serum-free DMEM in the range of 0.03 to 200 nM. 100 μl of each CDC dilution was added to the wells with the cells. Reaction mixture without CDCs was used as a negative control of lysis. The plates were incubated for 1 h at 37 °C and 5 % CO_2. Twenty μl of MTS reagent (Promega) was added to the wells and incubated for 4 h at 37 °C 5 % CO_2. The absorbance at 630 nm and 490 nm wavelengths was measured. A_{630nm} values were subtracted from A_{490nm}. The wells with cells untreated with CDCs were used as a negative control of lysis. Percentage of maximal lysis (positive control of lysis acquired from the wells without cells) was evaluated for each data point. The cell lysis versus CDC concentration was fitted with a four-parameter dose-response curve using GraphPad Prism. Each experiment was repeated three times. EC50 value that represented the CDC concentration inducing half-maximal cell lysis was calculated for each data set together with standard deviation. For better visualisation of the different effect of CDCs on CHO and HEK293 (or CHO-CD59) cells the ratios of EC50 values for CHO and HEK293 (or each clone of CHO-CD59) cells were calculated and the variance of the ratios was evaluated by 95 % confidence intervals.

5   Construction of the homology-based VLY structural model

As the crystal structure of VLY was not known at the time of the study, we aimed to generate a homology model would guide us in designing the VLY mutants for structural and functional studies.

The model was constructed using HHPRED software (Söding et al., 2005) relying on the closest structural template of ILY (PDB ID: 1S3R) (Polekhina et al., 2005) with the sequence identity of 58 %. As an additional reference of which the crystal structure was known (Rossjohn et al., 1997), a homology model of PFO was constructed using the same ILY crystal structure as a template (41 % sequence identity). Assessment of model quality was evaluated by ProSA Z-score using ProSA knowledge-based energy potentials (the more negative the ProSA Z score, the more energetically favourable the model) (Sippl, 1993).

6   Flow cytometric cell binding assay

VLY binding to the cell surface was evaluated by treating the cells with non-lytic VLY variants that were probed with primary anti-VLY and secondary fluorescently labelled Abs and analysed using flow cytometry.

Subconfluent CHO and CHO-CD59 cells were detached from the surface using StemPro Accutase enzyme (Gibco by Life Technologies), washed, resuspended in PBS and counted. For each sample 1×10^5 cells (40 μl) were mixed with 10 μl of VLY variant to the final concentration of 15 nM, 30 nM or 100 nM, as stated, and incubated for 30 min at 37 °C. The sample mixture without VLY was used as a negative control. After incubation, the cells were washed twice with 1.5 ml of incubation buffer (PBS supplemented with 1 % heat-inactivated FBS and 0.1 % NaN_3) followed by centrifugation (for 5 min at 200 RCF). After washing, the cells were incubated with an excess of primary mouse anti-VLY MAbs (clone 9B4 or 21A5) for 30 min at RT. The cells were washed twice and subsequently incubated with an excess of secondary PE-conjugated goat anti-mouse IgG Abs for 30 min at RT (Cat. No. 550589, BD Biosciences). After washing, the cells were fixed using BD CytoFix (BD Biosciences) for 10 min at 4 °C. After washing, the cells were transferred to 200 μl of incubation buffer and analysed by CyFlow Space flow cytometer (Partec, Muenster). Flow cytometry data were analysed using FlowJo software. The median of fluorescence intensity (MFI) was normalised dividing it by the values of the negative control (cells directly probed with antibodies only). Each experiment was repeated three times. Normalised MFI

(nMFI) values, together with standard deviation, were used to evaluate the binding of VLY variants to the surface of the cells.

7 ELISA

7.1 Indirect ELISA

Indirect enzyme-linked immunosorbent assay (ELISA) was used to determine the apparent dissociation constants (K_d) between VLY (or its mutants) and anti-VLY MAbs (9B4 and 21A5 clones).

Purified recombinant VLY (or its mutants) was immobilised on the surface of 96-well plates (Nunc MaxiSorp, Thermo Fisher Scientific) by adding 100 µl of 5 µg/ml VLY (or its variants) diluted in 50 mM Na-carbonate, (pH 9.5 at 25 °C) buffer and incubated overnight at 4 °C. Blocking was carried out by incubating the plates with 250 µl of 1 % BSA dissolved in PBS for 1 h at RT. The plates were washed with PBS supplemented with 0.1 % Tween-20. The plates were incubated with 100 µl of serially diluted mouse anti-VLY MAbs (clone 9B4 or 21A5) in the range of 1.9×10^{-7} to 3.3×10^{-12} M concentration in PBS supplemented with 0.1 % Tween-20 for 1 h at RT. After washing, the plates were incubated with 100 µl of HRP-conjugated goat anti-mouse IgG Abs (Cat. No. 5178-2504, Bio-Rad) diluted 1:5000 in PBS supplemented with 0.1 % Tween-20 for 1 h at RT. After washing, bound MAbs were quantified using HRP enzymatic reaction by adding 50 µl of ready-to-use TMB liquid substrate reagent (Sigma-Aldrich). The reaction was stopped by adding 25 µl of 3.6 % H_2SO_4 solution, and the absorbance at 620 nm was subtracted from the absorbance at 450 nm. The concentration of MAb that gave one-half of the maximal absorbance was averaged from three replicates that defined an apparent K_d for each antigen-MAb pair.

7.2 Sandwich ELISA

Sandwich ELISA was used for quantification of VLY in *G. vaginalis* growth media. For this purpose, two non-competitive mouse anti-VLY MAb clones were used, namely 12E1 and 9B4, which were previously generated in our laboratory (Zvirbliene et al., 2010). 100 µl of 5 µg/ml 12E1 (diluted in 50 mM Na-carbonate pH 9.5 (pH 9.5 at 25 °C)) was immobilised on the surface of 96-well plate by incubating it overnight at 4 °C (Nunc MaxiSorp, Thermo Fisher Scientific). The plates were blocked with 1 % of BSA (dissolved in PBS) for 1 hour at RT. *G. vaginalis* growth media was serially diluted in PBS supplemented with 0.1 % Tween-20, 100 µl of each dilution

was added to the wells and incubated for 1 h at RT with shaking. After washing, the plates were incubated with HRP-labelled mouse anti-VLY 9B4 MAbs (conjugation was carried out as described in *Methods* 7.2.1 section) for 1 h at RT with shaking. 100 μl of ready-to-use TMB reagent was added to the wells. The reaction was stopped by adding 25 μl of 3.6 % H_2SO_4. The absorbances at 620nm and 450nm were measured. The absorbance at 620 nm was subtracted from the absorbance at 450 nm.

A calibration curve was obtained using recombinant VLY protein dilutions in the range of 1 ng/ml to 1 μg/ml. Recombinant VLY was diluted in fresh *G. vaginalis* growth media The absorbance data points were plotted against the recombinant VLY concentrations. The linear part of the calibration curve was used as a standard to evaluate VLY concentrations in experimental *G. vaginalis* samples

G. vaginalis growth media supernatants were provided by Miglė Janulaitienė (Lithuanian National Public Health Surveillance Laboratory, Vilnius, Lithuania) growing the bacteria for 24 h or 48 h.

7.2.1 MAb conjugation with HRP

MAb conjugation with horseradish peroxidase (HRP) was based on periodate linkage. Anti-VLY MAb clone 9B4 was purified from the hybridoma media using Protein A Sepharose CL-4B (GE Healthcare) according to the manufacturer's recommendations. 5 mg of MAb was dialysed against 0.2 M Na-carbonate buffer pH 9.5 (pH 9.5 at 25 °C) overnight at 4 °C. HRP (Merck Millipore, Cat. No. 516531) (5 mg) was dissolved in 1 ml of deionised water and mixed with 0.25 ml of freshly prepared 0.2 M $NaIO_4$ and incubated for 2 h at RT in the dark. The solution of HRP was exchanged into 1 mM sodium acetate (pH 4.5 at 25 °C) using Sephadex G-25 PD-10 column (GE Healthcare). Activated HRP was mixed with Mab solution followed by pH adjustment to pH 9.5 (at 25 °C) by adding 0.2 M sodium carbonate (pH 9.5 at 25 °C). The mixture was incubated for 24 °C. Finally, the solution was dialysed against PBS, followed by the addition of BSA up to 2 % and glycerol up to 50 %.

8   Membrane-immobilised cholesterol dot blot analysis

The direct interaction between VLY and cholesterol was assessed using membrane-immobilised cholesterol dot blot technique.

Cholesterol was dissolved in chloroform to concentrations ranging from 32.5 to 0.01 mM (*w/v*). Polyvinylidene fluoride (PVDF) membrane (pore size

0.45 μm) was prewetted with 100 % methanol and washed in PBS. The dots with different amounts of immobilised cholesterol were formed by loading 2 μl of serially diluted cholesterol solution. The membrane was dried and blocked with 3 % low-fat milk powder dissolved in PBS for 1 h at RT. After blocking, the membrane was incubated with wild-type or mutated VLY diluted in blocking solution supplemented 0.01 % Tween-20 for 1 h at RT. After washing with PBS supplemented with 0.01 % Tween-20, the membrane was incubated with primary mouse anti-VLY MAb 9B4 in blocking solution supplemented with 0.01 % Tween-20 for 1 h at RT. After washing, the membrane was incubated with secondary goat anti-mouse HRP-labelled Abs (Cat. No. 5178-2504, Bio-Rad) (diluted 1:5000 in blocking solution supplemented with 0.01 % Tween-20) for 1 h at RT. After washing, the membranes were incubated with ready-to-use TMB substrate reagent (Sigma-Aldrich) for 1 min followed by placing the membrane into the water to terminate the reaction. The experiment for each VLY variant was repeated at least three times, and the representative membranes were imaged.

9   Liposome-based assays

9.1   The preparation of liposomes

Lipids were dissolved in chloroform and premixed according to the required composition to the final amount of 2 mg (Table 2). The lipid film was prepared by evaporating chloroform. Dry lipids were hydrated in 1 ml of 10 mM HEPES (pH 7.5 at 25 °C), 150 mM NaCl buffer by vigorous vortexing for 10 min followed by three freeze-thaw cycles. The hydrated lipid solution was extruded 11 times through a 100 nm polycarbonate membrane. Liposomes were stored at 4 °C and used within a week of preparation.

Table 2. The compositions of the liposomes that were used.

1	DOPC/cholesterol	45/55 mol%
2		60/40 mol%
3		70/30 mol%
4	DOPC	100 mol%
5	POPC/POPS/DGS-NTA(Ni)/cholesterol	49/10/1/40 mol%
6	POPC/POPS/DGS-NTA(Ni)	89/10/1 mol%

9.2   Liposome co-sedimentation assay

Liposome co-sedimentation assay was used to assess the binding of 6xHis-tagged CD59 to 18:1 DGS-NTA(Ni) containing liposomes.

100 μl (2 mg/ml) of liposomes were incubated with 15 μl of 72 μM CD59 for 30 min at RT. The samples were ultracentrifuged for 30 min at 67,000 rpm 15 °C (Beckman Coulter TLA 100.4 rotor). The supernatant was collected, and the pellet was resuspended in 115 μl 10 mM HEPES (pH 7.5 at 25 °C), 150 mM NaCl buffer and ultracentrifuged again. The supernatant was discarded, and the pellet was resuspended in reducing SDS-PAGE loading buffer. After heating for 5 min at 95 °C, the samples of the supernatant and the pellet were analysed using SDS-PAGE.

9.3   Liposome leakage assay

Functional CDC pore formation was assessed by liposome leakage assay. A fluorescent dye, sulforhodamine B (SRB), was encapsulated into the liposomes, which self-quenches at high concentrations, whereas upon pore formation the dye leaks out of the liposomes and is diluted in a buffer resulting in the increase of fluorescent signal.

SRB dye encapsulation was carried out during liposome preparation – 50 mM SRB was added into the buffer (10 mM HEPES (pH 7.5 at 25 °C), 150 mM NaCl), which was used to hydrate lipid film. Hydration was performed by vortexing the sample for 10 min, followed by three freeze-thaw cycles. Hydrated liposomes were extruded 11 times through a 100 nm polycarbonate membrane. To remove non-encapsulated SRB dye, the sample was buffer-exchanged into 10 mM HEPES (pH 7.5 at 25 °C), 150 mM NaCl using PD-10 desalting columns (GE Healthcare). After PD-10 equilibration with buffer, 1 ml of liposome sample was loaded followed by 2 ml of buffer and eluted by loading 2 ml of buffer. For liposome leakage assay, two compositions (No. 5 and 6 described in Table 2) of liposomes were used. Where indicated, liposomes were decorated with soluble C-terminally 6xHis-tagged CD59 by overnight incubation at 4 °C. To remove most of the unbound CD59, liposomes were run through the PD-10 column. Liposome leakage assay was carried out in 96-well plates, and the fluorescence was measured at 25 °C every 10 sec using Agilent Stratagene Mx3005 Real-Time PCR machine. Triton X-100 at the final concentration of 3 % was used as a complete lysis control. The data points over time were plotted and fitted with two-phase accumulation curve using GraphPad Prism. Each experiment was repeated four times. To define the rate of liposome leakage, the rate constant of the fast-phase (KFast) with standard deviation were evaluated.

9.4 SDS-agarose gel electrophoresis

SDS-agarose gel electrophoresis (SDS-AGE) was used to fractionate high molecular weight oligomers of CDC proteins after incubation with liposomes. The protocol was adapted from Shepard et al. (Shepard et al., 2000).

The gel was prepared from TopVision LE GQ agarose (Thermo Fisher Scientific) dissolved in Tris-glycine SDS buffer (Pierce, Thermo Fisher Scientific) to the final concentration of 1.5 % (*w/v*). In a reaction mixture of 20 µl, CDCs (53.7 pmol VLY, 54.6 pmol PLY or 52.4 pmol ILY) were incubated alone or with 15 nmol (total lipid) of liposomes for 30 min at 37 °C or 4 °C, as indicated. The 5x sample loading dye (300 mM Tris-HCl (pH 6.8 at 25 °C), 0.05% bromophenol blue 50 % glycerol) with or without 2 % (*w/v*) of SDS was added to the sample mixture and incubated for 2 min at 37 °C followed by heating for 7 min at 95 °C unless stated otherwise. The samples were loaded onto a gel, and the electrophoresis was performed. The gel was stained with the staining solution (0.25 % (*w/v*) Coomassie Brilliant Blue R, 10 % (*v/v*) acetic acid, 40 % (*v/v*) methanol) followed by destaining with destaining solution (5 % (*v/v*) acetic acid and 20 % (*v/v*) methanol). High molecular weight thyroglobulin protein was used as a reference. Thyroglobulin is known to exist as a dimer of ~670 kDa and a monomer of ~335 kDa.

9.5 Transmission electron microscopy

The ability of VLY to form oligomers was visualised using negative-stain transmission electron microscopy imaging the liposomes after incubation with VLY.

20 µl sample of liposomes (2 mg/ml total lipid concentration) were incubated with 3 µg of VLY (0.15 mg/ml final concentration) for 30 min at 37 °C. 3.5 µl of the sample was then loaded onto a C-flat carbon-coated grid (Cat. No. CF300-Cu-50, Electron Microscopy Sciences) and incubated for 1 min and dried using filter paper. Subsequently, the top side of the grid was immersed into the drop of MiliQ H_2O and dried again. After repeating the washing two more times, the top side of the grid was immersed in uranyl formate, dried, immersed again and incubated for 1 min before drying it out. The samples were imaged using FEI T12 transmission electron microscope operating at 120 kV. Imaging was performed by Dr Tao Ni (University of Oxford, Division of Structural biology).

10 Analytical ultracentrifugation

The state of VLY after incubation with CD59 protein in solution was assessed using analytical ultracentrifugation performing sedimentation velocity experiments.

Analytical ultracentrifugation (AUC) was performed for three samples – the mixture of VLY and CD59 as well as the individual proteins, VLY and CD59. The protein samples were mixed and incubated for 30 min at 37 °C. The reference samples were prepared by mixing the buffers at the same ratios as in the protein samples. AUC experiment was performed using a Beckman Optima XL-1 machine at 40,000 rpm 20 °C. Sedimentation data was collected using absorbance optics at the wavelength of 210 nm and interference optics every 6 min (120 scans in total). The data was analysed using Sedfit software using the protocols of sedimentation coefficient distribution, c(s) and two-dimensional c(s,f/f$_0$). The data points were plotted using GraphPad Prism.

RESULTS

1 Isolation of VLY and other cholesterol-dependent cytolysins

In the study of vaginolysin (VLY) from *Gardnerella vaginalis,* we included two other CDCs for comparison – intermedilysin (ILY) from *Streptococcus intermedius* and pneumolysin (PLY) from *Streptococcus pneumoniae*. ILY is a CD59-dependent cytolysin, and its pore-forming activity strictly depends on human protein CD59 (hereafter, CD59). PLY does not have a preference for CD59-expressing cells and does not engage a known protein receptor during its pore formation.

We used recombinantly expressed CDC proteins. The genes encoding VLY, ILY, PLY proteins were cloned into bacterial pET28a(+) vector fusing with N-terminal 6xHis-tag and expressed in either *E. coli* Tuner (DE3) or BL21 (DE3) strains. The constructs contained a thrombin cleavage site between the 6xHis-tag and the CDC. The thrombin-catalysed cleavage was performed to remove the 6xHis-tag from VLY and PLY proteins for the experiments with liposomes containing 18:1 DGS-NTA(Ni) lipids (*Results* 9, 10 sections). CDCs were purified using Ni-chelating affinity and ion-exchange chromatography followed by size-exclusion chromatography.

The functional activity of recombinant CDC proteins was confirmed using human erythrocyte-based haemolytic assay. The addition of generated CDCs to human erythrocytes lysed the cells in a concentration-dependent manner.

A collection of monoclonal antibodies (MAbs) against VLY were generated in our laboratory previously (Zvirbliene et al., 2010). Three anti-VLY MAbs were used, namely clones 9B4, 21A5 and 12E1.

2 VLY displays species tropism towards human cells

Previous insights into the cytolytic activity of VLY showed that it is directed towards human cells, e.g. human erythrocytes. In addition to being dependent on cholesterol, VLY engages human protein CD59 (Gelber et al., 2008). One of our attempts to demonstrate and characterise species tropism of VLY was performed using a CHO cell line (derived from Chinese hamster) and human HEK293 cell line. The end-point cell viability measurements were conducted using the MTS assay.
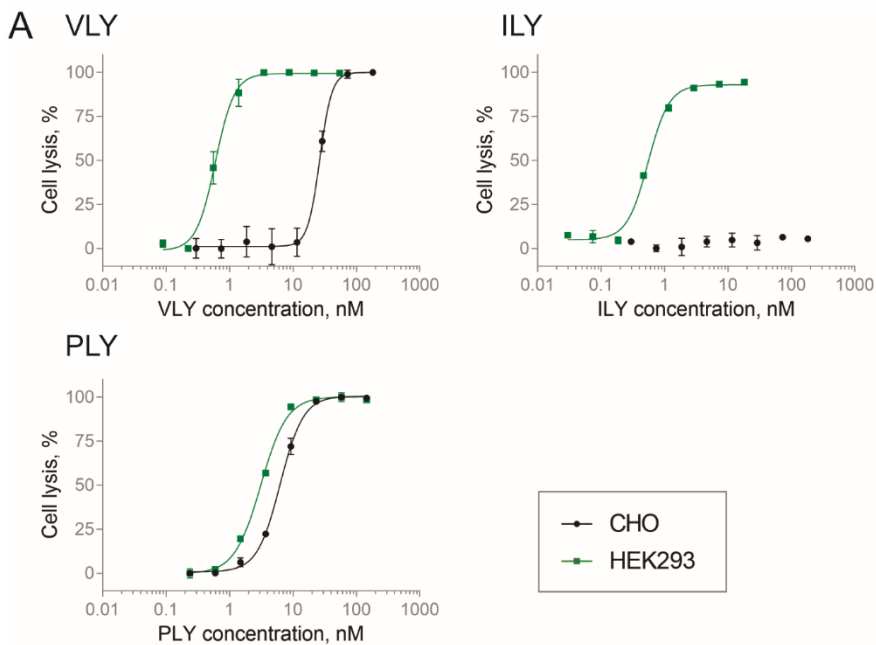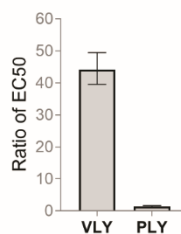
Figure 10. Vaginolysin (VLY) and intermedilysin (ILY) are directed towards human cells.
A – Cytolytic activity of VLY, ILY, pneumolysin (PLY) on CHO and HEK293 cells measured using MTS assay; data points were fitted with a four-parameter dose-response curve using GraphPad Prism; error bars show standard deviation; N=3. B – EC50 values of cells lysis by VLY, ILY, and PLY with standard deviation. The barplot represents ratios of EC50 value for the cytolysis of CHO to HEK293 cells by VLY and PLY; error bars show 95 % confidence intervals; N=3.

The results on CDC-induced concentration-dependent cell lysis are presented in Figure 10, A. The cell lysis was evaluated by determining the EC50 value (half-maximal effective concentration) that refers to the concentration of toxin able to lyse half of the cells (Figure 10, A). HEK293 cells were susceptible to lysis by all three CDCs. However, in the case of CHO cells, clear differences were seen. ILY did not affect the viability of CHO cells, even at very high concentration of 200 nM (Figure 10, A). Unlike ILY, VLY did lyse CHO cells, but approximately 40 times more toxin was required

than for HEK293 cells (Figure 10, A). PLY had a similar effect for both CHO cells and HEK293 cells (Figure 10, A). The ratio of EC50 value for CHO to EC50 for HEK293 cells emphasises VLY tropism towards human cells that was not seen in the case of PLY (Figure 10, B).
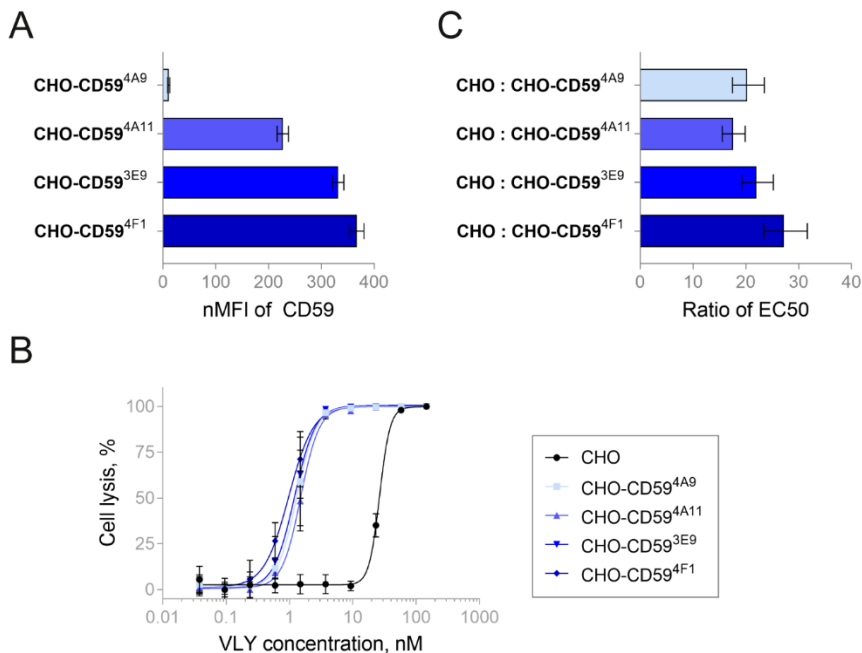
Figure 11. CD59 enhances the cytolytic activity of vaginolysin (VLY) in an amount-independent manner. A – the relative amount of surface-exposed CD59 in CHO-CD59 cell lines was evaluated using flow cytometry analysis by labelling cells with mouse anti-human CD59 FITC-conjugated antibodies; the barplot visualises normalised median fluorescence intensity (nMFI); error bars show standard deviation; N=3. B – the cytolytic activity of VLY for CHO and CHO-CD59 cells measured using MTS assay; error bars show standard deviation; N=3. C – ratios of EC50 values for the cytolysis of CHO cells to EC50 for CHO-CD59 cells by VLY; error bars show 95 % confidence intervals; N=3.

To provide more insight into the role of CD59 in VLY-induced cell lysis, stable CHO cell lines expressing different levels of GPI-anchored CD59 protein were generated by transfecting CHO cells with human protein CD59-encoding plasmid. The relative amount of surface-exposed CD59 was evaluated by labelling cells with mouse anti-human CD59 FITC-conjugated antibodies (Abs) and subsequently analysing them using flow cytometry. Four stably transfected cell lines (CHO-CD59[4A9], CHO-CD59[4A11], CHO-CD59[3E9], CHO-CD59[4F1] – listed in order from the lowest to the highest amount of CD59) were selected for further study (Figure 11, A). MTS assay was used to investigate the effect of the amount of CD59 for VLY-induced cell lysis

(Figure 11, B). The ratios of EC50 value for CHO to EC50 for CHO-CD59 cell lines clearly showed that CD59 significantly enhanced the cytolytic activity of VLY. However, the increase of cell lysis did not depend on the amount of CD59 as cells expressing very little CD59 (CHO-CD59[4A9], CHO-CD59[4A11]) were similarly susceptible to VLY-induced lysis as the ones expressing a high amount of it (CHO-CD59[3E9], CHO-CD59[4F1]) (Figure 11, C).
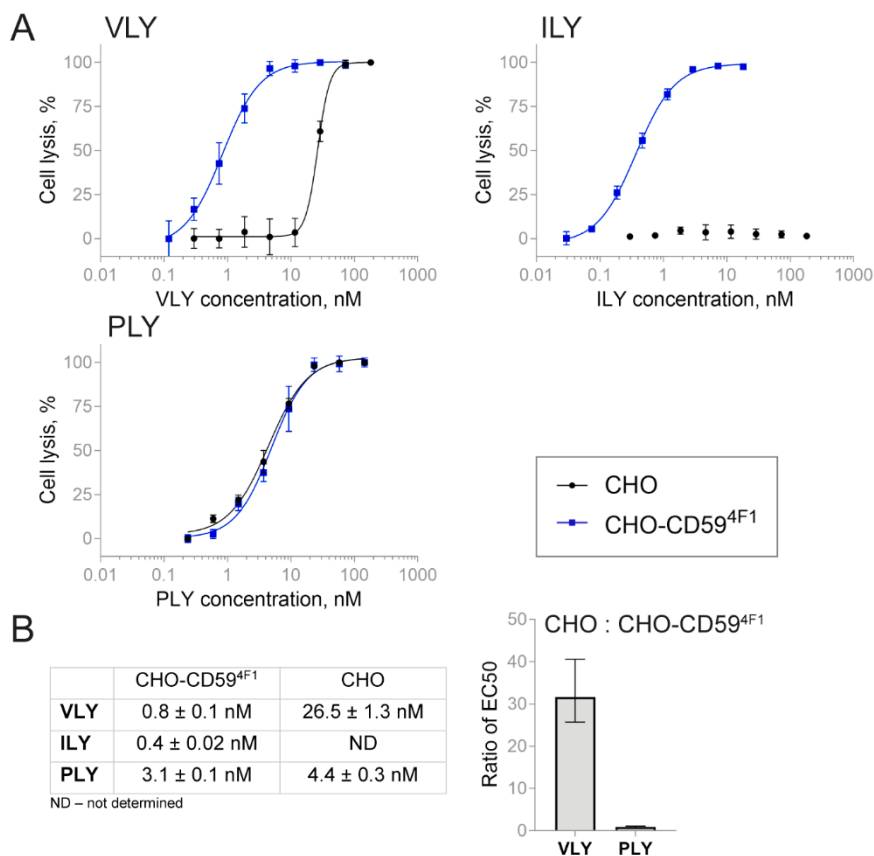
Figure 12. Vaginolysin (VLY) and intermedilysin (ILY) are directed towards CD59-expressing cells. A – the cytolytic activity of VLY, ILY and pneumolysin (PLY) for CHO and CHO-CD59[4F1] cells measured using MTS assay; data points were fitted with a four-parameter dose-response curve using GraphPad Prism; error bars show standard deviation; N=3. B – the table contains EC50 values of VLY, ILY and PLY with standard deviation; the barplot visualises ratios of EC50 values for cytolysis of CHO to EC50 for CHO-CD59[4F1] cells by VLY and PLY; error bars show 95 % confidence intervals; N=3.

CHO-CD59[4F1] cell line (the highest CD59 expression) was selected for a comparison of VLY activity with that of ILY and PLY. The comparison was performed to minimise the unpredicted cellular changes that could impact on higher cell sensitivity to CDCs unrelated to CD59. The cell lysis, monitored

by MTS assay, followed a similar trend as it was described above for HEK293 cells (Figure 12, A). CHO cells expressing CD59 became prone to ILY-induced lysis and were markedly more susceptible to the cytolytic activity of VLY. The ratio of EC50 values for VLY- or PLY-treated CHO cells to CHO-CD59[4F1] cells revealed the importance of CD59 enhancing the cytolytic action in the case of VLY but not PLY (Figure 12, B).

These findings suggested that species tropism of VLY towards human cells is directly related to human protein CD59 being incorporated in the cellular membrane. Furthermore, even a small amount of CD59 significantly increased VLY cytolytic activity.

3   Membrane cholesterol induces VLY oligomerisation

CDCs are known to form β-barrels that penetrate the cell membrane and open up pores. Oligomerisation itself is not enough to perforate the membrane, and a couple of maturation steps, including massive conformational changes, have to occur. As long as the CDC oligomer is above the membrane, it is called a prepore. In the late stage of oligomerisation, the prepore becomes an SDS-resistant oligomer followed by prepore-to-pore transition and the perforation of the membrane (van Pee et al., 2017; Shepard et al., 2000).

In our study, the SDS-resistance of oligomer was used as a characteristic of a late prepore or pore formation. Regarding oligomerisation, one of the questions was whether the cholesterol-rich bilayer alone could successfully trigger VLY oligomer formation. Thus, we aimed to investigate whether SDS-resistant VLY oligomers were formed. Unilamellar artificial cholesterol-rich liposomes were used as a model for simplified membrane containing POPC (1-palmitoyl-2-oleoyl-sn-glycero-3-phosphocholine) or DOPC (1,2-dioleoyl-sn-glycero-3-phosphocholine) phospholipids and 40 molar per cent (mol%) of cholesterol. VLY was incubated with liposomes, and then the sample was subjected to SDS-agarose gel, which was subsequently stained with Coomassie Blue stain.
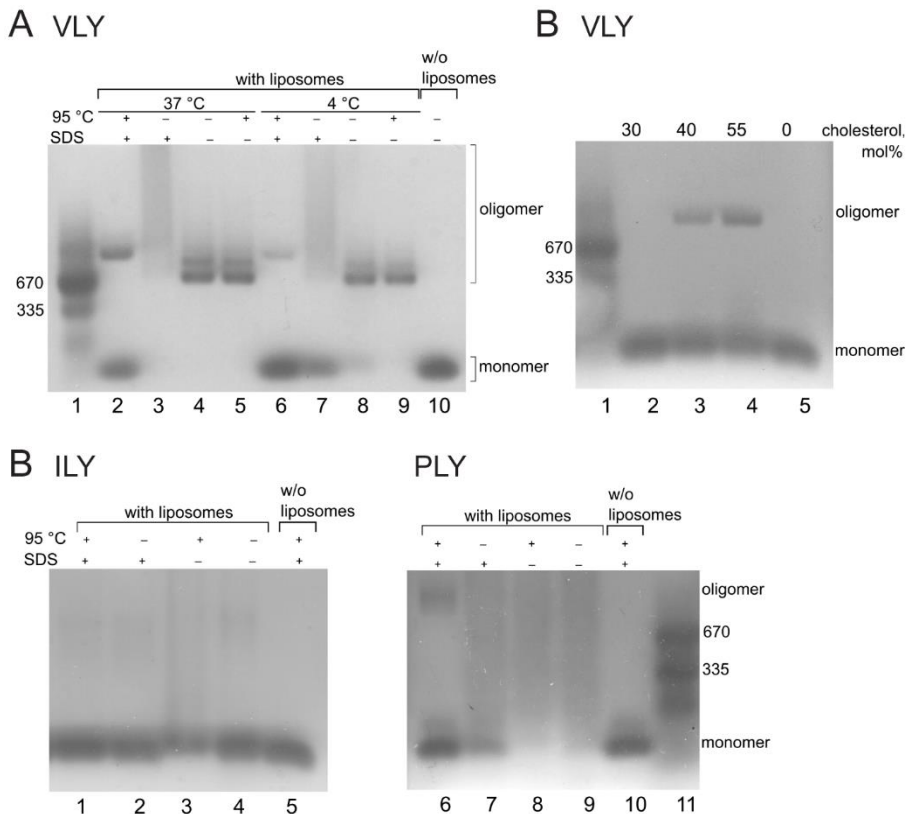
Figure 13. Vaginolysin (VLY) can form SDS-resistant oligomers on cholesterol-rich liposomes. A – SDS-agarose gel visualising VLY oligomers after incubation with DOPC:cholesterol (60 mol%:40 mol%) liposomes; the indication above the gel defines the temperature (37 °C or 4 °C) the incubation was carried on and the treatment of samples before loading into the gel. Lane 1 – thyroglobulin was used as a high molecular weight marker (a dimer of ~670 kDa and a monomer of ~335 kDa). B – SDS-agarose gel visualising VLY oligomers after incubation with liposomes containing varying concentrations of cholesterol (30 mol%, 40 mol% and 55 mol%) and the ones lacking cholesterol. Lane 1 – thyroglobulin was used as a high molecular weight marker (a dimer of ~670 kDa and a monomer of ~335 kDa). C – SDS-agarose gel visualising the capability of ILY and PLY to form oligomers after incubation with DOPC:cholesterol (60 mol%:40 mol%) liposomes; the captions above the gel indicate the treatment samples underwent before being loaded onto the gel. Lane 11 – thyroglobulin was used as a high molecular weight marker (a dimer of ~670 kDa and a monomer of ~335 kDa).

The experiment showed a clear difference between VLY state before and after incubation with cholesterol-rich liposomes (Figure 13, A). After incubation with liposomes, VLY formed SDS-resistant oligomers, which are indicative of late prepores or pores (lanes 2-9 in Figure 13, A). Incubation at 37 °C resulted in a higher amount of oligomers than at 4 °C. Furthermore, oligomers formed at 4 °C seemed to be more sensitive to SDS treatment (lanes

56

2-5 and lanes 6-9, Figure 13, A). Depending on the conditions the sample was treated before loading to the gel, the electrophoretic mobility for some of the conditions differed greatly. Heating of the samples did not have any impact on the electrophoretic mobility: both heated and non-heated samples migrated as oligomers of a high order and did not break down to monomers (lanes 4-5, lanes 8-9, Figure 13, A). When SDS was added directly to the sample before heating, the heterogeneity of oligomers increased (lanes 3, 7, Figure 13, A). The oligomers, which were formed at 4 °C, were more sensitive to SDS than the ones formed at 37 °C (lanes 3, 7, Figure 13, A). Once these SDS-treated oligomers were heated at 95 °C, a very distinct, high molecular weight band was formed while a great portion of VLY was reverted into the monomeric form (lanes 2, 6, Figure 13, A).

Next, we tested if VLY oligomerisation is related to the amount of cholesterol in the membrane. We used liposomes containing 30, 40, 55 mol% cholesterol and subjected them to the oligomerisation assay described above. The samples were treated with SDS, followed by heating at 95 °C for 7 min (Figure 13, A). As expected, no VLY oligomers were observed in the case of liposomes lacking cholesterol (lane 5, Figure 13, B). Interestingly, liposomes containing 30 mol% of cholesterol also did not produce a detectable amount of oligomers (lanes 2, 5, Figure 13, B). Judging by the band density, more VLY oligomers were formed on the liposomes containing 55 mol% cholesterol than those containing 40 mol% (lanes 3, 4, Figure 13, B).

For a more detailed comparison of the oligomerisation stage between the other CDCs, we assayed ILY and PLY with cholesterol-containing liposomes. As expected, ILY did not show a similar tendency of oligomerisation, because CD59 was not present on the liposomes. However, some higher oligomeric species were seen, although they did not resemble the pattern observed for VLY (Figure 13, C). PLY formed clear SDS-resistant oligomers, although PLY oligomers were more heterogeneous than VLY oligomers (Figure 13, C).

Thus, artificial cholesterol-rich liposomes were shown to act as a platform for VLY and PLY oligomerisation. Moreover, the cholesterol-rich membrane was demonstrated to be a necessary and sufficient component for VLY oligomers to form, as opposed to ILY, where no clear evidence for oligomer formation was generated. The oligomers of VLY and PLY were resistant to SDS treatment implying the formation of late prepore or functional pore structures.

4 VLY can bind cholesterol and CD59 independently

Cholesterol-dependent cytolysin, namely PFO, is being used for labelling cholesterol embedded in cellular membranes (Johnson et al., 2017a). Cholesterol binding is a defining feature of this class of proteins. It is, however, thought and in some cases proven by experimental data that cholesterol is not the only one membrane component, which defines the affinity of the toxin for the membrane (Gelber et al., 2008; Giddings et al., 2004; Shewell et al., 2014). We investigated whether CD59 plays a role in helping to attract more VLY to the surface of the attacked cells. And if so, does VLY bind to the cholesterol and the CD59 at the same time or is it possible for the toxin to bind to the cell through CD59 only?

4.1 Binding to cholesterol

Two conserved amino acid motif of Thr-Leu in the L1 loop of PFO D4 domain was shown to be responsible for the interaction with cholesterol (Farrand et al., 2010). We investigated whether Thr-Leu motif is engaged in the interaction between VLY and cholesterol and whether the interaction with cholesterol is necessary for the VLY-induced cell lysis.

To visualise the direct interaction between VLY and cholesterol, we performed a dot blot experiment. Decreasing amounts of cholesterol were immobilised on PVDF membrane starting from 65 nmol down to 0.02 nmol. The membrane was then incubated with VLY. The interaction between membrane-immobilised cholesterol and VLY was detected by primary anti-VLY 9B4 antibodies followed by secondary anti-mouse IgG antibodies conjugated with HRP enzyme (Figure 14, A). The intensities of the dots, indicative of the amount of VLY present, faded away as the amount of membrane-immobilised cholesterol was lowered, suggesting that VLY was binding in a cholesterol concentration-dependent manner.
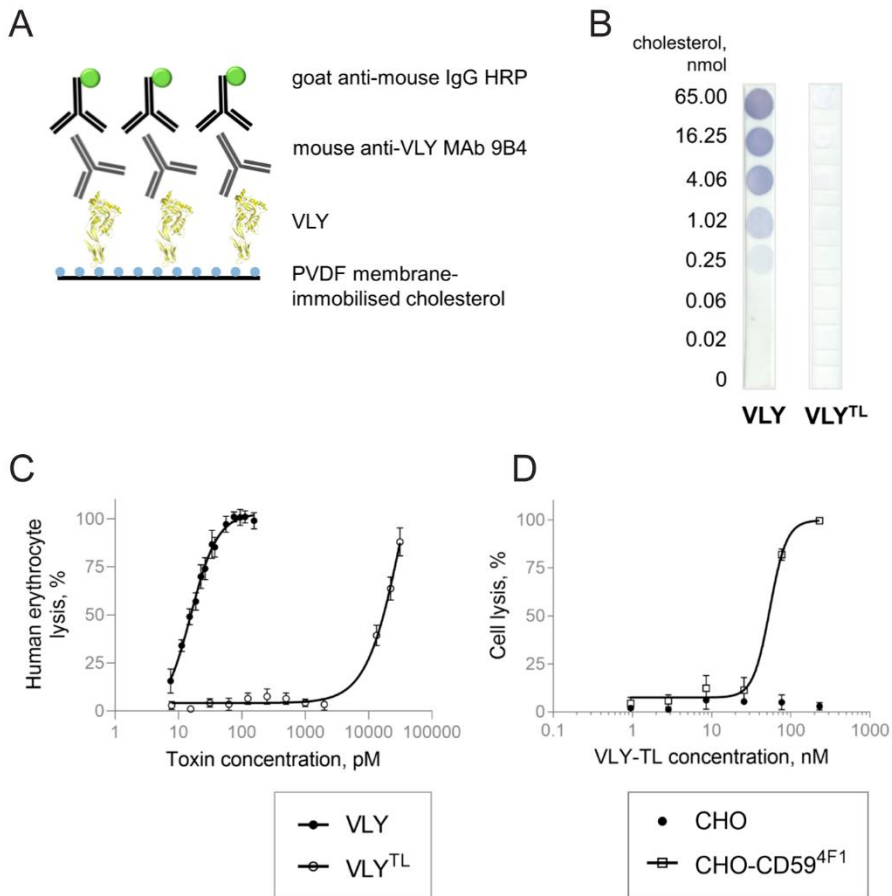
Figure 14. Thr-474/Leu-475 motif in the D4 domain plays a key role in VLY binding to cholesterol. A – schematic representation of dot blot experiment. B – dot blot images visualising VLY and VLY[TL] binding to PVDF membrane-immobilised cholesterol. C – the haemolytic activity of VLY and VLY[TL] by haemolytic assay using human erythrocytes; data points were fitted with a four-parameter dose-response curve using GraphPad Prism; error bars show standard deviation. N=2. D – the cytolytic activity of VLY, VLY[TL] for CHO and CHO-CD59[4F1] cells measured using MTS assay; data points were fitted with a four-parameter dose-response curve using GraphPad Prism; error bars show standard deviation; N=3.

By homology to PFO, the two amino acid motif of Thr-Leu in the L1 loop in the D4 domain of VLY was expected to be responsible for interaction with cholesterol. To prove this, we mutated the Thr-474/Leu-475 motif of VLY into Gly-Gly. The generated VLY mutant, named VLY[TL], was not able to bind to the membrane-immobilised cholesterol as we demonstrated using dot blot assay described above (Figure 14, B). It should be noted that the interaction of VLY[TL] with anti-VLY MAb 9B4 was not lost due to the mutation (Table 3). VLY[TL] mutant was able to induce human erythrocyte lysis, but an extremely high amount of this mutant was required that was about 1000-fold

higher as compared to wild-type VLY (Figure 14, C). Moreover, VLY^{TL} in high concentration lysed CHO-CD59^{4F1} cell line (with the highest amount of CD59) while non-transfected CHO cells remained intact (Figure 14, D).

Table 3. Apparent dissociation constants (K$_d$) of the affinity of anti-VLY monoclonal antibodies (MAbs) for wild-type vaginolysin (VLY), VLY^{GG} and VLY^{TL} mutants.

	VLY	VLY^{GG}	VLY^{TL}
9B4 MAb	3.0×10^{-10} M	2.2×10^{-10} M	2.5×10^{-10} M
21A5 MAb	2.7×10^{-10} M	9.0×10^{-10} M	7.0×10^{-10} M

Thr-Leu motif plays a key role in cholesterol recognition in VLY. Substitution of Thr-474/Leu-475 to Gly-Gly eliminated VLY binding to PVDF membrane-immobilised cholesterol and the ability to lyse CHO cells. Surprisingly, the ability to lyse CD59-expressing cells was maintained even though a much higher amount of VLY was required.

4.2   Binding to CHO and CHO-CD59 cells

Furthermore, we investigated whether CD59-driven enhancement of VLY cytolytic activity might be related to the higher affinity of VLY for the membrane. We aimed to measure whether CD59 bearing cells can attract more VLY than the ones lacking it. For this purpose, we needed a non-lytic mutant of VLY, which would mimic VLY binding to the membrane but would not lyse the cells.

Using site-directed mutagenesis, we generated a VLY^{GG} mutant (G308A·G309A), which had a substitution of the conserved Gly-Gly motif to Ala-Ala chosen by homology to PFO and its previously published mutation (Ramachandran et al., 2004). VLY^{GG} maintained binding to PVDF membrane-immobilised cholesterol and was recognised by anti-VLY 9B4 and 21A5 MAbs (Table 3, Figure 15, A). Importantly, the ability to lyse human erythrocytes was lost in the case of VLY^{GG} mutation (Figure 15, B).
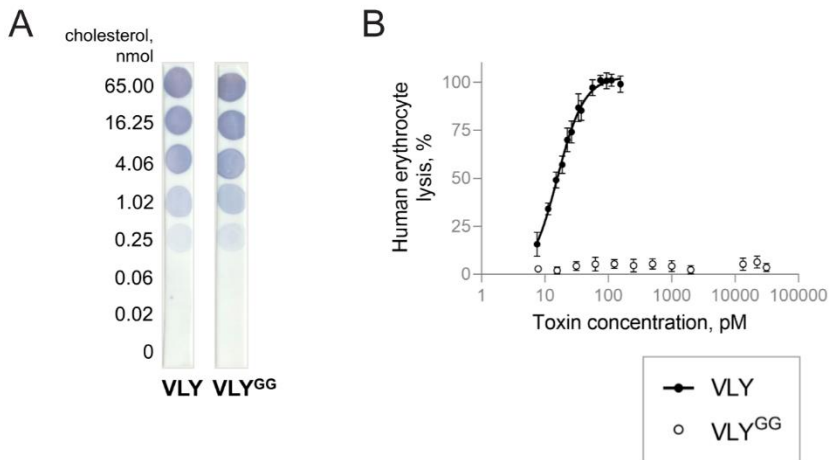
Figure 15. Mutation of Gly-308/Gly-309 motif in the D3 domain of VLY turns off its haemolytic activity but does not interrupt cholesterol binding. A – dot blot images visualising VLY and VLY[GG] binding to PVDF membrane-immobilised cholesterol detected by anti-VLY MAb 9B4. B – the haemolytic activity of VLY and VLY[GG] by haemolytic assay using human erythrocytes; data points were fitted with a four-parameter dose-response curve using GraphPad Prism; error bars show standard deviation. N=3.

Next, we set out an experiment to determine relative amounts of VLY[GG] and VLY[TL] that bind to the cell membranes containing or lacking CD59. To do so, we used flow cytometry for the detection of VLY mutants by primary anti-VLY MAbs and fluorescently labelled secondary goat anti-mouse IgG antibodies (Figure 16, A). Detection using both primary VLY-specific MAbs (clones 9B4 and 21A5) followed a similar trend (Figure 16, B, C). The lower detection level of 21A5 is probably related to its higher K_d (Figure 16, C; Table 3). VLY[GG] binding to CHO cells increased as its concentration was increased (Figure 16, B, C). CD59 helped to attract much more VLY[GG,] and no significant difference was seen between the two VLY[GG] concentrations of 75 nM and 300 nM (Figure 16, B, C). As expected, the binding of VLY[TL] to CHO cells was not detected as the cholesterol recognition site was disrupted (Figure 16, B, C). In contrast, the interaction between CHO-CD59[4F1] cells and VLY[TL] was detected by flow cytometry, suggesting that interaction with the membrane can be fulfilled through CD59 only (Figure 16, B, C).
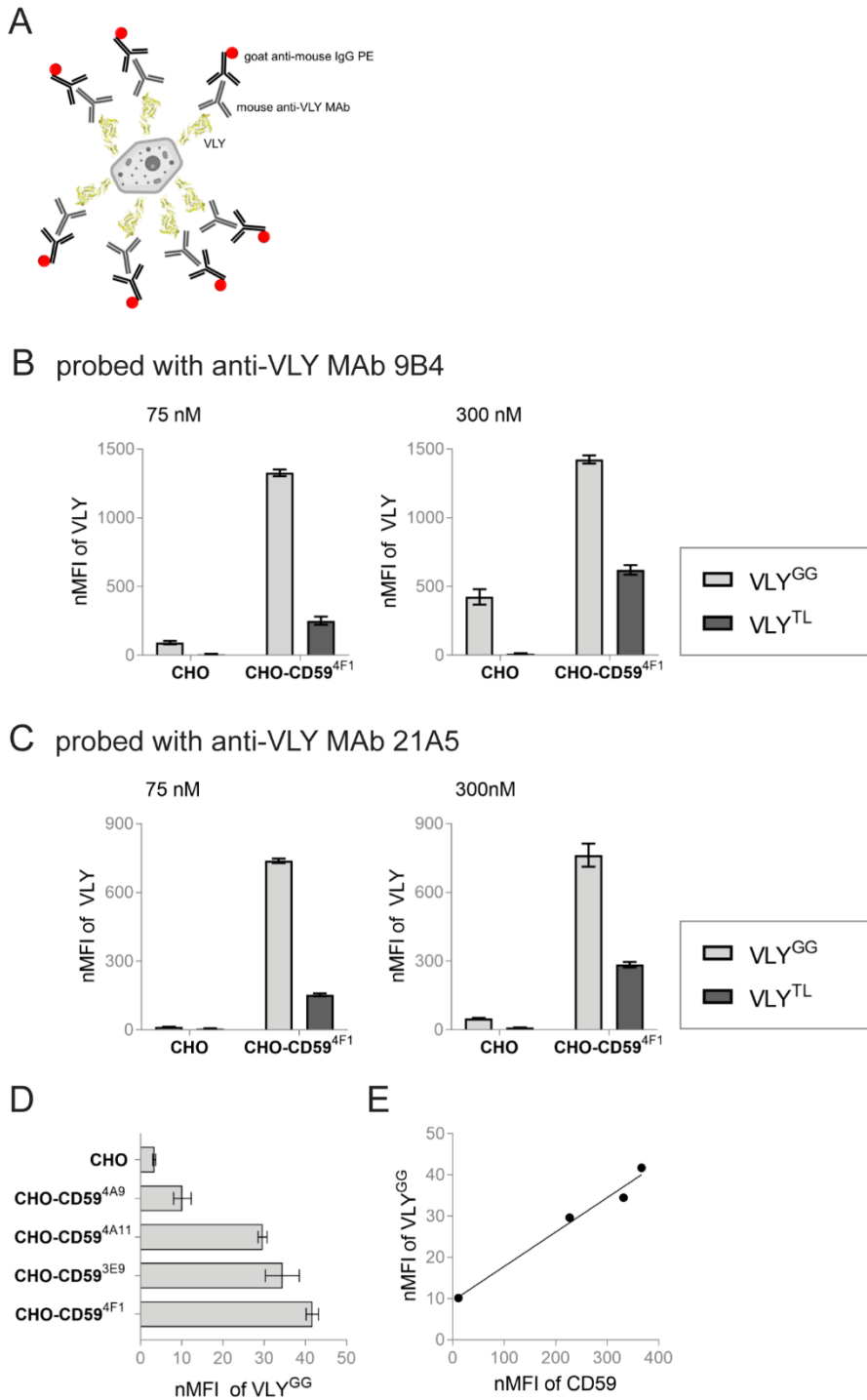
Figure 16. CD59 increases vaginolysin's (VLY) affinity for the membrane. A – schematic depiction of the experimental approach for the quantification of the amount of VLY bound to cells by labelling with primary MAbs, which were probed with secondary goat anti-mouse IgG

PE-labelled Abs. B – the relative amount of VLY^{GG} and VLY^{TL} bound to CHO and CHO-CD59^{4F1} cells; two VLY^{GG} and VLY^{TL} concentrations were used (75 nM and 300 nM); detection was carried out with anti-VLY MAb 9B4; bar plots show normalised median fluorescence intensity (nMFI) of the secondary goat anti-mouse IgG PE Abs; error bars show standard deviation; N=3. C – the relative amount of VLY^{GG} and VLY^{TL} bound to CHO and CHO-CD59^{4F1} cells; two VLY^{GG} and VLY^{TL} concentrations were used (75 nM and 300 nM); detection was carried out with anti-VLY MAb 21A5; bar plots show normalised median fluorescence intensity (nMFI) of the secondary goat anti-mouse IgG PE-conjugated Abs; error bars show standard deviation; N=3. D – the relative amount of VLY^{GG} bound to CHO-CD59 cells expressing a different amount of CD59 and CHO cells; bar plots evaluate nMFI of secondary goat anti-mouse IgG PE-conjugated Abs; error bars show standard deviation; N=3. E – linear correlation between the averaged amount of VLY^{GG} bound to the cell surface and the number of CD59 exposed on the cell surface that were detected using flow cytometric analysis.

For a better understanding of how CD59 attracts more VLY to the cellular membrane, we conducted a cell-binding experiment using four cell lines of CHO-CD59 expressing a different level of CD59 – CHO-CD59^{4A9}, CHO-CD59^{4A11}, CHO-CD59^{3E9}, CHO-CD59^{4F1}, listed in the order of surface-exposed CD59 expression level (Figure 11, A). Interestingly, VLY^{GG} binding to the cell surface increased with the increasing level of surface-exposed CD59 (Figure 16, D). Furthermore, the amount of VLY bound to cell surface suggested a linear correlation with the number of CD59 exposed on the surface of stably transfected CHO cells (Figure 16, E).

Thus, it can be concluded that VLY can bind to the cell surface either through cholesterol or CD59. We showed that CD59-harbouring cell membrane could attract much more VLY. Furthermore, an implication for a positive correlation between the amount of cell surface-exposed CD59 and the amount of VLY bound to these cells was demonstrated.

5 Mutagenesis study of VLY monomer-monomer and VLY-CD59 interactions

5.1 Construction of the homology-based VLY structural model

At the time the study was carried out, the crystal structure of VLY was not yet known. In collaboration with Prof. Dr Česlovas Venclovas (Vilnius University, Life Sciences Center, Institute of Biotechnology), we constructed a homology-based model of VLY.

VLY homology model was constructed with HHpred (Söding et al., 2005) using the crystal structure of ILY (PDB ID: 1S3R) (Polekhina et al., 2005) as the closest structural template (58% sequence identity). To assess the model quality, a homology-based model for PFO was constructed. Prosa Z-score of

VLY and PFO model structures and experimental ILY crystal structure were calculated (Sippl, 1993). Prosa Z-score of the VLY model was equal to -11.31 and placed VLY structure in between of the ILY structure with the score of -12.27 and PFO with the score of -11.08. This structural assessment suggested that the accuracy of VLY model was sufficient to provide the details of individual residues and hinted that structurally VLY is closer to ILY than PFO.

5.2 Disruption of VLY monomer-monomer interaction

The model for typical CDC monomer-monomer interaction is based on the β-sheet extension in D3 domain between neighbouring monomers (Dowd and Tweten, 2012; Ramachandran et al., 2004). Studies of PFO provided data that proper register between two β-strands is acquired with the help of π-stacking interaction (Ramachandran et al., 2004). However, other studied CDCs (VLY, ILY, PLY) do not have one of the respective aromatic amino acids. We investigated whether the same monomer-monomer interface is engaged by VLY.

Firstly, we investigated whether Tyr-165, one of the preserved aromatic residues, in β1 of VLY may still be important for monomer-monomer interface formation. Substitution of Tyr-165 to Ala (HD50=18 ± 1 pM) did not affect the haemolytic activity of mutant protein significantly comparing the HD50 values with wild-type VLY (HD50=10 ± 1 pM).

Another question we approached was whether VLY oligomerises through the same D3 region (β1- and β4-strands) as PFO. We aimed to prevent edge-to-edge interaction between D3 β1- and β4-strands of the neighbouring monomers. Using a homology-based model of VLY (*Results* 5.1 section), we designed a probable interface between β1- and β4-strands in D3 domain of two monomers. We chose to substitute Ala-304 and Ile-306 amino acids, which were likely to participate in the monomer-monomer interface (Figure 17, A). -NH groups of Ala-304 and Ile-306 are supposed to be oriented towards D3 β5-strand and after its rotation appearing accessible by the other monomer to interact with. Whereas Val-305 was taken as control, which forms a hydrogen bond with Tyr-262 in the β3-strand in individual monomer and does not contribute to the monomer-monomer interface (Figure 17, A). We attempted to mutate these amino acids to Pro to get rid of backbone -NH group serving hydrogen atom for a hydrogen bond. We succeeded in generating three mutants, namely VLY[V305P], VLY[I306P], VLY[A304P/I306P]. The starting point was to assess whether the overall structure of the mutants was not disrupted.
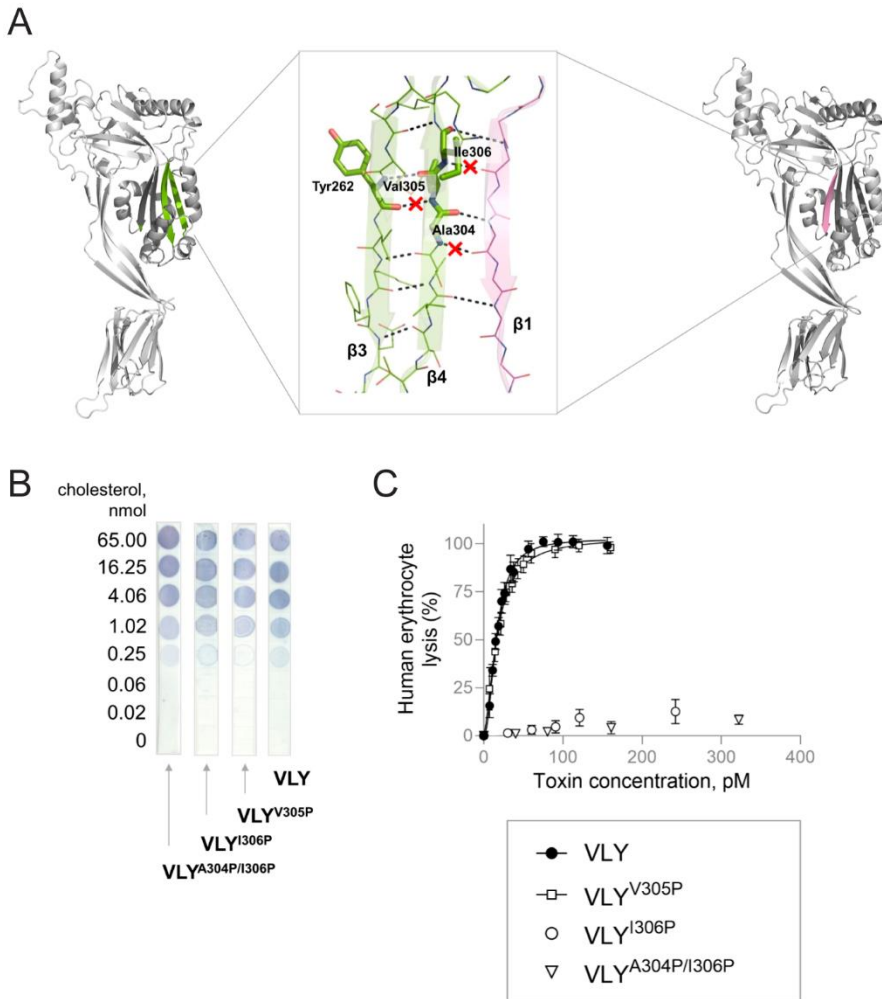
Figure 17. Vaginolysin (VLY) monomer-monomer interaction is maintained through β1- and β4-strands of neighbouring monomers. A – schematic interface between two VLY monomers highlighting the interaction of β1- and β4-strands; hydrogen bonds targeted to be disrupted by substitution to proline at positions 304-306 in β4 are indicated with red crosses. B – dot blot images visualising VLY, VLY^V305P, VLY^I306P, VLY^A304P/I306P binding to PVDF membrane-immobilised cholesterol detected by anti-VLY MAb 9B4. C – the haemolytic activity of VLY, VLY^V305P, VLY^I306P, VLY^A304P/I306P by hemolytic assay using human erythrocytes; data points were fitted with a four-parameter dose-response curve using GraphPad Prism; error bars show standard deviation. N=3.

For that reason, we performed dot blot assay, which showed that all mutants were able to bind to cholesterol immobilised on polyvinylidene fluoride (PVDF) membrane and can be detected by anti-VLY MAb 9B4 (Figure 17, B). Different outcomes were observed in the haemolytic assay as VLY^I306P, and VLY^A304P/I306P shared a non-haemolytic feature. Meanwhile, VLY^V305P

targeting an internal hydrogen bond maintained haemolytic activity similar to wild-type VLY (Figure 17, C).

Proline substitution was shown as an effective way to disrupt β-sheet extension between D3 domains at VLY monomer-monomer interface but not the overall structure of individual monomers. Ala-304 and Ile-306 amino acids positioned in the β4-strand were shown to take part in forming the interface of two neighbouring VLY molecules. Hence, the edge-to-edge β-sheet interface is maintained during VLY oligomerisation. However, π-stacking interaction is not required to either stabilise or align the respective β-strands to achieve a proper register of alignment.

5.3   Disruption of VLY-CD59 interaction

At the time the study was carried out only one crystal structure of the complex of CDC and CD59 had been solved. In 2013 Johnson and colleagues solved a crystal structure of ILY complexed with CD59 (Johnson et al., 2013). Two distinct interfaces between ILY and CD59 were suggested that were placed on the opposite sides of the ILY molecule. We investigated whether the interaction between VLY and CD59 resembled the interfaces of ILY-CD59 complex.

A set of amino acids that were incorporated in ILY-CD59 interface were selected for further mutagenesis study (listed in Table 4). Using the information from pairwise sequence alignment between ILY and VLY and homology modelling, ten amino acid positions in VLY were selected as candidates for single amino acid substitutions (Figure 18, A). Amino acids in the predicted interface between VLY and CD59 were substituted to alanines and introduced into the non-cytolytic VLY[GG]. Eight of 10 mutants were successfully generated (listed in Table 4). Using flow cytometry and the previously described experiment (*Results* 4.2 section), we measured the ability of these mutants to bind to CHO-CD59[4F1] cells. We evaluated median fluorescence intensities (MFI) for all the mutants that were normalised by dividing their MFI value by MFI value of negative control (cells treated with both antibodies only). Unexpectedly, single mutations did not have any effect on cell binding property (Figure 18, B).

Table 4. List of VLY mutants bearing single mutations targeting 1st or 2nd VLY-CD59 interfaces that were proposed from the crystal structure of ILY-CD59 (Johnson et al., 2013)**.**

The targeted interface of VLY-CD59	Name of mutant	Mutations
1st interface	VLY[D395A(GG)]	D395A / G308A / G309A
	VLY[E400A(GG)]*	E400A / G308A / G309A *
	VLY[D402A(GG)]	D402A / G308A / G309A
	VLY[Y406A(GG)]	Y406A / G308A / G309A
	VLY[V407A(GG)]	V407A / G308A / G309A
	VLY[S409A(GG)]	S409A / G308A / G309A
	VLY[R437A(GG)]*	R437A / G308A / G309A *
2nd interface	VLY[D50A(GG)]	D50A / G308A / G309A
	VLY[N53A(GG)]	N53A / G308A / G309A
	VLY[I401A(GG)]	I401A / G308A / G309A

* expression of soluble protein was not obtained;

A lack of effect of single substitutions to alanines brought us to a question whether the binding either through one or the other predicted interfaces might be strong enough and not so easily interfered. Moreover, we asked whether two interfaces can compensate each other. Hence, even some of the mutations did disrupt one of the interfaces, that might enable another interface masking the effect. To test these hypotheses, we designed more robust single or multiple mutations that would disrupt either two interfaces independently or both of them at the same time. All the mutations were designed as substitutions to alanine. Furthermore, Val-407, which might contribute to β-sheet extension between CD59 and ILY, was substituted to proline. We aimed to measure how these mutations affect VLY binding to CHO-CD59[4F1] cells and how they shape their haemolytic activity. Using site-directed mutagenesis, mutations were introduced either into cytolytically inactive VLY[GG] for cell binding experiment or into wild-type VLY for the measurement of haemolytic activity. For each experiment, ten mutants were generated, four of them were targeting the 1st interface of VLY-CD59 complex, two – targeting the 2nd interface and four – targeting both interfaces (listed in Table 5).
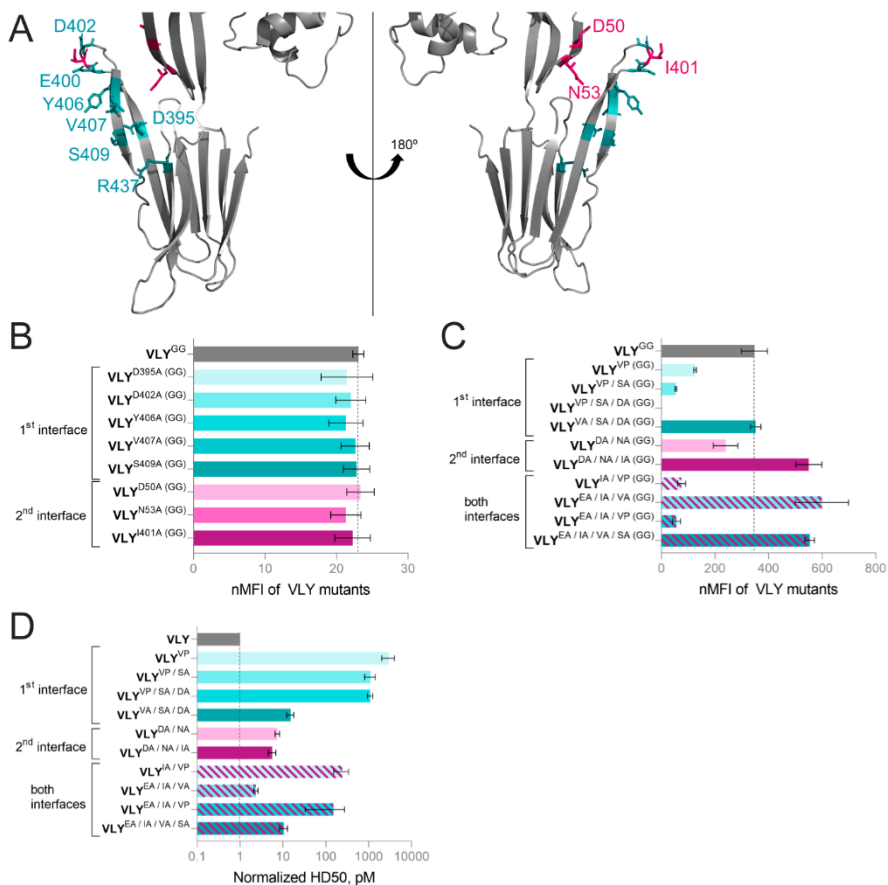
Figure 18. The interface of vaginolysin (VLY) and CD59 is based on β-sheet extension. A – visualisation of two proposed VLY-CD59 interfaces. Amino acid positions chosen for mutagenesis are highlighted in sticks model (the 1st interface in cyan, the 2nd interface in magenta). B – the relative amount of single VLY mutants (targeting the proposed VLY-CD59 interfaces) bound to CHO-CD59[4F1] cells; VLY[GG] was used as a reference; bar plots show normalised median fluorescence intensity (nMFI) of secondary anti-mouse IgG PE-conjugated Abs; error bars show standard deviation; N=3. C – the relative amount of single and multiple VLY mutants (targeting the proposed VLY-CD59 interfaces individually or together) bound to CHO-CD59[4F1] cells; VLY[GG] was used as a reference; red arrows highlight mutants containing V307P mutation; bar plots show normalized median fluorescence intensity (nMFI) of secondary goat anti-mouse IgG PE-conjugated Abs; error bars show standard deviation; N=3. D – the haemolytic activity of single and multiple VLY mutants (targeting the proposed VLY-CD59 interfaces individually and together) lysing human erythrocytes; VLY[GG] was used as a reference; bar plots show normalised HD50; error bars show standard deviation; N=3.

Mutations in the proposed 1st interface seemed to have more impact on VLY binding to cells than the 2nd interface. However, the mutations in the 2nd interface did influence haemolytic activity even though they did not hinder VLY binding to the cells.

Table 5. List of VLY mutants targeting the proposed VLY-CD59 interfaces, either separately or both at the same time. VLY mutants were generated for cell binding assay and haemolysis assay. Mutants for cell binding assay had additional G308A/G309A mutation, making them non-cytolytic.

Targeted interfaces of VLY-CD59	VLY mutants for cell binding assay		VLY mutants for hemolysis assay	
	Name of mutant	Mutations	Name of mutant	Mutations
1st interface	VLY$^{VP\,(GG)}$	V407P / G308A / G309A	VLY^{VP}	V407P
	VLY$^{VP\,/\,SA\,(GG)}$	V407P / S409A / G308A / G309A	VLY$^{VP\,/\,SA}$	V407P / S409A
	VLY$^{VP\,/\,SA\,/\,DA\,(GG)}$	V407P / S409A / D395A / G308A / G309A	VLY$^{VP\,/\,SA\,/\,DA}$	V407P / S409A / D395A
	VLY$^{VA\,/\,SA\,/\,DA\,(GG)}$	V407A / S409A / D395A / G308A / G309A	VLY$^{VA\,/\,SA\,/\,DA}$	V407A / S409A / D395A
2nd interface	VLY$^{NA\,/\,DA\,(GG)}$	N53A / D50A / G308A / G309A	VLY$^{NA\,/\,DA}$	N53A / D50A
	VLY$^{NA\,/\,DA\,/\,IA\,(GG)}$	N53A / D50A / I401A / G308A / G309A	VLY$^{NA\,/\,DA\,/\,IA}$	N53A / D50A / I401A
Both interfaces	VLY$^{EA\,/\,IA\,/\,VA\,(GG)}$	E400A / I401A / V407A / G308A / G309A	VLY$^{EA\,/\,IA\,/\,VA}$	E400A / I401A / V407A
	VLY$^{EA\,/\,IA\,/\,VP\,(GG)}$	E400A / I401A / V407P / G308A / G309A	VLY$^{EA\,/\,IA\,/\,VP}$	E400A / I401A / V407P
	VLY$^{EA\,/\,IA\,/\,VA\,/\,SA\,(GG)}$	E400A / I401A / V407A / S409A / G308A / G309A	VLY$^{EA\,/\,IA\,/\,VA\,/\,SA}$	E400A / I401A / V407A / S409A

Flow cytometry data on VLY mutant proteins' binding to CHO-CD59^{4F1} cells are presented in Figure 18, C. Binding of VLY^{GG} was held as a reference. Interestingly, only mutants carrying proline substitution (V407P, abbr. VP) shared significantly lower binding capabilities (Figure 18, C). For instance, VLY$^{VA\,/\,SA\,/\,DA(GG)}$ and VLY$^{EA\,/\,IA\,/\,VA(GG)}$ bound the cells to a similar or even

higher extent. However, analogous mutants bearing the substitution to proline, instead of alanine, namely $VLY^{VP \, / \, SA \, / \, DA(GG)}$ and $VLY^{EA \, / \, IA \, / \, VP(GG)}$, expressed significantly poorer cell-binding activities.

Haemolytic properties of VLY mutant proteins described above were evaluated by haemolytic assay, and HD50 values were calculated. HD50 values were normalised by dividing them by the HD50 value of wild-type VLY (Figure 18, D). The highest differences in HD50 were seen in the case of proline substitution mutants (Figure 18, D). Haemolytic activity appeared to be more sensitive to the introduced mutations. For instance, the binding of $VLY^{VA \, / \, SA \, / \, DA(GG)}$ to cells did not differ from VLY^{GG} while HD50 of its analogue $VLY^{VA \, / \, SA \, / \, DA}$ showed 10-fold lower haemolytic activity.

The mutagenesis data suggest that only the 1st interface proposed for ILY by Johnson et al. plays an important role in VLY pore formation and is based on the β-sheet extension. The disruption of intermolecular β-sheet can be easily disrupted by single proline substitution and strengthened by additional mutations.

6 Generation of recombinant CD59

For a more in-depth study of the interplay between VLY and CD59, we decided to generate a recombinant CD59 protein. Recombinant CD59 was produced in a mammalian cell expression system.

We cloned a gene encoding CD59 into pHLsec vector bearing a signal sequence to transport the target protein into the growth media. The gene did not contain a GPI-anchor attachment sequence. The internal known N-glycosylation site Asn-18 was mutated into Gln. The gene of CD59 was fused with C-terminal His-tag. Small-scale expression trial transiently transfecting HEK293T cells showed that protein is expressed and secreted into the media, but its amount was not high enough. One of the ways to increase the level of expression was to introduce an artificial N-glycosylation site at the C-terminus of the protein. 6xHis-tag was used for the first step of purification protocol using nickel-chelating affinity chromatography.
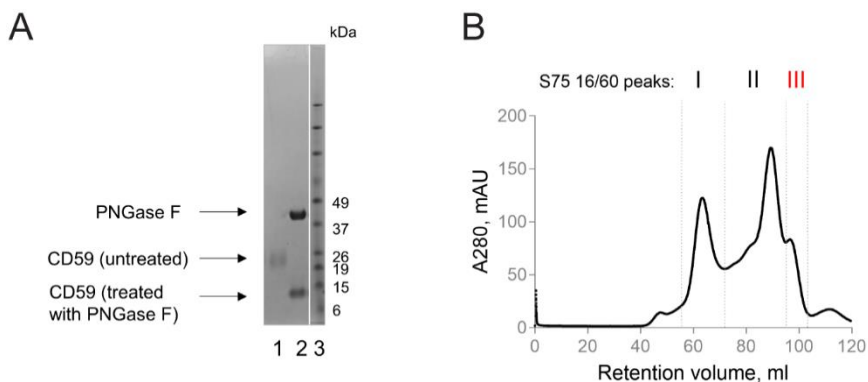
Figure 19. Artificially introduced C-terminal N-linked glycan can be cleaved by PNGase F glycosidase, and active form of CD59 can be purified by size-exclusion chromatography. A – SDS-PAGE of CD59 sample before cleavage by PNGase F and after; lane 1 – CD59 sample before treatment with PNGase F; lane 2 – CD59 cleaved by PNGase F, lane 3 – molecular marker PageRuler™ 26619. B – size-exclusion chromatogram of CD59 sample after cleavage by PNGase F; I, II, III highlights multiple UV absorption (280 nm) peaks of pure CD59, whereas only the third peak was found functionally active; Superdex 75 16/60 column was used.

We tested whether it was possible to cleave the artificially introduced N-linked glycan. The successful glycan cleavage was achieved using PNGase F glycosidase (Figure 19, A). We chose to use this strategy for the expression of CD59 for further study. The second purification step was carried out using size-exclusion chromatography. Pure CD59 was eluted in three major peaks from Superdex 75 size-exclusion column (Figure 19, B). Only fractions from the third peak (marked in red) were active in the liposome leakage experiment described in *Methods* 9.3 section.

7 VLY is a monomer in solution

PFO was shown to form antiparallel dimers in solution (Gilbert, 2005; Rossjohn et al., 2007). Thus, one of the hypotheses regarding this fact was related to the state of VLY in solution. We investigated whether CD59 may affect the state of VLY in solution and therefore unlock VLY molecules to bind to the membrane or oligomerise in solution.

To investigate the functional significance of VLY-CD59 interaction, we performed analytical ultracentrifugation (AUC) experiment. Using sedimentation velocity analysis, we assessed the state of VLY alone and after mixing it with soluble CD59. Firstly, we found that even at high concentrations (100 µM) VLY is a monomer – in continuous c(s) distribution,

its sedimentation coefficient is around 3.6 S (Figure 20). Using two-dimensional $c(s,f/f_0)$ analysis, the identity of the monomeric peak was confirmed via its molecular weight, which was determined as ~50kDa. Secondly, we failed to observe a significant amount of higher oligomeric particles either when analysing VLY alone or after mixing VLY with a 5-fold molar excess of soluble CD59 (Figure 20).
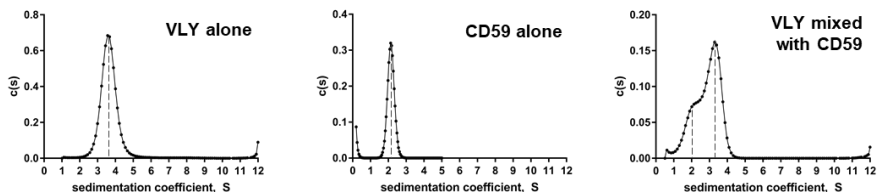
Figure 20. VLY is monomeric in solution. Analytical ultracentrifugation, using sedimentation velocity analysis of VLY, CD59 and the mixture of both, was carried out; the continuous c(s) distributions were plotted and curve-fitted using GraphPad Prism. VLY alone stays in the monomeric state in solution. The species of higher oligomeric order in either of the sample was not observed.

Thus, we concluded that VLY is monomeric even at 100 µM (5.6 mg/ml) concentration, and soluble CD59 is not capable of unlocking VLY oligomerisation.

8   CD59 can be reconstituted on the surface of the liposomes

To further investigate the role of CD59 in VLY pore formation, we aimed to make a simplified membrane model system that would have CD59 attached to it.
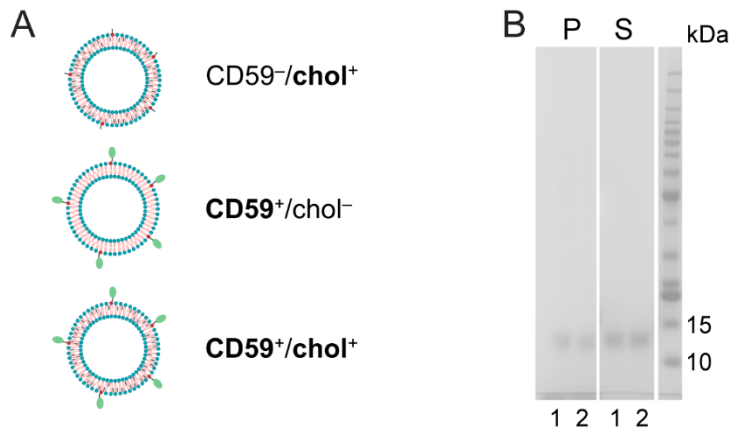
Figure 21. 6xHis-tagged CD59 binds to 18:1 DGS-NTA(Ni) phospholipid containing liposomes. A – schematic depiction of the liposomes used in the study. B – SDS-PAGE gel of the pellet (P) and supernatant (S) fractions of co-sedimentation assay; Lanes 1 – POPC/POPS/cholesterol/DGS-NTA(Ni) (69 mol%/10 mol%/20 mol%/1 mol%) liposomes were used; lanes 2 – POPC/POPS/DGS-NTA(Ni) (79 mol%/20 mol%/1 mol%) liposomes were used; M – unstained BenchMark ladder (Thermo Fisher Scientific, Cat. No. 10747012).

We designed a strategy to attach recombinant CD59 to the surface of artificial unilamellar liposomes (Figure 21, A). Recombinant CD59 described above was directly attached to NTA(Ni)-modified lipids through the C-terminal 6xHis-tag. Liposomes were prepared as previously discussed, with the addition of 1 % of 18:1 DGS-NTA(Ni) lipids into their composition. The attachment of CD59 was demonstrated by the co-sedimentation assay – pelleting liposomes after incubation with CD59 and running SDS-PAGE of the pellet and supernatant fractions. A fair amount of CD59 co-sedimented together with liposomes compared to CD59 that remained in the supernatant (Figure 21, B).

9   CD59 triggers VLY oligomerisation

As we previously found that soluble CD59 fails to unlock VLY oligomerisation in solution, we proceeded to use liposomes with reconstituted

CD59. Basic liposome composition used in the experiments below was POPC:cholesterol:DGS-NTA(Ni) (59 mol%/40 mol%/1 mol%) or POPC:DGS-NTA(Ni) (99 mol%/1 mol%) that were either preincubated with CD59 or not, depending on the experiment.

Firstly, we incubated VLY with liposomes bearing CD59, but no cholesterol (hereafter, CD59$^+$/chol$^-$) and visualised the samples using negative-stain transmission electron microscopy. Incomplete ring-shaped oligomers were observed that did not reflect functional pores as most of the oligomers were fallen off the liposomes (Figure 22, A). As resistance to SDS is indicative of the stage of oligomer maturity, we ran the samples on SDS-AGE. No higher oligomeric species were observed (Figure 22, B). Thus, the oligomers were sensitive to SDS, suggesting that the oligomers observed were intermediate prepores lacking the capability to perforate the membrane.
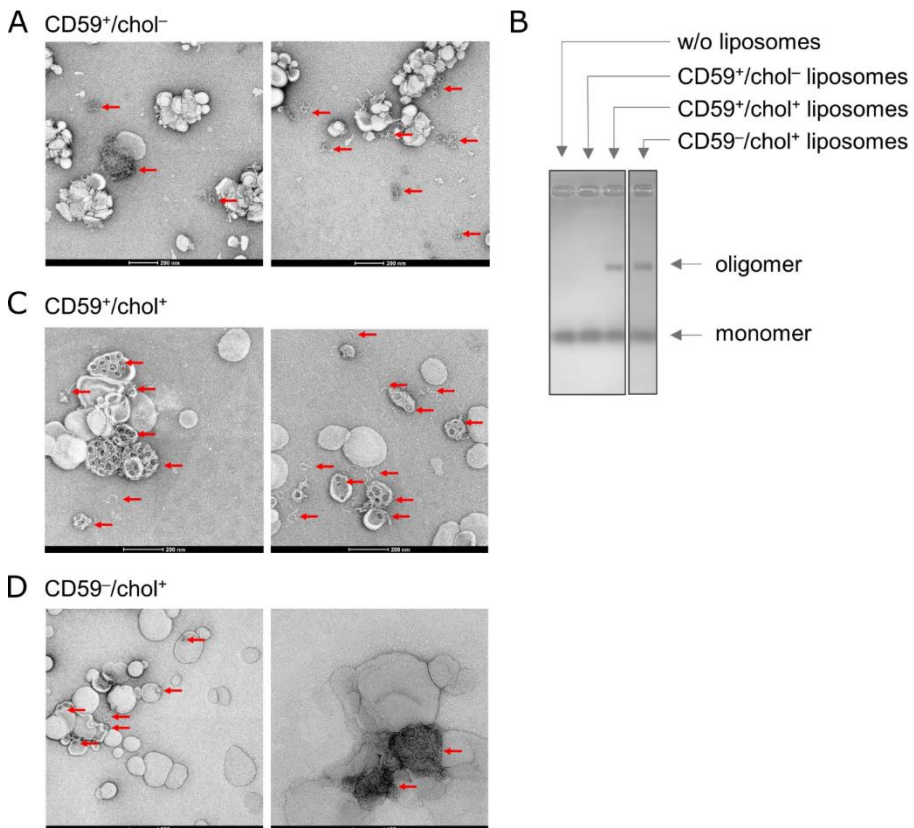
Figure 22. CD59 triggers SDS-sensitive vaginolysin (VLY) oligomer formation. A – representative negative-stain EM images of CD59$^+$/chol$^-$ liposomes preincubated with VLY; B – SDS-agarose gel of liposomes preincubated with VLY; C – representative negative-stain EM images of CD59$^+$/chol$^+$ liposomes preincubated with VLY; D – representative negative-stain EM images of CD59$^-$/chol$^+$ liposomes preincubated with VLY.

When CD59-bearing liposomes contained cholesterol (CD59$^+$/chol$^+$), incubation with VLY resulted in visually clear oligomers perforating the membrane observed in EM images (Figure 22, C). Cholesterol-rich liposomes lacking CD59 (CD59$^-$/chol$^+$) were capable of inducing visually observable VLY oligomers, which were seen in EM images (Figure 22, D). These oligomers were SDS-resistant by forming a distinct band on SDS-AGE gel (Figure 22, B). This is in agreement with the previous observation using DOPC/cholesterol (60 mol%/40 mol%) liposomes (*Results* 3 section).

10 CD59 enhances VLY pore-forming activity

To prove the functionality of pores, observed in negative-stain EM images, we encapsulated fluorescent dye sulforhodamine B (SRB) inside the liposomes, where dye's concentration was high enough to self-quench its fluorescence. The increase in fluorescence intensity of the sample is directly proportional to SRB release from liposomes and is indicative of the bilayer disruption by pore formation (Faudry et al., 2013).

We tested whether the treatment of these SRB-loaded liposomes with VLY would perforate the membrane and release the dye out of them (Figure 23, A). As expected, CD59$^-$/chol$^+$ and CD59$^+$/chol$^+$ liposomes were disrupted by VLY (Figure 23, B). Furthermore, CD59 had a clear impact on the increased liposome leakage over the broad range of VLY concentrations – from 5 nM to 325 nM (Figure 23, B). The same amount of VLY was able to perforate only a fraction of CD59$^-$/chol$^+$ liposomes, thus demonstrating the enhancer nature of CD59. The treatment of CD59$^+$/chol$^-$ liposomes with VLY did not induce any dye leakage, implying that the oligomers were early prepores (Figure 23, B).

We further tested the impact of CD59 on the liposome leakage by PLY (CDC that is non-dependent on CD59) to control for the unexpected effects of attaching CD59 to the liposomes in the manner described. CD59 did not affect the liposome leakage induced by PLY (Figure 23, C). The extent of liposome leakage was directly proportional to the concentration of PLY (Figure 23, C).
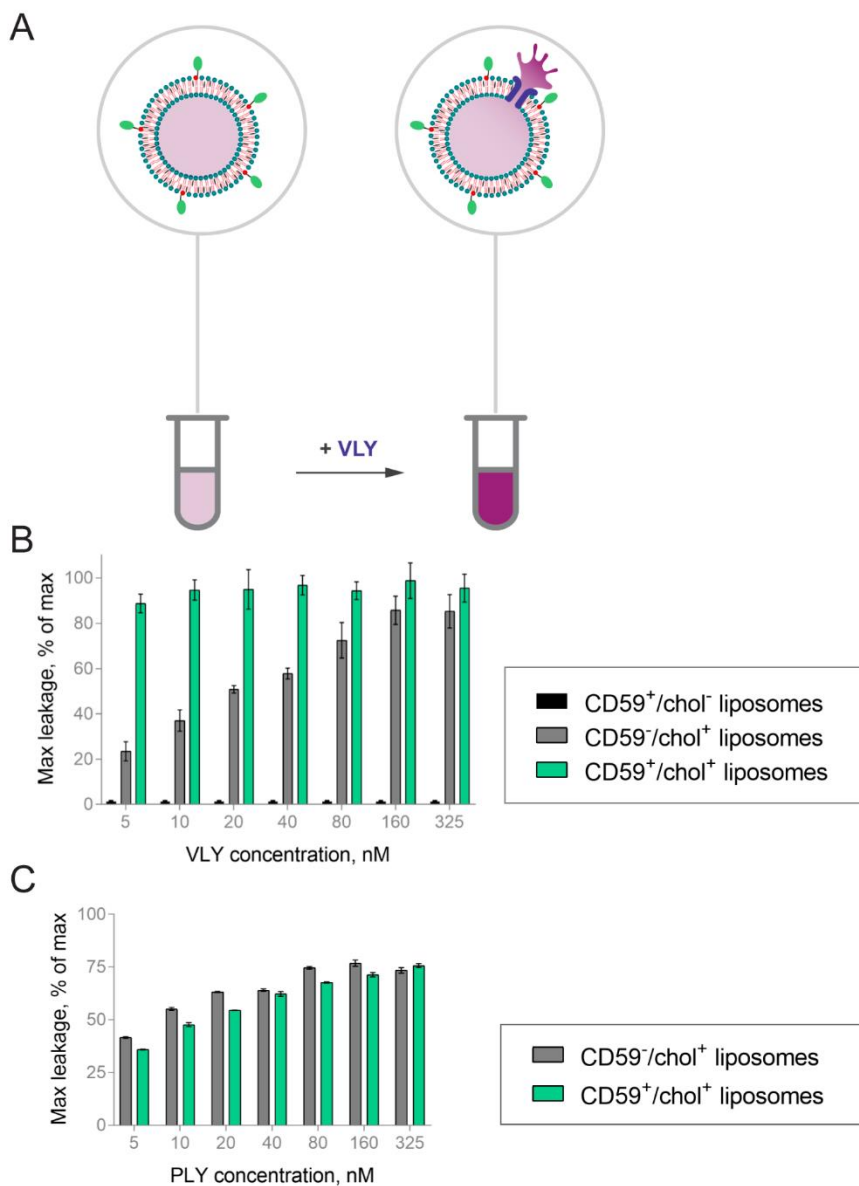
Figure 23. CD59 increases maximum sulforhodamine B (SRB) leakage from liposomes treated with vaginolysin (VLY) but is not sufficient to induce VLY pore formation. A – schematic depiction of the liposome leakage assay; violet colour intensity indicates the level of SRB dye fluorescence. B – bar plots show maximum leakage of liposomes treated with VLY concentrations ranging from 5 nM to 325 nM; error bars show standard deviation; N=4. C – bar plots show maximum leakage of liposomes treated with PLY concentrations ranging from 5 nM to 325 nM; error bars show standard deviation; N=4.

Thus, CD59 reconstituted on liposomes was able to induce VLY prepore formation. However, cholesterol was necessary for functional pores to be

formed. Furthermore, CD59 acted as an enhancer for the leakage from the liposomes treated with VLY, but not PLY.

10.1 Kinetics of VLY pore-forming activity on liposomes

We further postulated that we could elucidate the role of CD59 by monitoring VLY pore formation kinetics on liposomes of different compositions, i.e. containing either cholesterol, CD59 or both in the membrane, as used above.

To perform such observations, we monitored liposome leakage in near real-time. We optimised an assay to monitor the dye leakage from liposomes treated with VLY over 1.5 hours. The profile of the leakage over time resembled exponential two-phase association followed by the plateau of maximal leakage that remained steady over a long time. We evaluated the fast-phase rate constants (KFast) of liposome leakage as this allowed us to roughly compare VLY pore formation on liposomes of different composition.

We found a significant increase in the rate of $CD59^+/chol^+$ liposome leakage compared to $CD59^-/chol^+$ liposomes (Figure 24, A). In VLY concentration range of 5 nM – 325 nM the KFast of fitted two-phase curve varied from 0.27 to 0.79 min^{-1} and from 0.96 to 1.61 min^{-1} for $CD59^-/chol^+$ and $CD59^+/chol^+$ liposomes, respectively (Figure 24, B).
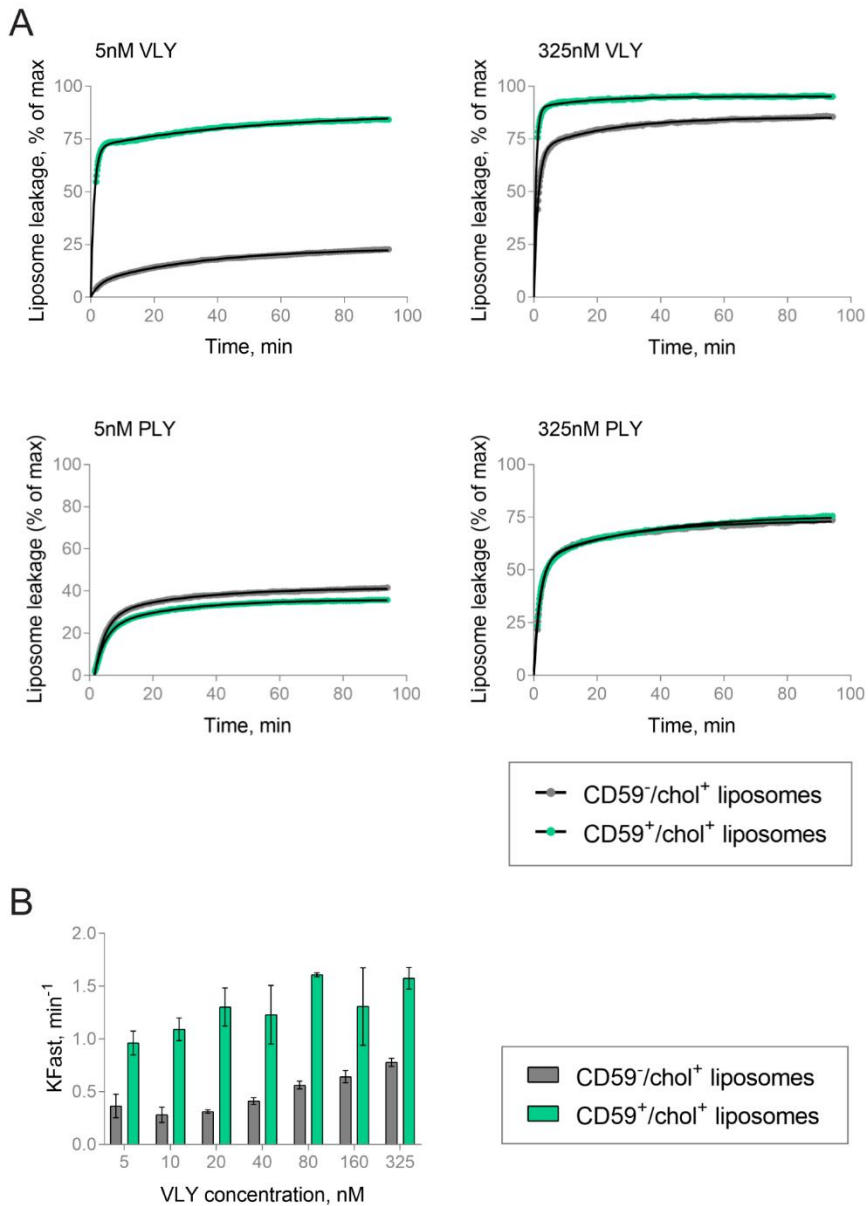
Figure 24. CD59 expedites the rate of liposome leakage treated with vaginolysin (VLY). A – representative profiles of liposome leakage over time after treatment with 5 nM and 325 nM VLY or PLY; data points were fitted with two-phase accumulation curve using GraphPad Prism. B – Fast-phase rate constants (KFast) of liposome leakage for CD59+/chol+ and CD59−/chol+ liposomes treated with VLY ranging in concentration from 5 nM to 325 nM; KFast was calculated from two-phase accumulation model using GraphPad Prism; error bars show standard deviation; N=4.

CD59 increases the KFast of the VLY-treated liposome leakage multiple times. This suggests that the role of CD59 in VLY pore formation is related to the rate of pore formation.

10.2 Increasing the distance of CD59 from the membrane reduces VLY pore-forming activity

We examined whether the orientation of CD59 in the context of the membrane is important in the enhancement of VLY activity. We aimed to sever VLY contacts with cholesterol from those with CD59 in time or space. To achieve this, we decided to place CD59 farther away from the membrane.
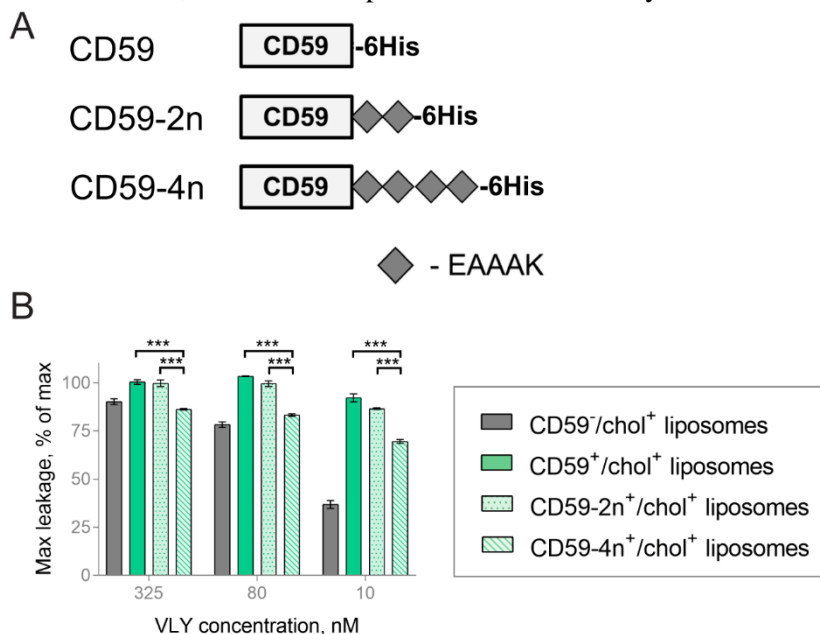
Figure 25. Vaginolysin pore-forming activity decreases as CD59 is placed farther away from the membrane. A – schematic representation of CD59 constructs used to distance the receptor from the membrane. B – liposome leakage after treatment with VLY concentrations of 10 nM, 80 nM, 325 nM visualised as maximum liposome leakage; t-test (alpha=0.05) p<0.001; error bars show standard deviation; N=4.

We generated two CD59 variants (hereafter referred to as CD59-2n$^+$ and CD59-4n$^+$) by introducing rigid helical linkers containing two and four repeats of EAAAK, respectively, at the C-terminal end of the CD59 protein (Figure 25, A). We showed that elongated CD59 binds to 1:18 DGS-NTA(Ni) containing liposomes to a similar extent to CD59 without a linker. After incubation of SRB-loaded cholesterol-rich liposomes bearing CD59-2n$^+$ and CD59-4n$^+$ (CD59-2n$^+$/chol$^+$ and CD59-4n$^+$/chol$^+$), we performed liposome leakage assay by treating the liposomes with serial dilutions of VLY ranging

from 5 nM to 325 nM, as described above for CD59$^+$/chol$^+$ liposomes (Figure 25, B). There was no significant difference in maximum liposome leakage in the case of CD59-2n$^+$/chol$^+$ liposomes, although CD59-4n$^+$/chol$^+$ liposomes did reduce the extent when compared to CD59-2n$^+$/chol$^+$ (Figure 25, B).

These results suggest that CD59 has to be at the correct distance away from the membrane. While some allowance can be made for the distance (CD59-2n$^+$), it seems that CD59 serves to bring VLY in proximity to the cholesterol in the membrane, which is hindered by the increased distance from the membrane. However, other, unforeseen, structural dynamics may be at play and cannot be yet excluded.

11 Detection of VLY in clinical samples

A case study was carried out in collaboration with Universite Pierre et Marie Curie to characterise *G. vaginalis* strain isolated from a 19-year-old female patient's blood. The patient experienced severe toxic encephalopathy that was related to a very rarely seen outcome of *G. vaginalis* infection – bacteremia (Flórez et al., 1994; Reimer and Reller, 1984). In collaboration with Lithuanian National Public Health Surveillance Laboratory (Vilnius, Lithuania), we succeeded in isolating *G. vaginalis* clinical strain, hereafter GV37, and cultivating it *in vitro*. One of the aims was to define the level of VLY secretion as a possible predictor of this strain's virulence when compared with other clinical isolates that are not related to the phenotype of severe bacteremia.
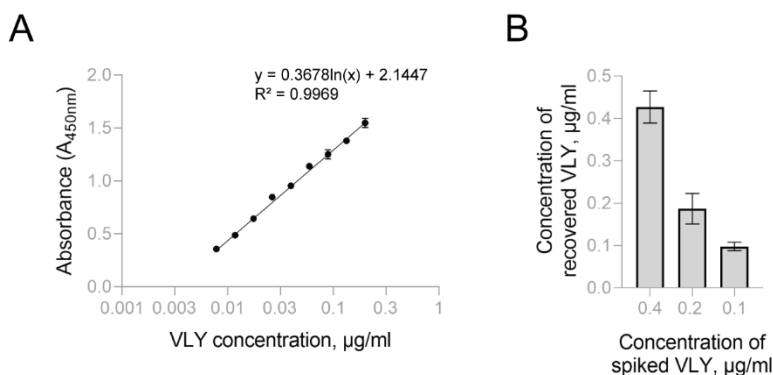
Figure 26. Sandwich-based ELISA is suitable for quantitative VLY detection in *G. vaginalis* growth media. A – representative calibration curve generated using serial dilutions of recombinant VLY detected by sandwich-based ELISA; error bars show standard deviation; N=3. B – barplot visualises recovery of spiked concentrations of recombinant VLY, which was diluted in fresh *G. vaginalis* growth media; error bars show standard deviation; N=3.

We optimised a quantitative detection system for VLY in *G. vaginalis* growth media. The detection was carried out using sandwich-based ELISA relying on VLY-specific binding of two non-competitive mouse anti-VLY MAbs (clone 12E1 as a coating MAb and clone 9B4 conjugated to HRP as a detection MAb) (Zvirbliene et al., 2010). The concentrations of VLY in *G. vaginalis* growth media was calculated from the calibration curves generated using serial dilutions of recombinant VLY protein (Figure 26, A). To assess the accuracy of the detection system and possible hindrance of VLY by the growth media components, we added known concentrations of recombinant VLY and measured them using our assay. We confirmed that the hindrance was minor, and the system is suitable for quantitative measurement of VLY concentration in the *G. vaginalis* growth media (Figure 26, B).
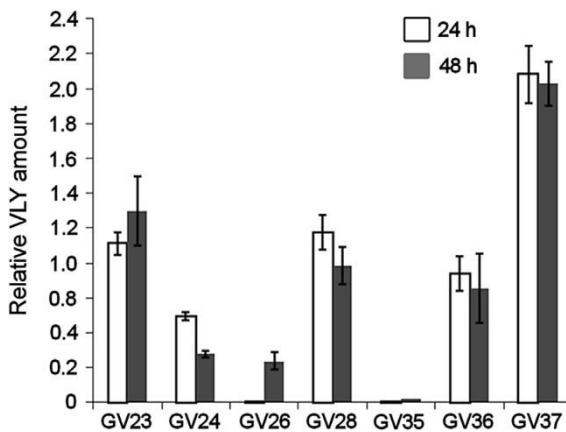
Figure 27. Clinical *G. vaginalis* strain GV37 possessed increased secretion of vaginolysin (VLY) when cultured *in vitro*. The relative amount of secreted VLY in the supernatants of clinical *G. vaginalis* strains (GV23, GV24, GV26, GV28, GV35, GV36, GV37) cultured *in vitro* was evaluated at specific time interval (24 h or 48 h) and normalised to OD_{600} by calculating the ratio of VLY concentration (µg/ml) to OD_{600}; error bars show standard deviation; N=3 (Tankovic et al., 2017).

The concentrations of VLY that were evaluated in the supernatants of clinical *G. vaginalis* growth media were normalised by dividing them by the optical density values (OD_{600nm}) defining the density of bacterial biomass in the sample. *G. vaginalis* isolate GV37 displayed a markedly higher secretion of VLY compared to other clinical isolates (Figure 27).

We propose that enhanced secretion of VLY in the case of *G. vaginalis* isolate GV37 may have contributed to a rarely observed severe bacteremia.

DISCUSSION

As CDCs are produced by a variety of bacterial pathogens, they are thought to play an important role in the pathogenesis of infectious diseases. More and more data appear to corroborate this idea, and new roles for CDCs in promoting bacterial virulence are found (Los et al., 2013). There are many hypotheses on the role of vaginolysin (VLY) in *Gardnerella vaginalis* virulence (Gelber et al., 2008; Nowak et al., 2018). However, an insufficient amount of direct evidence on its pathogenic effects has been found to date. During our study, we isolated a *G. vaginalis* strain from the blood of a 19-year old patient who experienced a severe toxic encephalopathy associated with *G. vaginalis* bacteremia. The strain secreted elevated levels of VLY when cultured *in vitro* compared to other strains unrelated to such a severe clinical outcome. As *G. vaginalis* genome variability is high between different strains, it is difficult to predict the pathogenic potential of a given strain on genetic grounds (Schellenberg et al., 2017). It is, however, hypothesised that the levels of secreted VLY might be directly related to the pathogenicity of the bacteria (Nowak et al., 2018). One of the classifications suggested up to date sorts *G. vaginalis* strains into four clades (Ahmed et al., 2012; Jayaprakash et al., 2012; Schellenberg et al., 2016). No clear correlation is found between the defined clades and their pathogenicity. However, one of the clades distinguishes itself as low-virulence, perhaps due to low levels of sialidase and VLY. Moreover, the pathogenic relevance of *G. vaginalis* is challenging to demonstrate as, despite its abundance, it is only one of many players of vaginal microbiota imbalance. The field is also lacking animal models that would have multicomponent microbiota similar to human microbiota. However, it may be the case that virulence factors in vaginal microbiota imbalance are species-specific or at least species preferential, and thus, the potential of any animal model might be limited at least.

This thesis was mainly focused on studying the pore-forming ability of VLY and the mechanism behind its binding to the cell surface, oligomerisation and membrane perforation of the targeted cell. VLY lyses erythrocytes from different species with different efficiencies, with a clear preference for human erythrocytes (Cauci et al., 1993). VLY species preference is mediated by human complement regulatory protein CD59 (Gelber et al., 2008). We investigated this previously observed phenomenon to understand the role of CD59 in VLY pore formation.

Firstly, transfected non-human cells (CHO) expressing GPI-anchored human CD59 were more susceptible to VLY-mediated lysis, similar to ILY-mediated lysis but distinct from PLY (*Results* Figure 12). The

mechanistic study on ILY carried out in parallel to our study by another group lead to a model for the ILY pore formation (Boyd et al., 2016). The model states that CD59 serves as primary contact with the cellular membrane and is required for oligomerisation, whereas during the vertical collapse and membrane perforation ILY disengages from CD59 and interacts with cholesterol (*Literature overview* Figure 6)

Our study on VLY highlighted the differences between the cytolytic mechanism of ILY and VLY. VLY can bind to the cell membrane in two distinct ways. One is through the interaction with human CD59 and the other one through cholesterol. Thus, our data support the attribution of VLY to a group of atypical CDCs in the mode of receptor-based classification introduced by Tabata et al. (Tabata et al., 2014). Notably, GPI-anchored CD59 proteins are known to colocalise with cholesterol in transient lipid rafts in the membrane (Kinoshita et al., 2017; Sezgin et al., 2017). Cholesterol is a hallmark of the eukaryotic cell membrane and the usual membrane target of CDCs, whereas CD59 proteins are unique for different species and do not share sequence-based or functional interchangeability with more distantly related species (Nagamune et al., 1996). The ability of VLY to engage both human protein CD59 and cholesterol when binding the target membrane shows only a partial tropism or preference for human cells whereas ILY strictly depends on the interaction with human CD59 when binding to the cell surface.

We found that apart from binding, CD59-bearing CHO cells were more susceptible to VLY pore formation compared to untransfected CHO cells. Therefore, we hypothesised that VLY binding to the cell surface might be the critical step that governs its cytolytic activity. The high toxin affinity for the membrane may play an essential role for all CDCs in physiological conditions, where the toxin concentration is likely to be low, especially during early infection. We showed that CD59 containing cells (HEK293, CHO-CD59) could attract much more VLY than untransfected CHO cells (*Results* Figure 16, B, C). The higher the number of CD59 molecules was exposed on the surface of the cells, the more VLY was bound to those cells (*Results* Figure 16, E). Thus, the interaction between VLY and CD59 directly influences and enhances VLY affinity for the membrane.

Furthermore, negative-stain EM visualisation of the liposomes, which had CD59 attached to them but lacked cholesterol, showed that CD59 could trigger VLY oligomerisation. However, the oligomers formed in the absence of cholesterol were early prepores – sensitive to SDS and incapable of perforating the membrane. This finding is in agreement with the model proposed for ILY pore formation, highlighting the role of CD59 in the initial

stages of pore formation (Boyd et al., 2016). The closer look into the oligomer interface with CD59 would benefit the further understanding of CD59's role. Unfortunately, we were not able to evaluate the stoichiometry between VLY and CD59 to detect how many molecules of CD59 are required to induce VLY oligomerisation. This feature is not known for ILY or any other CD59-dependent CDC. We hypothesise that VLY:CD59 ratio is far from 1:1 and not every VLY molecule has to bind to CD59.

Although the more CD59 cells had, the more VLY they attracted, but more CD59 did not enhance the overall cell lysis. Interestingly, the end-point measurement of liposome leakage revealed that the presence of CD59 ($CD59^+/chol^+$) causes maximal liposome leakage independent of VLY concentration in the range tested. In contrast, in the case of cholesterol-rich liposomes lacking CD59 ($CD59^-/chol^+$), a clear VLY concentration-dependent pattern of liposome leakage was observed. Next, we investigated the kinetic aspect of the liposome leakage. Liposome leakage over time followed a biphasic exponential trend of increasing overall leakage with increasing VLY concentration. Aside from the maximal liposome leakage, we observed 2- to 3-fold higher rate constants in perforation of the $CD59^+/chol^+$ liposomes compared to $CD59^-/chol^+$ liposomes.

Independently from CD59, cholesterol can successfully mediate VLY pore formation even though the amount of VLY needed to reach the level of pore formation similar to the one enhanced by CD59 is significantly higher. Comparing CHO and CHO-CD59 cells, at least 30 times more VLY is required to get the same lysis outcome in CHO cells.

Interestingly, our study indicates that oligomers formed in both cases may be similar. We managed to obtain SDS-resistant VLY oligomers upon treating cholesterol-rich liposomes with VLY both in the presence and absence of CD59. Surprisingly, after heating the samples, the oligomers formed a compact band on SDS-agarose gel, suggesting a specific single species of SDS- and heat-resistant oligomers. Besides, the electrophoretic mobility of SDS and heat-treated oligomers did not depend on the presence of CD59. Unfortunately, we were not able to estimate the size of the oligomers. However, we observed the leakage of liposome-encapsulated sulforhodamine B dye both in the presence and absence of CD59 that indicated that the obtained SDS- and heat-resistant oligomers were functional pores. In addition to findings directly related to our work, we demonstrated that simple unilamellar liposomes could serve as a platform for VLY pore formation.

In the studies with artificial liposomes, cholesterol concentration in the bilayer needs to be above 30-40 molar per cent of the total lipids for VLY pore to be formed. This requirement is likely related to the amount of cholesterol

that is surface-exposed and, hence, accessible from the solution, although the threshold for the amount of cholesterol depends on the rest of the lipids as they influence the accessibility of cholesterol (Flanagan et al., 2009). Furthermore, cholesterol influences the physical properties of the membrane, such as fluidity and thickness. This challenges the understanding of CDC interaction with the cholesterol because cholesterol distribution across the bilayer is uncertain. On the other hand, CDCs can be used as a tool to map or track membrane cholesterol accessible from solution (Johnson et al., 2017a).

It is unclear whether VLY binds to cholesterol or CD59 first or whether binding occurs simultaneously. Interestingly, CD59-dependent CDCs contain an atypical undecapeptide (UDP) sequence. Crystal structure of monomer-locked VLY (VLY^{ML}) in the complex with CD59 revealed that UDP could occupy two distinct conformations. One of the conformations is similar to that of ILY, and the other is similar to that of PFO (Lawrence et al., 2016). If the UDP could switch between these conformations depending on the membrane in its proximity, it may tailor the way VLY binds to the membrane that contains CD59 or is cholesterol-rich only.

VLY homology modelling based on the structure of ILY and ILY-CD59 complex that at the time was the only solved CDC-CD59 complex structure allowed us to predict and determine the positions of the interface between VLY and CD59 (Johnson et al., 2013). The first ILY-CD59 crystal structure suggested that two interfaces may exist between the two proteins, even though any clear mechanistic evidence was not provided (Johnson et al., 2013). We aimed to disrupt these interfaces between VLY and CD59. We succeeded in disrupting the 1st interface. Interestingly, even a single amino acid substitution to proline in the β-strand of VLY D4 domain resulted in the hindrance of the mutant binding to CHO-CD59 cells. However, we could not find any clear evidence to prove the existence of the 2nd interface. Our data turned out to be in a strong agreement with the crystal structure of VLY-CD59 complex that found only one interface (Figure 28) (Lawrence et al., 2016). Moreover, mutations in VLY D4 domain, that strengthened the interaction with CD59 did not enhance VLY haemolytic activity but, oppositely, decreased it. This finding is in accordance with the view that PFPs need to release their protein receptors during the membrane perforation as it was previously demonstrated for ILY (LaChapelle et al., 2009).
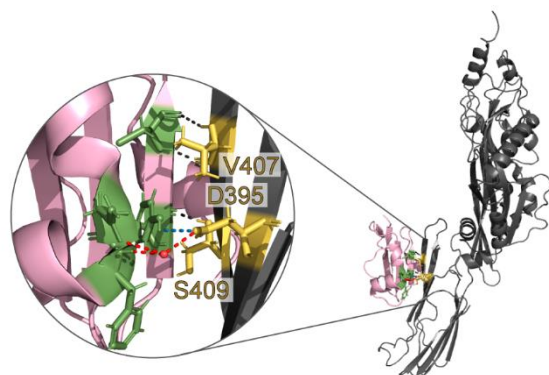
Figure 28. Key amino acids maintaining vaginolysin (VLY) interaction with CD59. VLY is coloured in grey; CD59 – in pink. Our mutagenesis study of VLY revealed D395, V407, S409 (depicted in yellow sticks) as key amino acids in VLY and CD59 interface, which are visualised in the crystal structure of VLY-CD59 complex (PDB ID: 5IMY, Lawrence et al., 2016). These amino acids participate in hydrogen bonding between VLY D4 domain and CD59. Backbone-based hydrogen bonds are visualised in black, water-based hydrogen bonds – in red, hydrogen bonds through side chains – in blue dashed lines.

Moreover, both membrane partners of VLY are known to cluster in lipid rafts suggesting that CD59 may help to attract VLY molecules to cholesterol. Pore formation at the distinct localisation in a particular membrane microdomain may be much more efficient as the physical properties of the bilayer differ due to its composition. Cholesterol clustering is known to thicken the bilayer as it changes the organisation of the surrounding phospholipids into a more ordered state. Huge β-barrel structures of CDCs are likely to be able to perforate membranes of a limited range of thicknesses and, therefore, targeting particular membrane microdomains may help to meet this requirement.

Thus, VLY dependence on CD59 is not strict *in vitro* as we showed in this study. However, the picture *in vivo* might be quite different. For instance, arcanolysin form *Arcanobacterium haemolyticum* relies on sphingomyelin-specific phospholipase D to enhance its rate of pore formation (Gellings and McGee, 2018). Sphingomyelin and cholesterol also tend to cluster in lipid rafts. Moreover, due to membrane packing, sphingomyelin largely obscures cholesterol. Therefore phospholipase D removes the choline head of sphingomyelin and exposes cholesterol for arcanolysin to act upon (Gellings and McGee, 2018). We propose that, similarly, VLY may use CD59 not only as a species-specific receptor but also as a lipid raft beacon that serves to guide VLY to cholesterol.

The proper alignment between the β-strands extending β-sheets is believed to be required for a stable pore to form. π-stacking interaction between

neighbouring monomers was shown to play an essential role in the case of PFO between the β1- and β4-strands in D3 domain (Ramachandran et al., 2004). A large number of CDCs, including VLY, do not contain one of the aromatic amino acids that could participate in π-stacking, which was shown to stabilise the monomer-monomer interface of PFO. Moreover, mutating the existing VLY aromatic residue (Tyr-165) to alanine did not affect VLY haemolytic activity. As this suggested that π-stacking interaction did not play a part in the establishment of the monomer-monomer interface, we investigated whether the VLY monomer-monomer interface was typical in comparison to other CDCs. Results of site-directed mutagenesis within β4-strand showed the necessity of the backbone -NH hydrogen for hydrogen bonding in the β-sheet extension as even single substitution to proline significantly decreased VLY haemolytic activity. However, it is still not obvious how the proper register between the β1- and β4-strand is ensured.

Moreover, we hypothesised that CD59 serves as a tether to force VLY monomers into the correct orientation against the plane of the membrane and therefore increases oligomerisation by increasing the chance that two monomer molecules meet in the correct orientation, simply because only one of them has degrees of freedom and the other is locked in position. This may allow the oligomer to grow efficiently to become large enough to perforate the membrane. To answer this, we introduced linkers at the C-terminal end of CD59. When we attached a distanced CD59 to cholesterol-rich liposomes, we still observed an enhancement of VLY pore formation compared to CD59$^-$/chol$^+$ liposomes in liposome leakage assay. When the length of the linker was increased, liposome leakage decreased – although not much. It may be the case that we have failed to place CD59 far enough to get a definitive answer. However, it is clear that CD59 attracts and likely concentrates and/or orients VLY with respect to the membrane.

However, the role of CD59 to attract and properly orient VLY molecules cannot be its only function, as even alone, it induces prepore formation on the membrane, as discussed above. Therefore, we investigated the role of CD59 in unlocking VLY pore-formation. For example, PFO forms antiparallel dimers in solution that are used to avoid premature oligomerisation before encountering the membrane. PFO dimers are subsequently disrupted by binding to the cholesterol-rich membrane (Gilbert, 2005; Rossjohn et al., 2007). Hence, we hypothesised that CD59 might work similarly to separate preformed VLY dimers. If VLY dimers exist, the enhancement of the cytolytic activity we observed could be attributed to CD59 disrupting the dimers. Using analytical ultracentrifugation, we demonstrated that VLY is a monomer in solution even at a relatively high concentration. Furthermore, we

did not observe any significant higher oligomeric state products after incubating the toxin with CD59 in solution. This suggests that interaction with CD59 itself does not induce sufficient changes in the VLY molecule itself or if it induces these changes, they may not be enough to trigger VLY oligomerisation in solution. All these considerations strengthen the hypothesis that CD59 might be essential in concentrating and orientating VLY on the plane of the membrane (Figure 29).
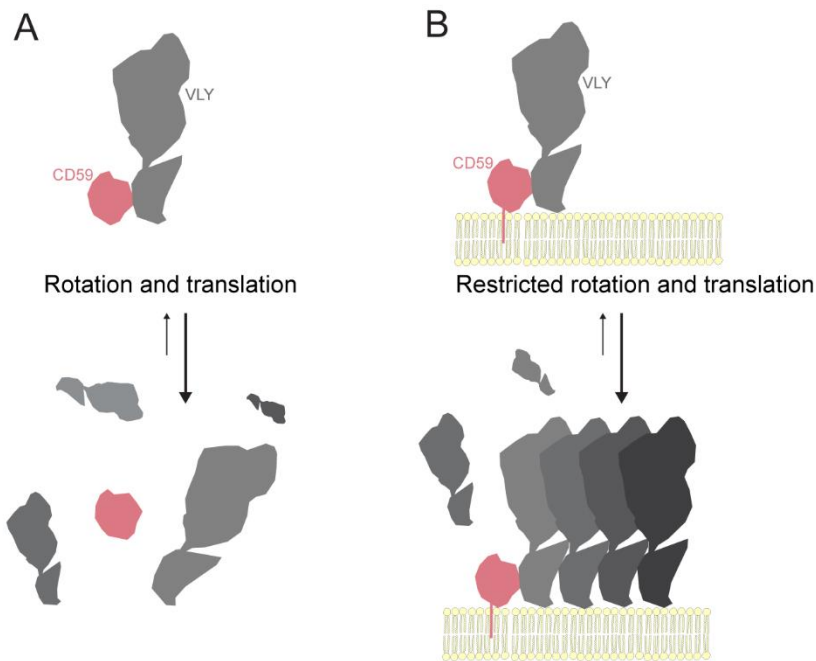
Figure 29. Proposed model of membrane-bound CD59 role in VLY concentration and orientation. A – in the hypothetical case of soluble CD59, VLY may form short-lived complexes with it; however, before this complex could meet another VLY monomer in a correct orientation and position, it dissociates. This happens because all free monomers have rotational and translational degrees of freedom, and short-lived CD59-VLY complexes can rotate and translate as well. B – in the case of membrane-bound CD59, membrane-bound VLY (through the contacts with CD59 and cholesterol-rich membrane) has almost no degrees of freedom and are thus more likely to meet VLY monomers in a correct or close to correct orientation thus greatly facilitating oligomerisation. Explicitly, we hypothesise that CD59-VLY complexes or small oligomers do not survive long enough to reach a stable size, whereas, on the membrane, they do.

In this study, we present novel insights about VLY from *G.vaginalis*, which shares some key features with other CDCs but also has a unique dependence on CD59, that our findings help to explain. Furthermore, our attempts in disentangling the role of CD59 from the role of cholesterol bore

fruit in the realisation that the enhancer nature of CD59 in VLY pore formation likely resides in CD59 acting similar to a guide-post of lipid rafts and cholesterol therein. However, as CD59 alone fails to induce oligomerisation of VLY in solution, but readily does it when tethered to the membrane, we hypothesise, that it orients a growing oligomer against the plane of the membrane thus effectively reducing degrees of freedom of the whole pore-forming system (Figure 29).

CONCLUSIONS

1) Vaginolysin (VLY), similarly to pneumolysin, is able to lyse cells of non-human origin. In contrast to intermedilysin, VLY does not necessarily need human protein CD59 for its cytolytic activity.

2) Artificial liposomes bearing membrane-embedded cholesterol and human protein CD59, designed during this study, represent a suitable tool for the monitoring of VLY pore formation dynamics.

3) CD59 boosts the cytolytic activity of VLY by improving the affinity of VLY for cholesterol-rich membrane and accelerating VLY pore formation. Membrane-attached CD59 is able to initiate VLY oligomerisation, while cholesterol is required for VLY pore formation.

4) Cholesterol is necessary and sufficient for VLY pore formation, although, in the absence of CD59, notably higher amount of VLY is required for the same level of pore formation to be achieved.

5) VLY monomer-monomer interface is based on the β-sheet extension via hydrogen bonding between β1- and β4-strands in D3 domains of the respective monomers.

6) The interface between VLY and CD59 is based on the β-sheet extension via hydrogen bonding between CD59 and the D4 domain of VLY. The key amino acids of VLY involved in the interaction with CD59 are Val-407, Ser-409, Asp-395.

REFERENCES

1. Ahmed, A., Earl, J., Retchless, A., Hillier, S.L., Rabe, L.K., Cherpes, T.L., Powell, E., Janto, B., Eutsey, R., Hiller, N.L., et al. (2012). Comparative Genomic Analyses of 17 Clinical Isolates of Gardnerella vaginalis Provide Evidence of Multiple Genetically Isolated Clades Consistent with Subspeciation into Genovars. J. Bacteriol. *194*, 3922–3937.

2. Albert, A.Y.K., Chaban, B., Wagner, E.C., Schellenberg, J.J., Links, M.G., Van Schalkwyk, J., Reid, G., Hemmingsen, S.M., Hill, J.E., Money, D., et al. (2015). A study of the vaginal microbiome in healthy Canadian women utilizing cpn60-based molecular profiling reveals distinct Gardnerella subgroup community state types. PLoS One *10*, 1–21.

3. Alonzo, F., and Torres, V.J. (2014). The Bicomponent Pore-Forming Leucocidins of Staphylococcus aureus. Microbiol. Mol. Biol. Rev. *78*, 199–230.

4. Amino, R., Giovannini, D., Thiberge, S., Gueirard, P., Boisson, B., Dubremetz, J.F., Prévost, M.C., Ishino, T., Yuda, M., and Ménard, R. (2008). Host Cell Traversal Is Important for Progression of the Malaria Parasite through the Dermis to the Liver. Cell Host Microbe *3*, 88–96.

5. Amsel, R., Totten, P.A., Spiegel, C.A., Chen, K.C., Eschenbach, D., and Holmes, K.K. (1983). Nonspecific vaginitis: diagnostic criteria and microbial and epidemiologic associations. Am. J. Med. *74*, 14–22.

6. Anderluh, G., and Gilbert, R. (2014). MACPF/CDC Proteins - Agents of Defence, Attack and Invasion (Springer Netherlands).

7. Anderluh, G., and Lakey, J.H. (2008). Disparate proteins use similar architectures to damage membranes. Trends Biochem. Sci. *33*, 482–490.

8. Aricescu, A.R., Lu, W., and Jones, E.Y. (2006). A time- and cost-efficient system for high-level protein production in mammalian cells. Acta Crystallogr. Sect. D Biol. Crystallogr. *62*, 1243–1250.

9. Awad, M.M., Ellemor, D.M., Boyd, R.L., Emmins, J.J., and Rood, J.I. (2001). Synergistic effects of alpha-toxin and perfringolysin O in Clostridium perfringens-mediated gas gangrene. Infect. Immun. *69*, 7904–7910.

10. Bakrač, B., Gutiérrez-Aguirre, I., Podlesek, Z., Sonnen, A.F.P., Gilbert, R.J.C., Maček, P., Lakey, J.H., and Anderluh, G. (2008). Molecular determinants of sphingomyelin specificity of a eukaryotic pore-forming toxin. J. Biol. Chem. *283*, 18665–18677.

11. Balaj, L., Lessard, R., Dai, L., Cho, Y., Pomeroy, S.L., Breakefield, X.O., and Skog, J. (2011). NIH Public Access. Nat. Commun. *2*, 1–19.

12. Balashov, S. V., Mordechai, E., Adelson, M.E., and Gygax, S.E. (2014). Identification, quantification and subtyping of Gardnerella vaginalis in noncultured clinical vaginal samples by quantitative PCR. J. Med. Microbiol. *63*, 162–175.

13. Bavdek, A., Kostanjšek, R., Antonini, V., Lakey, J.H., Dalla Serra, M., Gilbert, R.J.C., and Anderluh, G. (2012). pH dependence of listeriolysin O aggregation and pore-forming ability. FEBS J. *279*, 126–141.

14. Bayraktar, R., Van Roosbroeck, K., and Calin, G.A. (2017). Cell-to-cell communication: microRNAs as hormones. Mol. Oncol. *11*, 1673–1686.

15. Bhakdi, S., and Tranum-Jensen, J. (1991). Alpha-Toxin of Staphylococcus aureus. Microbiol. Rev. *55*, 733–751.

16. Bhattacharjee, P., and Keyel, P.A. (2018). Cholesterol-dependent cytolysins impair pro-inflammatory macrophage responses. Sci. Rep. *8*, 1–15.

17. Birmingham, C.L., Canadien, V., Kaniuk, N.A., Steinberg, B.E., Higgins, D.E., and Brumell, J.H. (2008). Listeriolysin O allows Listeria monocytogenes replication in macrophage vacuoles. Nature *451*, 350–354.

18. Bokori-Brown, M., Petrov, P.G., Khafaji, M.A., Mughal, M.K., Naylor, C.E., Shore, A.C., Gooding, K.M., Casanova, F., Mitchell, T.J., Titball, R.W., et al. (2016). Red Blood Cell Susceptibility to Pneumolysin: Correlation with Membrane Biochemical and Physical Properties. J. Biol. Chem. *291*, 10210–10227.

19. Borgnia, M., Nielsen, S., Engel, A., and Agre, P. (1999). Cellular and molecular biology of the aquaporin water channels. Annu Rev Biochem *68*, 425–458.

20. Boyd, C.M., Parsons, E.S., Smith, R.A.G.G., Seddon, J.M., Ces, O., and Bubeck, D. (2016). Disentangling the roles of cholesterol and CD59 in intermedilysin pore formation. Sci. Rep. *6*, 38446.

21. Bräuning, B., and Groll, M. (2018). Structural and Mechanistic Features of ClyA-Like α-Pore-Forming Toxins. Toxins (Basel). *10*, 343.

22. Brown, M.S., and Goldstein, J.L. (1997). The SREBP pathway: Regulation of cholesterol metabolism by proteolysis of a membrane-bound transcription factor. Cell *89*, 331–340.

23. Burnet, F.M. (1929). The Exotoxins of Staphylococcus pyogenes aureus. J. Pathol. Bacteriol. *32*, 717–734.

24. Catlin, B.W. (1992). Gardnerella vaginalis : Characteristics, Clinical Considerations, and Controversies. Clin. Microbiol. Rev. *5*, 213–237.

25. Cauci, S., Monte, R., Ropele, M., Missero, C., Not, T., Quadrifoglio, F., and Menestrina, G. (1993). Pore-forming and haemolytic properties of the Gardnerella vaginalis cytoiysin. Mol. Microbiol. *9*, 1143–1155.

26. Cauci, S., Scrimin, F., Driussi, S., Ceccone, S., Monte, R., Fant, L., and Quadrifoglio, F. (1996). Specific immune response against Gardnerella vaginalis hemolysin in patients with bacterial vaginosis. Am. J. Obstet. Gynecol. *175*, 1601–1605.

27. Cauci, S., Guaschino, S., Driussi, S., De Santo, D., Lanzafame, P., and Quadrifoglio, F. (2002). Correlation of Local Interleukin-8 with Immunoglobulin A against Gardnerella vaginalis Hemolysin and with Prolidase and Sialidase Levels in Women with Bacterial Vaginosis. J. Infect. Dis. *185*, 1614–1620.

28. Chakrabarti, R.S., Ingham, S.A., Kozlitina, J., Gay, A., Cohen, J.C., Radhakrishnan, A., and Hobbs, H.H. (2017). Variability of cholesterol accessibility in human red blood cells measured using a bacterial cholesterol-binding toxin. Elife *6*, 1–27.

29. Chang, H. (2017). Cleave but not leave: Astrotactin proteins in development and disease. IUBMB Life *69*, 572–577.

30. Christie, M.P., Johnstone, B.A., Tweten, R.K., Parker, M.W., and Morton, C.J. (2018). Cholesterol-dependent cytolysins: from water-soluble state to membrane pore. Biophys. Rev. *10*, 1337–1348.

31. Cirauqui, N., Abriata, L.A., Van Der Goot, F.G., and Dal Peraro, M. (2017). Structural, physicochemical and dynamic features conserved within the aerolysin pore-forming toxin family. Sci. Rep. *7*, 1–12.

32. Cooper, S.T., and McNeil, P.L. (2015). Membrane Repair: Mechanisms and Pathophysiology. Physiol. Rev. *95*, 1205–1240.

33. Črnigoj Kristan, K., Viero, G., Dalla Serra, M., Maček, P., and Anderluh, G. (2009). Molecular mechanism of pore formation by actinoporins. Toxicon *54*, 1125–1134.

34. Cywes-Bentley, C., Hakansson, A., Christianson, J., and Wessels, M.R. (2005). Extracellular group A Streptococcus induces keratinocyte apoptosis by dysregulating calcium signalling. Cell. Microbiol. *7*, 945–955.

35. Czajkowsky, D.M., Hotze, E.M., Shao, Z., and Tweten, R.K. (2004). Vertical collapse of a cytolysin prepore moves its transmembrane b-hairpins to the membrane. EMBO J. *23*, 3206–3215.

36. Dal Peraro, M., and Van der Goot, F.G. (2016). Pore-forming toxins: ancient, but never really out of fashion. Nat. Rev. Microbiol. *14*, 77–92.

37. Davies, A., and Lachmann, P.J. (1993). Membrane defence against complement lysis: the structure and biological properties of CD59. Immunol. Res. *12*, 258–275.

38. Davies, A., Simons, D.L., Hale, G., Harrison, R.A., Tighe, H., Lachmann, P.J., and Waldmann, H. (1989). CD59, an LY-6 protein expressed in human lymphoid cells, regulates the action of the complement membrane attack complex on homologous cells. *170*, 637–654.

39. Davis, B.K., Wen, H., and Ting, J.P.-Y. (2011). The Inflammasome NLRs in Immunity, Inflammation, and Associated Diseases. Annu. Rev. Immunol. *29*, 707–735.

40. Derrington, I.M., Butler, T.Z., Collins, M.D., Manrao, E., Pavlenok, M., Niederweis, M., and Gundlach, J.H. (2010). Nanopore DNA sequencing with MspA. Proc. Natl. Acad. Sci. *107*, 16060–16065.

41. Diep, D.B., Nelson, K.L., Raja, S.M., Pleshak, E.N., and Buckley, J.T. (2002). Glycosylphosphatidylinositol Anchors of Membrane Glycoproteins Are Binding Determinants for the Channel-forming Toxin Aerolysin. J. Biol. Chem. *273*, 2355–2360.

42. Dowd, K.J., and Tweten, R.K. (2012). The cholesterol-dependent cytolysin signature motif: a critical element in the allosteric pathway that couples membrane binding to pore assembly. PLoS Pathog. *8*, e1002787.

43. Dumont, A.L., and Torres, V.J. (2014). Cell targeting by the Staphylococcus aureus pore-forming toxins: It's not just about lipids. Trends Microbiol. *22*, 21–27.

44. Farrand, A.J., LaChapelle, S., Hotze, E.M., Johnson, A.E., and Tweten, R.K. (2010). Only two amino acids are essential for cytolytic toxin recognition of cholesterol at the membrane surface. Proc. Natl. Acad. Sci. *107*, 4341–4346.

45. Farrand, S., Hotze, E., Friese, P., Hollingshead, S.K., Smith, D.F., Cummings, R.D., Dale, G.L., and Tweten, R.K. (2008). Characterization of a Streptococcal Cholesterol-Dependent Cytolysin with a Lewis y and b Specific Lectin Domain [†]. Biochemistry *47*, 7097–7107.

46. Faudry, E., Perdu, C., and Attrée, I. (2013). Bacterial Cell Surfaces. In Methods in Molecular Biology, A.H. Delcour, ed. (Humana Press), pp. 173–185.

47. Feil, S.C., Lawrence, S., Mulhern, T.D., Holien, J.K., Hotze, E.M., Farrand, S., Tweten, R.K., and Parker, M.W. (2012). Structure of the lectin regulatory domain of the cholesterol-dependent cytolysin lectinolysin reveals the basis for its lewis antigen specificity. Structure *20*, 248–258.

48. Feng, D., Dai, S., Liu, F., Ohtake, Y., Zhou, Z., Wang, H., Zhang, Y., Kearns,

A., Peng, X., Zhu, F., et al. (2016). Cre-inducible human CD59 mediates rapid cell ablation after intermedilysin administration. *126*, 2321–2333.

49. Flanagan, J.J., Tweten, R.K., Johnson, A.E., and Heuck, A.P. (2009). Cholesterol Exposure at the Membrane Surface Is Necessary and Sufficient to Trigger Perfringolysin O Binding. Biochemistry *48*, 3977–3987.

50. Flórez, C., Muchada, B., Nogales, M., Aller, A., and Martin, E. (1994). Bacteremia Due to Gardnerella vaginalis: Report of Two Cases. Clin. Infect. Dis. *18*, 125.

51. Gardner, H.L., and Dukes, C.D. (1955). Haemophilus vaginalis vaginitis. A newly defined specific infection previously classified "nonspecific" vaginitis. Am. J. Obstet. Gynecol. *69*, 962–976.

52. Gelber, S.E., Aguilar, J.L., Lewis, K.L.T., and Ratner, A.J. (2008). Functional and phylogenetic characterization of vaginolysin, the human-specific cytolysin from Gardnerella vaginalis. J. Bacteriol. *190*, 3896–3903.

53. Gellings, P.S., and McGee, D.J. (2018). Arcanobacterium haemolyticum phospholipase D enzymatic activity promotes the hemolytic activity of the cholesterol-dependent cytolysin arcanolysin. Toxins (Basel). *10*, 1–13.

54. Giddings, K.S., Johnson, A.E., and Tweten, R.K. (2003). Redefining cholesterol's role in the mechanism of the cholesterol-dependent cytolysins. Proc. Natl. Acad. Sci. U. S. A. *100*, 11315–11320.

55. Giddings, K.S., Zhao, J., Sims, P.J., and Tweten, R.K. (2004). Human CD59 is a receptor for the cholesterol-dependent cytolysin intermedilysin. Nat. Struct. Mol. Biol. *11*, 1173–1178.

56. Gilbert, R.J.C. (2005). Inactivation and activity of cholesterol-dependent cytolysins: What structural studies tell us. Structure *13*, 1097–1106.

57. Gilbert, R.J.C., and Sonnen, A.F.-P. (2016). Measuring kinetic drivers of pneumolysin pore structure. Eur. Biophys. J. *45*, 365–376.

58. Gilbert, R.J.C., Serra, M.D., Froelich, C.J., Wallace, M.I., and Anderluh, G. (2014). Membrane pore formation at protein–lipid interfaces. Trends Biochem. Sci. *39*, 510–516.

59. Gill, S., Chow, R., and Brown, A.J. (2008). Sterol regulators of cholesterol homeostasis and beyond: The oxysterol hypothesis revisited and revised. Prog. Lipid Res. *47*, 391–404.

60. Gonzalez, M.R., Bischofberger, M., Pernot, L., Van Der Goot, F.G., and Frêche, B. (2008). Bacterial pore-forming toxins: The (w)hole story? Cell. Mol. Life Sci. *65*, 493–507.

61. Greenwood, J.R., and Pickett, M.J. (1980). Transfer of Haemophilus vaginalis Gardner and Dukes to a New Genus, Gardnerella: G. vaginalis (Gardner and Dukes) comb. nov. Int. J. Syst. Bacteriol. *30*, 170–178.

62. Hadders, M.A., Bubeck, D., Roversi, P., Hakobyan, S., Forneris, F., Morgan, B.P., Pangburn, M.K., Llorca, O., Lea, S.M., and Gros, P. (2012). Assembly and Regulation of the Membrane Attack Complex Based on Structures of C5b6 and sC5b9. Cell Rep. *1*, 200–207.

63. Hamon, M.A., Batsche, E., Regnault, B., Tham, T.N., Seveau, S., Muchardt, C., and Cossart, P. (2007). Histone modifications induced by a family of bacterial toxins. Proc. Natl. Acad. Sci. *104*, 13467–13472.

64. Hardy, L., Cerca, N., Jespers, V., Vaneechoutte, M., and Crucitti, T. (2017). Bacterial biofilms in the vagina. Res. Microbiol. *168*, 865–874.

65. Heuck, A.P., Tweten, R.K., and Johnson, A.E. (2003). Assembly and topography of the prepore complex in cholesterol-dependent cytolysins. J. Biol. Chem. *278*, 31218–31225.

66. Hill, J.E., Swee, H.G., Money, D.M., Doyle, M., Li, A., Crosby, W.L., Links, M., Leung, A., Chan, D., and Hemmingsen, S.M. (2005). Characterization of vaginal microflora of healthy, nonpregnant women by chaperonin-60 sequence-based methods. Am. J. Obstet. Gynecol. *193*, 682–692.

67. Hirst, R.A., Kadioglu, A., O'Callaghan, C., and Andrew, P.W. (2004). The role of pneumolysin in pneumococcal pneumonia and meningitis. Clin. Exp. Immunol. *138*, 195–201.

68. Hotze, E.M., Heuck, A.P., Czajkowsky, D.M., Shao, Z., Johnson, A.E., and Tweten, R.K. (2002). Monomer-Monomer Interactions Drive the Prepore to Pore Conversion of a β-Barrel-forming Cholesterol-dependent Cytolysin. *277*, 11597–11605.

69. Hotze, E.M., Le, H.M., Sieber, J.R., Bruxvoort, C., McInerney, M.J., and Tweten, R.K. (2013). Identification and characterization of the first cholesterol-dependent cytolysins from gram-negative bacteria. Infect. Immun. *81*, 216–225.

70. Hu, W., Ferris, S.P., Tweten, R.K., Wu, G., Radaeva, S., Gao, B., Bronson, R.T., Halperin, J.A., and Qin, X. (2007). Rapid conditional targeted ablation of cells expressing human CD59 in transgenic mice by intermedilysin. Nat. Med. *14*, 98–103.

71. Huang, S., and Czech, M.P. (2007). The GLUT4 Glucose Transporter. Cell Metab. *5*, 237–252.

72. Iacovache, I., Degiacomi, M.T., Pernot, L., Ho, S., Schiltz, M., Dal Peraro, M., and van der Goot, F.G. (2011). Dual chaperone role of the c-terminal

propeptide in folding and oligomerization of the pore-forming toxin aerolysin. PLoS Pathog. *7*.

73. Iacovache, I., De Carlo, S., Cirauqui, N., Dal Peraro, M., Van Der Goot, F.G., and Zuber, B. (2016). Cryo-EM structure of aerolysin variants reveals a novel protein fold and the pore-formation process. Nat. Commun. *7*, 1–8.

74. Janulaitiene, M., Paliulyte, V., Grinceviciene, S., Zakareviciene, J., Vladisauskiene, A., Marcinkute, A., and Pleckaityte, M. (2017). Prevalence and distribution of Gardnerella vaginalis subgroups in women with and without bacterial vaginosis. *17*, 1–9.

75. Janulaitiene, M., Gegzna, V., Baranauskiene, L., Bulavaitė, A., Simanavicius, M., and Pleckaityte, M. (2018). Phenotypic characterization of Gardnerella vaginalis subgroups suggests differences in their virulence potential. PLoS One *13*, e0200625.

76. Jayaprakash, T.P., Schellenberg, J.J., and Hill, J.E. (2012). Resolution and Characterization of Distinct cpn60-Based Subgroups of Gardnerella vaginalis in the Vaginal Microbiota. PLoS One *7*, e43009.

77. Jeon, T.-I., and Osborne, T.F. (2012). SREBPs: Metabolic integrators in physiology and metabolism. Trends Endocrinol. Metab. *23*, 65–72.

78. Johnson, B.B., Breña, M., Anguita, J., and Heuck, A.P. (2017a). Mechanistic Insights into the Cholesterol-dependent Binding of Perfringolysin O-based Probes and Cell Membranes. Sci. Rep. *7*, 1–14.

79. Johnson, S., Brooks, N.J., Smith, R.A.G.G., Lea, S.M., and Bubeck, D. (2013). Structural Basis for Recognition of the Pore-Forming Toxin Intermedilysin by Human Complement Receptor CD59. Cell Rep. *3*, 1369–1377.

80. Johnson, T.K., Henstridge, M.A., and Warr, C.G. (2017b). MACPF/CDC proteins in development: Insights from Drosophila torso-like. Semin. Cell Dev. Biol. *72*, 163–170.

81. Jørgensen, P.L., and Andersen, J.P. (1988). Structural basis for E1-E2 conformational transitions in Na, K-pump and Ca-pump proteins. J. Membr. Biol. *103*, 95–120.

82. Kafsack, B.F., Pena, J. DO, Coppens, I., Ravindran, S., Boothroyd, J.C., and Carruthers, V.B. (2009). Rapid Membrane Disruption by a Perforin-Like Protein Facilitates Parasite Exit from Host Cells. Science (80-.). *323*, 530–533.

83. Kinoshita, M., Suzuki, K.G.N., Matsumori, N., Takada, M., Ano, H., Morigaki, K., Abe, M., Makino, A., Kobayashi, T., Hirosawa, K.M., et al. (2017). Raft-based sphingomyelin interactions revealed by new fluorescent

sphingomyelin analogs. J. Cell Biol. *216*, 1183–1204.

84. LaChapelle, S., Tweten, R.K., and Hotze, E.M. (2009). Intermedilysin-receptor interactions during assembly of the pore complex. Assembly intermediates increase host cell susceptibility to complement-mediated lysis. J. Biol. Chem. *284*, 12719–12726.

85. Lakey, J.H., Massotte, D., Heitz, F., Dasseux, J. -L, Faucon, J. -F, Parker, M.W., and Pattus, F. (1991). Membrane insertion of the pore-forming domain of colicin A: A spectroscopic study. Eur. J. Biochem. *196*, 599–607.

86. Lakey, J.H., Gisou van der Goot, F., and Pattus, F. (1994). All in the family: the toxic activity of pore-forming colicins. Toxicology *87*, 85–108.

87. Lawrence, S.L., Feil, S.C., Morton, C.J., Farrand, A.J., Mulhern, T.D., Gorman, M.A., Wade, K.R., Tweten, R.K., and Parker, M.W. (2015). Crystal structure of Streptococcus pneumoniae pneumolysin provides key insights into early steps of pore formation. Sci. Rep. *5*, 1–13.

88. Lawrence, S.L., Gorman, M.A., Feil, S.C., Mulhern, T.D., Kuiper, M.J., Ratner, A.J., Tweten, R.K., Morton, C.J., and Parker, M.W. (2016). Structural Basis for Receptor Recognition by the Human CD59-Responsive Cholesterol-Dependent Cytolysins. Structure *24*, 1–11.

89. Lee, A.A., Senior, M.J., Wallace, M.I., Woolley, T.E., and Griffiths, I.M. (2016). Dissecting the self-assembly kinetics of multimeric pore-forming toxins. J. R. Soc. Interface *13*, 1–8.

90. Lemon, J.K., and Weiser, J.N. (2015). Degradation Products of the Extracellular Pathogen Streptococcus pneumoniae Access the Cytosol via Its Pore-Forming Toxin. *6*, 1–10.

91. Leopold, S. (1953). Heretofore undescribed organism isolated from the genitourinary system. U.S. Armed Forces Med. J. *4*, 263–266.

92. Lesieur, C., Frutiger, S., Hughes, G., Kellner, R., Pattus, F., and van der Goot, F.G. (1999). Increased Stability upon Heptamerization of the Pore-forming Toxin Aerolysin. J. Biol. Chem. *274*, 36722–36728.

93. Leung, C., Dudkina, N. V, Lukoyanova, N., Hodel, A.W., Farabella, I., Pandurangan, A.P., Jahan, N., Damaso, M.P., Osmanovi, D., Reboul, C.F., et al. (2014). Stepwise visualization of membrane pore formation by suilysin , a bacterial cholesterol-dependent cytolysin. *3*, 1–17.

94. Lewis, A.L., and Lewis, W.G. (2012). Host sialoglycans and bacterial sialidases: A mucosal perspective. Cell. Microbiol. *14*, 1174–1182.

95. Lewis, W.G., Robinson, L.S., Gilbert, N.M., Perry, J.C., and Lewis, A.L. (2013). Degradation, foraging, and depletion of mucus sialoglycans by the

vagina-adapted actinobacterium Gardnerella vaginalis. J. Biol. Chem. *288*, 12067–12079.

96. Lipsitch, M., and Moxon, E.R. (1997). Virulence and transmissibility of pathogens: What is the relationship? Trends Microbiol. *5*, 31–37.

97. Los, F.C.O., Randis, T.M., Aroian, R. V., and Ratner, A.J. (2013). Role of Pore-Forming Toxins in Bacterial Infectious Diseases. Microbiol. Mol. Biol. Rev. *77*, 173–207.

98. Lukoyanova, N., Hoogenboom, B.W., and Saibil, H.R. (2016). The membrane attack complex, perforin and cholesterol-dependent cytolysin superfamily of pore-forming proteins. J. Cell Sci. *129*, 2125–2133.

99. Ma, B., Forney, L.J., and Ravel, J. (2012). Vaginal Microbiome: Rethinking Health and Disease. Annu. Rev. Microbiol. *66*, 371–389.

100. Machado, A., and Cerca, N. (2015). Influence of biofilm formation by gardnerella vaginalis and other anaerobes on bacterial vaginosis. J. Infect. Dis. *212*, 1856–1861.

101. Marshall, J.E., Faraj, B.H.A., Gingras, A.R., Lonnen, R., Sheikh, M.A., El-Mezgueldi, M., Moody, P.C.E., Andrew, P.W., and Wallis, R. (2015). The Crystal Structure of Pneumolysin at 2.0 Å Resolution Reveals the Molecular Packing of the Pre-pore Complex. Sci. Rep. *5*, 1–11.

102. Matthias, K.A., Roche, A.M., Standish, A.J., Shchepetov, M., and Weiser, J.N. (2014). Neutrophil-Toxin Interactions Promote Antigen Delivery and Mucosal Clearance of Streptococcus pneumoniae. J. Immunol. *180*, 6246–6254.

103. Mim, C., and Unger, V.M. (2012). Membrane curvature and its generation by BAR proteins. Trends Biochem. Sci. *37*, 526–533.

104. Mitchel, C., and Marrazzo, J. (2014). Bacterial vaginosis and the cervicovaginal immune response. Am. J. Reprod. Immunol. *71*, 555–563.

105. Mueckler, M., Caruso, C., Baldwin, S.A., Panico, M., Blench, I., Morris, H.R., Allard, W.J., Lienhard, G.E., and Lodish, H.F. (1985). Sequence and structure of a human glucose transporter. Science (80-.). *229*, 941–945.

106. Mueller, M., Grauschopf, U., Maier, T., Glockshuber, R., and Ban, N. (2009). The structure of a cytolytic α-helical toxin pore reveals its assembly mechanism. Nature *459*, 726–730.

107. Nagamune, H., Ohnishi, C., Katsuura, A., Fushitani, K., Whiley, R.A., and Matsuda, Y. (1996). Intermedilysin , a novel cytotoxin specific for human cells secreted by Streptococcus intermedius UNS46 isolated from a human liver abscess . Intermedilysin , a Novel Cytotoxin Specific for Human Cells ,

Secreted by Streptococcus intermedius UNS46 Isolate. *64*, 3093–3100.

108. Nel, J.G., Theron, A.J., Durandt, C., Tintinger, G.R., Pool, R., Mitchell, T.J., Feldman, C., and Anderson, R. (2016). Pneumolysin activates neutrophil extracellular trap formation. Clin. Exp. Immunol. *184*, 358–367.

109. Ni, T., and Gilbert, R.J.C. (2017). Repurposing a pore: Highly conserved perforin-like proteins with alternative mechanisms. Philos. Trans. R. Soc. B Biol. Sci. *372*, 20160212.

110. Nivala, J., Marks, D.B., and Akeson, M. (2013). Unfoldase-mediated protein translocation through an α-hemolysin nanopore. Nat. Biotechnol. *31*, 247–250.

111. Nowak, R.G., Randis, T.M., Desai, P., He, X., Robinson, C.K., Rath, J.M., Glover, E.D., Ratner, A.J., Ravel, J., and Brotman, R.M. (2018). Higher levels of a cytotoxic protein, vaginolysin, in lactobacillus-deficient community state types at the vaginal mucosa. Sex. Transm. Dis. *45*, e14–e17.

112. Nugent, R.P., Krohn, M.A., and Hillier, S.L. (1991). Reliability of Diagnosing Bacterial Vaginosis Is Improved by a Standardized Method of Gram Stain Interpretation. J. Clin. Microbiol *29*, 297-301.

113. O'Brien, D.K., and Melville, S.B. (2004). Effects of Clostridium perfringens Alpha-Toxin (PLC) and Perfringolysin O (PFO) on Cytotoxicity to Macrophages, on Escape from the Phagosomes of Macrophages, and on Persistence of C. perfringens in Host Tissues. Infect. Immun. *72*, 5204–5215.

114. Onderdonk, A.B., Delaney, M.L., and Fichorova, R.N. (2016). The Human Microbiome during Bacterial Vaginosis. Clin. Microbiol. Rev. *29*, 223–238.

115. Palmer, M., Harris, R., Freytag, C., Kehoe, M., Tranum-Jensen, J., and Bhakdi, S. (1998). Assembly mechanism of the oligomeric streptolysin O pore: The early membrane lesion is lined by a free edge of the lipid membrane and is extended gradually during oligomerization. EMBO J. *17*, 1598–1605.

116. Parker, M.W., Pattus, F., Tucker, A., and Tsernoglou, D. (1989). Structure of the membrane-pore-forming fragment of colicin A. Nature *337*, 93–96.

117. Pee, K. Van, Mulvihill, E., Müller, D.J., and Yildiz, Ö. (2016). Unraveling the pore forming steps of pneumolysin from Streptococcus pneumoniae. Nano Lett. *16*, 7915–7924.

118. van Pee, K., Neuhaus, A., D'Imprima, E., Mills, D.J., Kühlbrandt, W., Yildiz, Ö., D'Imprima, E., Mills, D.J., Kühlbrandt, W., Yildiz, Ö., et al. (2017). CryoEM structures of membrane pore and prepore complex reveal cytolytic mechanism of Pneumolysin. Elife *6*, 1–22.

119. Perez-Pascual, D., Monnet, V., and Gardan, R. (2016). Bacterial cell-cell

communication in the host via RRNPP peptide-binding regulators. Front. Microbiol. *7*, 1–8.

120. Pernas, L., and Scorrano, L. (2015). Mito-Morphosis: Mitochondrial Fusion, Fission, and Cristae Remodeling as Key Mediators of Cellular Function. Annu. Rev. Physiol. *78*, 505–531.

121. Podobnik, M., Marchioretto, M., Zanetti, M., Bavdek, A., Kisovec, M., Cajnko, M.M., Lunelli, L., Dalla Serra, M., and Anderluh, G. (2015). Plasticity of Listeriolysin O Pores and its Regulation by pH and Unique Histidine. Sci. Rep. *5*, 1–10.

122. Polekhina, G., Giddings, K.S., Tweten, R.K., and Parker, M.W. (2005). Insights into the action of the superfamily of cholesterol-dependent cytolysins from studies of intermedilysin. Proc. Natl. Acad. Sci. *102*, 600–605.

123. Pollard, T., Earnshaw, W., Lippincott-Schwartz, J., and Johnson, G. (2017). Cell Biology (Elsevier).

124. Pybus, V., and Onderdonk, A.B. (1997). Evidence for a Commensal, Symbiotic Relationship between Gardnerella vaginalis and Prevotella bivia Involving Ammonia: Potential Significance for Bacterial Vaginosis. J. Infect. Dis. *175*, 406–413.

125. Ramachandran, R., Tweten, R.K., and Johnson, A.E. (2004). Membrane-dependent conformational changes initiate cholesterol-dependent cytolysin oligomerization and intersubunit beta-strand alignment. Nat. Struct. Mol. Biol. *11*, 697–705.

126. Ramachandran, R., Tweten, R.K., and Johnson, A.E. (2005). The domains of a cholesterol-dependent cytolysin undergo a major FRET-detected rearrangement during pore formation. Proc. Natl. Acad. Sci. *102*, 7139–7144.

127. Reboul, C.F., Whisstock, J.C., and Dunstone, M.A. (2016). Giant MACPF/CDC pore forming toxins: A class of their own. Biochim. Biophys. Acta - Biomembr. *1858*, 475–486.

128. Reimer, L., and Reller, L. (1984). Gardnerella vaginalis bacteremia: a review of thirty casestle. Obs. Gynecol *64*, 170–172.

129. Rojko, N., and Anderluh, G. (2015). How Lipid Membranes Affect Pore Forming Toxin Activity. Acc. Chem. Res. *48*, 3073–3079.

130. Rojko, N., Dalla Serra, M., Mačєk, P., and Anderluh, G. (2016). Pore formation by actinoporins, cytolysins from sea anemones. Biochim. Biophys. Acta - Biomembr. *1858*, 446–456.

131. Rosado, C.J., Buckle, A.M., Law, R.H., Butcher, R.E., Kan, W.-T., H, B.C.,

Ung, K., Browne, K.A., Baran, K., Bashtannyk-Puhalovich, T.A., et al. (2007). A Common Fold Mediates Vertebrate Defense and Bacterial Attack. *317*, 1548–1551.

132. Rosado, C.J., Kondos, S., Bull, T.E., Kuiper, M.J., Law, R.H.P., Buckle, A.M., Voskoboinik, I., Bird, P.I., Trapani, J.A., Whisstock, J.C., et al. (2008). The MACPF/CDC family of pore-forming toxins. Cell. Microbiol. *10*, 1765–1774.

133. Rossjohn, J., Feil, S.C., McKinstry, W.J., Tweten, R.K., and Parker, M.W. (1997). Structure of a Cholesterol-Binding, Thiol-Activated Cytolysin and a Model of Its Membrane Form. Cell *89*, 685–692.

134. Rossjohn, J., Polekhina, G., Feil, S.C., Morton, C.J., Tweten, R.K., and Parker, M.W. (2007). Structures of Perfringolysin O Suggest a Pathway for Activation of Cholesterol-dependent Cytolysins. J. Mol. Biol. *367*, 1227–1236.

135. Ruan, Y., Rezelj, S., Bedina Zavec, A., Anderluh, G., and Scheuring, S. (2016). Listeriolysin O Membrane Damaging Activity Involves Arc Formation and Lineaction – Implication for Listeria monocytogenes Escape from Phagocytic Vacuole. PLoS Pathog. *12*, 1–18.

136. Sathyanarayana, P., Maurya, S., Behera, A., Roy, R., Ravichandran, M., Visweswariah, S.S., Ayappa, K.G., and Roy, R. (2018). Cholesterol promotes Cytolysin A activity by stabilizing the intermediates during pore formation. Proc. Natl. Acad. Sci. *115*, E7323–E7330.

137. Savinov, S.N., and Heuck, A.P. (2017). Interaction of Cholesterol with Perfringolysin O: What Have We Learned from Functional Analysis? Toxins (Basel). *9*, 381.

138. Schellenberg, J.J., Jayaprakash, T.P., Withana Gamage, N., Patterson, M.H., Vaneechoutte, M., and Hill, J.E. (2016). Gardnerella vaginalis Subgroups Defined by cpn60 Sequencing and Sialidase Activity in Isolates from Canada, Belgium and Kenya. PLoS One *11*, e0146510.

139. Schellenberg, J.J., Patterson, M.H., and Hill, J.E. (2017). Gardnerella vaginalis diversity and ecology in relation to vaginal symptoms. Res. Microbiol. *168*, 837–844.

140. Schön, P., García-Sáez, A.J., Malovrh, P., Bacia, K., Anderluh, G., and Schwille, P. (2008). Equinatoxin II permeabilizing activity depends on the presence of sphingomyelin and lipid phase coexistence. Biophys. J. *95*, 691–698.

141. Schroeder, F., Huang, H., McIntosh, A.L., Atshaves, B.P., Martin, G.G., and Kier, A.B. (2010). Caveolin, sterol carrier protein-2, membrane cholesterol-rich microdomains and intracellular cholesterol trafficking. In Cholesterol Binding and Cholesterol Transport Proteins, (Springer), pp. 279–318.

142. Sezgin, E., Levental, I., Mayor, S., and Eggeling, C. (2017). The mystery of membrane organization: Composition, regulation and roles of lipid rafts. Nat. Rev. Mol. Cell Biol. *18*, 361–374.

143. Shak, J.R., Ludewick, H.P., Howery, K.E., Sakai, F., Yi, H., Harvey, R.M., Paton, J.C., Klugman, K.P., and Vidal, J.E. (2013). Novel Role for the Streptococcus pneumoniae Toxin Pneumolysin in the Assembly of Biofilms. MBio *4*, 1–10.

144. Shatursky, O., Heuck, A.P., Shepard, L.A., Rossjohn, J., Parker, M.W., Johnson, A.E., and Tweten, R.K. (1999). The mechanism of membrane insertion for a cholesterol-dependent cytolysin: A novel paradigm for pore-forming toxins. Cell *99*, 293–299.

145. Shaughnessy, L.M., Hoppe, A.D., Christensen, K.A., and Swanson, J.A. (2006). Membrane perforations inhibit lysosome fusion by altering pH and calcium in Listeria monocytogenes vacuoles. Cell. Microbiol. *8*, 781–792.

146. Shepard, L. a, Shatursky, O., Johnson, A.E., and Tweten, R.K. (2000). The Mechanism of Pore Assembly for a Cholesterol-Dependent Cytolysin : Formation of a Large Prepore Complex Precedes the Insertion of the. Biochemistry *39*, 10284–10293.

147. Shepard, L.A., Heuck, A.P., Hamman, B.D., Rossjohn, J., Parker, M.W., Ryan, K.R., Johnson, A.E., and Tweten, R.K. (1998). Identification of a Membrane-Spanning Domain of the Thiol-Activated Pore-Forming Toxin Clostridium perfringens Perfringolysin O: An α-Helical to β-Sheet Transition Identified by Fluorescence Spectroscopy. Biochemistry *37*, 14563–14574.

148. Shewell, L.K., Harvey, R.M., Higgins, M.A., Day, C.J., Hartley-Tassell, L.E., Chen, A.Y., Gillen, C.M., James, D.B.A., Alonzo, F., Torres, V.J., et al. (2014). The cholesterol-dependent cytolysins pneumolysin and streptolysin O require binding to red blood cell glycans for hemolytic activity. Proc. Natl. Acad. Sci. *111*, E5312–E5320.

149. Simons, K., and Toomre, D. (2000). Lipid rafts and signal transduction. Nat. Rev. Mol. Cell Biol. *1*, 31–41.

150. Sippl, M.J. (1993). Recognition of Errors in Three-Dimensional Structures of Proteins. Proteins Struct. Funct. Genet. *17*, 355–362.

151. Slade, D.J., Lovelace, L.L., Chruszcz, M., Minor, W., Lebioda, L., and Sodetz, J.M. (2008). Crystal Structure of the MACPF Domain of Human Complement Protein C8α in Complex with the C8γ Subunit. J. Mol. Biol. *379*, 331–342.

152. Söding, J., Biegert, A., and Lupas, A.N. (2005). The HHpred interactive server for protein homology detection and structure prediction. Nucleic Acids Res. *33*, 244–248.

153. Soltani, C.E., Hotze, E.M., Johnson, A.E., and Tweten, R.K. (2007). Specific protein-membrane contacts are required for prepore and pore assembly by a cholesterol-dependent cytolysin. J. Biol. Chem. *282*, 15709–15716.

154. Sonnen, A.F.P., Plitzko, J.M., and Gilbert, R.J.C. (2014). Incomplete pneumolysin oligomers form membrane pores. Open Biol. *4*, 1–10.

155. Subramanian, K., Neill, D.R., Malak, H.A., Spelmink, L., Khandaker, S., Dalla Libera Marchiori, G., Dearing, E., Kirby, A., Yang, M., Achour, A., et al. (2018). Pneumolysin binds to the mannose receptor C type 1 (MRC-1) leading to anti-inflammatory responses and enhanced pneumococcal survival. Nat. Microbiol. *4*, 62.

156. Szczesny, P., Iacovache, I., Muszewska, A., Ginalski, K., van der Goot, F.G., and Grynberg, M. (2011). Extending the Aerolysin Family: From Bacteria to Vertebrates. PLoS One *6*, e20349.

157. Tabata, A., Ohkura, K., Ohkubo, Y., Tomoyasu, T., Ohkuni, H., Whiley, R.A., and Nagamune, H. (2014). The diversity of receptor recognition in cholesterol-dependent cytolysins. Microbiol. Immunol. *58*, 155–171.

158. Tanaka, K., Caaveiro, J.M.M., Morante, K., and Tsumoto, K. (2017). Haemolytic actinoporins interact with carbohydrates using their lipid-binding module. Philos. Trans. R. Soc. B Biol. Sci. *372*, 1–9.

159. Tankovic, J., Timinskas, A., Janulaitiene, M., Zilnyte, M., Baudel, J.L., Maury, E., Zvirbliene, A., and Pleckaityte, M. (2017). Gardnerella vaginalis bacteremia associated with severe acute encephalopathy in a young female patient. Anaerobe *47*, 132–134.

160. Thompson, J.R., Cronin, B., Bayley, H., and Wallace, M.I. (2011). Rapid Assembly of a Multimeric Membrane Protein Pore. *101*, 2679–2683.

161. Tilley, S.J., and Orlova, E. V (2005). Structural Basis of Pore Formation by the Bacterial Toxin Pneumolysin. Cell *121*, 247–256.

162. Timmer, A.M., Timmer, J.C., Pence, M.A., Hsu, L.C., Ghochani, M., Frey, T.G., Karin, M., Salvesen, G.S., and Nizet, V. (2009). Streptolysin O promotes group A streptococcus immune evasion by accelerated macrophage apoptosis. J. Biol. Chem. *284*, 862–871.

163. Tweten, R.K., Hotze, E.M., and Wade, K.R. (2015). The Unique Molecular Choreography of Giant Pore Formation by the Cholesterol-Dependent Cytolysins of Gram-Positive Bacteria. Annu. Rev. Microbiol. *69*, 323–340.

164. Varkouhi, A.K., Scholte, M., Storm, G., and Haisma, H.J. (2011). Endosomal Escape Pathways for Delivery of Biologics. J. Control. Release *151*, 220–228.

165. Vasta, G.R., Mario Amzel, L., Bianchet, M.A., Cammarata, M., Feng, C., and Saito, K. (2017). F-Type Lectins: A highly diversified family of fucose-binding proteins with a unique sequence motif and structural fold, involved in self/non-self-recognition. Front. Immunol. *8*, 1–18.

166. Verstraelen, H., Verhelst, R., Vaneechoutte, M., and Temmerman, M. (2010). The epidemiology of bacterial vaginosis in relation to sexual behaviour. BMC Infect. Dis. *10*, 1–11.

167. Wade, K.R., Hotze, E.M., Kuiper, M.J., Morton, C.J., Parker, M.W., and Tweten, R.K. (2015). An intermolecular electrostatic interaction controls the prepore-to-pore transition in a cholesterol-dependent cytolysin. Proc. Natl. Acad. Sci. *112*, 2204–2209.

168. Wickham, S.E., Hotze, E.M., Farrand, A.J., Polekhina, G., Nero, T.L., Tomlinson, S., Parker, M.W., and Tweten, R.K. (2011). Mapping the intermedilysin-human CD59 receptor interface reveals a deep correspondence with the binding site on CD59 for complement binding proteins C8α and C9. J. Biol. Chem. *286*, 20952–20962.

169. Wirth, C.C., Glushakova, S., Scheuermayer, M., Repnik, U., Garg, S., Schaack, D., Kachman, M.M., Weißbach, T., Zimmerberg, J., Dandekar, T., et al. (2014). Perforin-like protein PPLP2 permeabilizes the red blood cell membrane during egress of Plasmodium falciparum gametocytes. Cell. Microbiol. *16*, 709–733.

170. Yu, J., Abagyan, R., Dong, S., Gilbert, A., Nussenzweig, V., and Tomlinson, S. (1997). Mapping the Active Site of CD59. J. Exp. Med. *185*, 745–754.

171. Zafar, M.A., Wang, Y., Hamaguchi, S., and Weiser, J.N. (2017). Host-to-Host Transmission of Streptococcus pneumoniae Is Driven by Its Inflammatory Toxin, Pneumolysin. Cell Host Microbe *21*, 73–83.

172. Zhang, G., and Yang, P. (2017). A novel cell-cell communication mechanism in the nervous system: exosomes. J. Neurosci. Res. *96*, 45–52.

173. Zhao, X.J., Zhao, J., Zhou, Q., and Sims, P.J. (1998). Identity of the residues responsible for the species-restricted complement inhibitory function of human CD59. J. Biol. Chem. *273*, 10665–10671.

174. Zvirbliene, A., Pleckaityte, M., Lasickiene, R., Kucinskaite-Kodze, I., and Zvirblis, G. (2010). Production and characterization of monoclonal antibodies against vaginolysin: Mapping of a region critical for its cytolytic activity. Toxicon *56*, 19–28.

LIST OF PUBLICATIONS

Publications included in this thesis

Zilnyte, M., Venclovas, Č., Zvirbliene, A., Pleckaityte, M. (2015) The cytolytic activity of vaginolysin strictly depends on cholesterol and is potentiated by human CD59. Toxins, *7*, 110-128.

Tankovic, J., Timinskas, A., Janulaitiene, M., **Zilnyte, M.**, Baudel, J.L., Maury, E., Zvirbliene, A., Pleckaityte, M. (2017) *Gardnerella vaginalis* bacteremia associated with severe acute encephalopathy in a young female patient. Anaerobe, 47, 132-134.

Publication not included in this thesis

Kuncinskaite-Kodze, I., Pleckaityte, M., Bremer, C.M., Seiz, P., **Zilnyte, M.**, Bulavaite, A., Mickiene, G., Zvirblis, G., Sasnauskas, K., Glebe, D., Zvirbliene, A. (2015) New broadly reactive neutralizing antibodies against hepatitis B virus surface antigen. Virus research, *211*, 209-211.

LIST OF CONFERENCES

Zilnyte, M., Venclovas, Č., Zvirbliene, A., Pleckaityte, M. The cytolytic mechanisms of bacterial toxins. Conference for young scientists held by Lithuanian Academy of Sciences. Vilnius, Lithuania, 9 December 2014 (oral talk).

Zilnyte, M., Venclovas, Č., Zvirbliene, A., Pleckaityte, M. The Cytolytic Activity of Vaginolysin Strictly Depends on Cholesterol and Is Potentiated by Human CD59. The 3rd Prato Conference On Pore Forming Proteins. Prato, Italy, 11-14 May 2015 (poster presentation).

Zilnyte, M., Venclovas, Č., Penkauskas, T., Valincius, G., Zvirbliene, A., Pleckaityte, M. Probing the functional basis for pore-forming activity of cholesterol-dependent cytolysin vaginolysin. 18th World Congress of the International Society on Toxinology. Oxford, United Kingdom, 25-30 September 2015 (poster presentation).

Zilnyte, M., Ni, T., Gilbert, RJC. Insights into the role of CD59 in vaginolysin pore formation. The 4th Prato Conference On Pore Forming Proteins. Prato, Italy, 24-27 September 2018 (poster presentation).

CV

Milda Zilnytė
Date of birth: 1989-02-18
Tel. no. +447708 066565
Email: milda.zilnyte@magd.ox.ac.uk, milda.zilnyte@gmail.com
Address: Flat 3 186 Iffley Road, OX4 1SD, Oxford, United Kingdom

EDUCATION

2017-2018	**13-month internship in Prof. Robert Gilbert laboratory at the University of Oxford, Division of Structural Biology** Supervisor: Prof. Dr Robert Gilbert
2014-2018	**4-year Biochemistry PhD Programme at Vilnius University, Institute of Biotechnology, Department of Immunology and Cell biology** **Thesis title:** "Characterization of pore-forming toxin vaginolysin from *Gardnerella vaginalis*" Supervisors: Prof. Dr Aurelija Žvirblienė (2016-2018), Dr Milda Plečkaitytė (2014-2016)
2012-2014	**MSc Biochemistry at Vilnius University** **Thesis title:** "A study of the mechanism of cytolytic activity of bacterial toxin vaginolysin" Supervisor**:** Dr Milda Plečkaitytė
2008-2012	**BSc Biochemistry at Vilnius University** **Thesis title:** "Identification and analysis of CRISPR regions in bacteria *Gardnerella vaginalis*" Supervisor: Dr Milda Plečkaitytė

EMPLOYMENT

Since 01/04/2019		Postdoctoral Research Associate, University of Oxford, Magdalen College, Calleva Research Centre
01/07/2018 22/03/2019	–	Junior scientist at Vilnius University, Life Sciences Center, Institute of Biotechnology, Department of Immunology and Cell Biology
01/08/2011 30/06/2018	–	Laboratory assistant at Vilnius University, Life Sciences Center, Institute of Biotechnology, Department of Immunology and Cell Biology

AWARDS

2018	Grant for conference attendance in Prato, Italy from Research Council of Lithuania
2017-2018	One-year Erasmus+ scholarship for my internship at the University of Oxford from Vilnius University
2016, 2018	One-year promotional scholarships awarded for my academic achievements from Research Council of Lithuania
2015	Winner prize for the best poster presentation at Prato Pore-forming Proteins conference

NOTES

NOTES